REPUBLIC OF TURKEY
YILDIZ TECHNICAL UNIVERSITY
GRADUATE SCHOOL OF NATURAL AND APPLIED SCIENCES

DEVELOPING PHOSPHA-CARBORANE CONTAINING POLYMERS

GİZEM KAHRAMAN

PhD THESIS
DEPARTMENT OF CHEMISTRY
PROGRAM OF PHYSICAL CHEMISTRY

ADVISER
PROF. DR. TARIK EREN

İSTANBUL, 2019

REPUBLIC OF TURKEY

YILDIZ TECHNICAL UNIVERSITY

GRADUATE SCHOOL OF NATURAL AND APPLIED SCIENCES

DEVELOPING PHOSPHA-CARBORANE CONTAINING POLYMERS

A thesis submitted by Gizem KAHRAMAN in partial fulfillment of the requirements for the degree of **DOCTOR OF PHILOSOPHY** is approved by the committee on … in Department of Chemistry, Physical Chemistry.

Thesis Adviser

Prof. Dr. Tarık EREN

Yıldız Technical University

Co- Adviser

Prof. Dr. Dr. h.c. mult. Evamarie HEY-HAWKINS

Leipzig University

Approved By the Examining Committee

Prof. Dr. Tarık EREN

Yıldız Technical University ______________________

Prof. Dr. Nergis ARSU

Yıldız Technical University ______________________

Assoc. Prof. Dr. Hale OCAK

Yıldız Technical University ______________________

Assoc. Prof. Dr. Ece BULAK

Boğaziçi University ______________________

Assoc. Prof. Dr. Ersin ACAR

Boğaziçi University ______________________

This study was supported by the Scientific and Technological Research Council of Turkey (TUBITAK) Grant No: 114Z666, TUBITAK 2214-A International Research Fellowship Programme for PhD Students, COST Action CM1302 Short Term Scientific Mission (STSM) and German Academic Exchange Service (DAAD) Short Term Research Grant.

ACKNOWLEDGEMENTS

Foremost, I would like to express my sincere gratitude to my advisor, Prof. Dr. Tarik Eren for the continuous support of my PhD study and research, for his patience, motivation, enthusiasm, and immense knowledge. His guidance helped me in all the time of research and writing of the thesis. Besides my advisor, I would like to thank my co-advisor, Prof. Dr. Dr. h.c. mult. Evamarie Hey-Hawkins for her countless hours of reflecting, reading, and most of all patience throughout the entire process. They are excellent role models for someone who really know how to balance scientific and teaching.

My sincere thanks also goes to Prof. Dr. Markus Gallei and Dr. De-Yi Wang for offering me the short term research opportunities in their groups and leading me working on diverse exciting projects. I am also thankful to Assoc. Prof. Dr. Demet Karaca Balta for photo-studies and her regarding suggestions.

I also thank my fellow labmates and very close friends of mine, Ecem Işıksel, Naime Ceren Süer and Ceren Demir for the stimulating discussions and for the intense days we were working together. I am also very grateful to Rafaella Precker and Minghui Cong for their sincere friendship during last years in Leipzig. I would also like to thank my colleague and friend Dr. Toni Grell for all his help during submission of my dissertation. Furthermore, I want to thank all the members of Eren and Hey-Hawkins research groups for the friendly working atmosphere.

My special thanks to Tolga Çeper for being such an amazing person and very supportive in any circumstances. Thank you very much for all your contribution to my life.

Last but not least, I would love to thank my family; my parents Nilüfer Kahraman and Selçuk Kahraman, my little brother Uğur Kahraman for supporting me spiritually throughout my life. Love you so much.. iyi ki varsınız.

July, 2019

Gizem KAHRAMAN

TABLE OF CONTENTS

LIST OF SYMBOLS

B	Boron
C	Carbon
H	Hydrogen
Fe_3O_4	Iron Oxide
O	Oxygen
P	Phosphorus
T_g	Transmission Temperature

LIST OF ABBREVIATIONS

CB	Carborane
DSC	Differential Scanning Calorimetry
ESI-MS	Electrospray Ionization-Mass Spectrometry
FT-IR	Fourier Transform Infrared Spectroscopy
GPC	Gel Permeation Chromatography
ICP-MS	Inductively Coupled Plasma-Mass Spectrometry
MCC	Micro Combustion Calorimeter
NMR	Nuclear Magnetic Resonance
ROMP	Ring Opening Metathesis Polymerization
ROP	Ring Opening Polymerization
TEM	Transmission Electron Microscopy
TGA	Thermogravimetric Analysis
UV-Vis	Ultraviolet Visible

LIST OF FIGURES

Page

LIST OF TABLES

Page

ABSTRACT

DEVELOPING PHOSPHA-CARBORANE CONTAINING POLYMERS

Gizem KAHRAMAN

Department of Chemistry

PhD. Thesis

Adviser: Prof. Dr. Tarık EREN

Co-adviser: Prof. Dr. Dr. h.c. mult. Evamarie HEY-HAWKINS

The research presented in this thesis focuses on the development of novel functional hybrid architectures by carborane and phosphorus or anthracene units bearing polymers. The motivation behind this work was to understand the structure-property relationship with the incorporation of inorganic boron clusters and phosphorus or anthracene units into a variety of polymeric architectures. The aim was the incorporation of carborane cluster for the development of novel hybrid materials possesing multifunctional properties that can be used in different field. Development of heat resistance polymers without any additives is one of the challenges for the advancement of fire resistance polymers towards technological applications. Synergistic effect of phosphorus and carborane units enhance the thermal properties. Photocleavage and photodimerization properties of anthracene units highlights the improvement and implementation of the stimuli responsive polymers.

In the first part of the study, the synthesis of a silyl-protected oxanorbornene imide carborane and a phosphorus containing monomer were synthesized as well as they were copolymerized by ring-opening metathesis polymerization (ROMP) to investigate their heat resistance properties. The cleavage of the phosphonate ester present at the backbone of copolymer resulted in phosphonic acid units which were then used for coating of iron oxide nanoparticules. The first part of the study also illustrates some of the potential target applications in particular those containing boron and phosphorous derived compounds. Therefore, the heat resistance effect of both boron and phosphorous groups have been investigated by using thermal gravimetric analysis (TGA) and micro combustion calorimeter (MCC) techniques. Encapsulation of iron oxide nanoparticles with carborane clusters is a potential application for magnetically induced targeting and diagnosis boron neutron capture therapy in cancer treatment.

The second part of the study illustrates the carborane-phosphorus based condensation type polymers possesing hydroxyl functional end groups. Furthermore, a hydroxyl terminated carborane-phosphorus oligomer is used in the commercial epoxy resin formulation as a curing agent with a different loading by weight. Thermal properties and curing kinetics were investigated by using TGA, MCC and differential scanning calorimetry (DSC) techniques. The advantage offered by the presence of phosphorus and carborane groups is described.

The third and last part of the study is based on the copolymerization of carborane and anthracene units. The polymers with varying compositions of carborane and anthracene units have been obtained and characterized. The structural and thermal properties of these materials have been evaluated and compared to the literature known compounds. The effect of the presence of silyl carborane and anthracene units on the thermal properites is described. Furthermore, the photoswiching behaviour through anthracene units has been investigated to afford smart materials.

Monomer and polymer structures were analyzed by using NMR (^{1}H NMR, ^{13}C NMR, ^{31}P NMR, ^{11}B NMR), FTIR, GPC techniques. Solution and surface morphology were also analyzed by trasmission electron microscope (TEM) techniques. Efficiency of iron nanoparticles loading was evaluted via inductively coupled plasma mass spectrometry (ICP-MS). Photocleavage and photodimerization properties were investigated by using utraviolet–visible spectroscopy (UV–Vis).

Key words: ROMP (Ring opening methathesis polymerization), carborane, phosphonate, anthracene, heat resistance, amphiphilic block copolymer

ÖZET

FOSFA-KARBORAN ICEREN POLIMERLERIN GELISTIRILMESI

Gizem KAHRAMAN

Kimya Anabilim Dalı

Doktora Tezi

Tez Danışmanı: Prof. Dr. Tarık EREN

Eş Danışman: Prof. Dr. Dr. h.c. mult. Evamarie HEY-HAWKINS

Bu tez kapsamında yapılan çalışmaların odak noktası; içerisinde hem organik hem de inorganik kısımlar bulunduran fonksiyonlandırılmış yeni ikosahedral karboran ve fosfor ve ya antrasen türevi polimerlerin geliştirilmesi ve araştırılmasıdır. Bu çalışmaların arkasındaki motivasyon ise inorganik bor gruplarını içerisinde bulunduran iyi dizayn edilmiş çeşitli polimer yapılarına ışık tutmak ve bu bağlamda literatürde daha önce dikkat çekilmiş sorunlara çözüm aramaktır. Burada ki çalışmalar yeni hibrit malzemelerin teknolojik uygulamalara yönelik geliştirilmesi ve uygulanmasının yanı sıra bu konudaki bilimsel anlayışın ilerleyebilmesi içinde kritiktir. Herhangi bir katkı maddesi kullanılmaksızın elde edilen yangın geciktirici polimerlerin geliştirilmesi gnümüz teknolojisinin önemli bir parçasıdır. Karboran ve fosfor içerikli malzemeler sinerjik bir efekt yaratarak termal olarak daha dayanımlı hale gelmektedirler. Bunun yanında antrasenin fotodimimerizasyon ve fotoyarılma özellikleri sayesinde stimuli-responsive polimerlerin gelişmesi sağlanmaktadır.

Tezin ilk kısmında sillil koruması yapılmış oksanorbornen imid karboran ve fosfor içerikli monomerler sentezlenmiş, bu monomerler kullanılarak halka açılma metatez polimerizasyonu yöntemi (ROMP) ile kopolimerleri elde edilmiş ve sentezlenen polimerlerin yangın geciktirici özelliği incelenmiştir. Buna ek olarak, burada sentezlenen bu fosfonat esteri ve karboran bazlı polimerler, hidrojenasyon yöntemi ile fosfonik asit ve karboran içerikli bir hale getirilip yapıdaki fosfonik asit aracılığı ile demir oksit nanopartiküllerine bağlanmaları sağlandı. Bu bağlamda, tezin bu kısmında k çalışmalar aynı zamanda potansiyel bazı uygulamalarada ışık tutmaktadır. Burada polimerlerin yangın geciktiri özellikleri termal gravimetrik analiz (TGA) ve mikro

yanma kalorimetresi (MCC) kullanılarak araştırıldı. Karboran bağlı demir nanopartiküllerinin kapsülasyonu ise kanser tedavisinde (boron nötron yakalama terapi) ve manyetik tanı takibinde kullanılmak için potansiyel bir uygulama alanıdır.

Bu çalışmanın ikinci kısmı karboran ve fosfor bazlı kondenzasyon polimerlerine ışık tutmaktadır. Sentezlenen hidoksi ile kapanan bu karboran-fosfor oligomerleri, ticari epoksi reçine içerisinde belirli yüzdelerde karıştırılarak yanmazlık çalışmaları yapılmıştır. Bu malzemelerin termal özellikleri ve ışık kinetikleri TGA, MCC ve DSC (differential scanning calorimetry).

Çalışmanın üçüncü ver son kısmı ise karboran-monool (CB-Monool) ve antrasen türevi monomerlerin kopolimerizasyon çalışmalarını konu edinmektedir. Çeşitli polimer yapıları elde edilmiş ve hidrojenasyon reaksiyonu uygulanmıştır. Daha sonrasında polimerlerin yapısında bulunan antrasen birimlerinden kaynaklı olacak foto değişim (fotosel) özellikleri incelenmiş ve akıllı malzeme (Smart Materials) konusunda bu yapıların kullanabilirliğine ışık tutulmuştur.

Bu tez kapsamında sentezlenen ve kullanılan tüm malzemelerin yapısal ve termal özellikleri incelenerek literatürde bilinen bileşikler ile karşılaştırıldı. Elde edilen monomerler ve polimerler NMR (^{1}H NMR, ^{13}C NMR, ^{31}P NMR, ^{11}B NMR), FTIR, GPC teknikleri kullanılarak analiz edildi. Yüzey morfolojisinin tespiti için Geçiş Elektron Mikroskobu (TEM), polimerlerin termal dayanımlarının ncelenmesinde ise Termal Gravimetrik Analiz (TGA) ve Mikro Yanma Kalorimetresi (MCC) kullanıldı.

Anahtar Kelimeler: ROMP (Halka Açılma Metatez Polimerizasyonu), karboran, fosfonat, antrasen, yangın geciktirici, amfifilik blok kopolimer

REFERAT

ENTWICKLUNG PHOSPHA-CARBORANHALTIGER POLYMERE

Gizem KAHRAMAN

Department of Chemistry
PhD. Thesis

Adviser: Prof. Dr. Tarık EREN
Co-adviser: Prof. Dr. Dr. h.c. mult. Evamarie HEY-HAWKINS

Die vorliegende Arbeit beschäftigt sich mit der Entwicklung von Polymeren als neuartige funktionale Hybridarchitekturen welche Carborane sowie Phosphor- oder Anthraceneinheiten aufweisen. Die Motivation dieser Untersuchungen ist das Verständis des Wechselspiels von Struktur und Eigenschaften durch die Einführung von anorganischen Bor-Clustern und Phosphor- sowie Anthraceneinheiten in eine Vielzahl von polymeren Architekturen. Das Ziel war dabei die Einführung von Carboran-Clustern um neuartiger Hybridmaterialien mit Mutlifunktionseigenschaften zu entwickeln welche in verschiedensten Gebieten Anwendung finden können. Die Entwicklung hitzestabiler Polymere ohne jegliche Additive ist eine der Herausforderungen für die Verbesserung feuerresistenter Polymere hin zu neuen technologischen Anwendungen. Synergieeffekte von Phosphor- und Carboran-Einheiten verbessern hierbei die thermischen Eigenschaften. Die Photolyse sowie Photodimerization der Anthracen-Einheiten heben darüber hinaus die Verbesserung dieser Stimuli-risponsiven Polymere heraus

Im ersten Teil dieser Arbeit wird die Synthese eines Silyl-geschützten Imidocarborans und eines phosphorhaltigen Monomers beschrieben sowie ihre Ringöffnungs-Metathese-polymerisation (ROMP) und die Untersuchung der entsprechenden Hitzestabiltitätseigenschaften. Die Spaltung des Phosphonatesters im Rückgrat des Copolymers führte zur Bildung von Phosphonsäure-Einheiten welche für das Coating der Eisenoxid-Nanopartikel verwendet wurde. Darüber hinaus werden potenzielle Anwendungen einzelner Verbindungen herausgestellt, insbesondere jener welche Bor und Phosphor enthalten. Zu diesem Zweck wurden die Hitzestabilität von sowohl Bor-

als auch Phosphorgruppe mittels Thermogravimetrie (TGA) und Mikro-Verbrennungs-Kalorimetrie (MCC) untersucht. Die Einkapselung der Eisenoxid-Nanopartikel mit Carboran-Clustern ist eine potenzielle Anwendung für die magneitsch-induzierte gerichtete Diagnose und Behandlung von Krebs mit Bor-Neutronen-Einfang-Therapie.

Der zweite Teil befasst sich mit den Carboran-Phosphor-basierten Kondensationspolymeren welche eine endständige Hydroxylgruppe aufweisen. Des Weiteren wurden die Carboran-Phosphor-Oligomere mit terminalen Hydroxylgruppen mit der käuflich erwerblichen Epoxy-Resin-Formel als Härter mit verschiedenen Massenbeladungen getestet. Die thermischen Eigenschaften sowie Härtungsraten wurden dabei mittels TGA, MCC sowie DSC (differential scanning calorimetry) untersucht. Hierbei wird der Vorteil der vorhandenen Phosphor- und Carboran-Gruppen beschrieben.

Im dritten und letzten Teil der Arbeit wird die Copolymerisation von Carboran- und Anthracen-Einheite beschrieben. Dabei wurden Polymere mit verschiedenen Zusammensetzungen der entsprechenden Einheiten erhalten und charakterisiert. Ihre strukturellen sowie thermischen Eigenschaften wurden daraufhin evaluiert und mit literaturbekannten Verbindungen verglichen. Dabei wird der Effekt der Einführung der Silylcarboran- und Anthraceneinheiten auf die thermischen Eigenschaften beschrieben. Des Weiteren wurde das photoschaltbare verhalten der Anthracen-Einheiten untersucht um “smart materials” zu erhalten.

Alle Monomer- und Polymerstrukturen wurden charaktisiert durch NMR-Spektroskopie (^{1}H-, ^{13}C-, ^{31}P-, ^{11}B-NMR), FTIR-Spektroskopie sowie Gel-Permeations-Chromatographie (GPC). Die Morphologien der Lösungen und Oberflächen wurde untersucht mittels Transmissionselektronenmikroskopie (TEM). Die Effiktivität der Eisen-Nanopartikel-Beladung wurde evaluiert anhand von Messungen mit Massenspektrometrie mit induktiv gekoppeltem Plasma (ICP-MS). Die Photolyse sowie Photodimerisation wurden untersucht durch UV/VIS-Spektroskopie.

Stichwörter: ROMP (Ringöffnungs-Metathese-polymerisation), Carborane, Phosphonate, Anthracen, Hitzestabilität, Amphiphile Blockcopolymer

CHAPTER 1

INTRODUCTION

1.1 Literature Review

One of the most challenging jobs in materials science is that of building nanostructures, whose shape and dimension are formed in a controlled way. There is a special interest in amphiphilic block copolymers thanks to their capability to self-assemble on the nanoscale. There are many potential applications of amphiphilic block copolymers forming micelles, such as biosensors [1], gene therapy [2] and drug delivery [3]. Ring-opening metathesis polymerization (ROMP) is a specific method to synthesize monodisperse block copolymers using ruthenium-based catalysts. In the literature, numerous block copolymers, having both hydrophilic and hydrophobic units obtained via the ROMP method, have been examined and utilized to assemble into micelles [4], [5], [6], [7], [8], [9], [10], [11], [12], [13] or as drug delivery materials [14]. The carborane-based block copolymers with amphiphilic nature, which are able to form micelles in aqueous media with average hydrodynamic radius of 41 nm, have been developed before [15]. It is known that these copolymers exploit the hydrophobicity of carboranes. One approach to make amphiphilic polymers is to add hydrophilic groups such as phosphoric acids to the backbone, e.g. phosphoric acid-type amphiphilic block copolymers can be synthesized via ROMP using 3rd generation Grubbs catalyst, with a broad range of micelle dimensions, depending on the block copolymer composition [16]. The phosphonates and phosphoric acid-derived anions can also be used as surface modifiers for metals and their oxides [17], e.g. iron oxide nanoparticle surfaces have successfully been coated with phosphoric acid-containing compounds [18]. In this regard, the surface modification of magnetic nanoparticles with polymers bearing phosphoric acid has not been widely investigated.

Carboranes, which are also called “carbaboranes”, are clusters with some particular electronic and thermal properties as aromatic molecules. Icosahedral carboranes are carbon–boron molecular clusters, featuring a fully delocalized system of 26 skeletal electrons via 3c–2e bonding between tangential p orbitals and radial sp orbitals [19], [20]. Such clusters are aromatic molecules having 3-D aromaticity (σ aromaticity) [21], which are different from classical 2-D aromatic molecules such as benzenes (π aromaticity) [22]. On the other hand, both classes of molecules share some common features such as thermal stability and ability to undergo electrophilic substitution reactions [23], [24], [25]. They include both boron and carbon atoms in the polyhedral form. Among others, icosahedral carborane isomers have two carbon, ten boron and twelve hydrogen atoms ($C_2B_{10}H_{12}$) in skeletal cage structure, which have very stable molecular architectures. Isomers of carboranes can be converted into one another, e.g. 1,7-$C_2B_{10}H_{12}$ (*m*-carborane), can be obtained via heat treatment of 1,2-$C_2B_{10}H_{12}$ (*o*-carborane) at 400 to 500 °C, and 1,12-$C_2B_{10}H_{12}$ (*p*-carborane) after heating at 700 °C. Figure 1.1 shows icosahedral carborane isomers *ortho* (*o*-), *meta* (*m*-) and *para* (*p*-). The numbering of the atoms in carborane compounds begins with the apex atom of lowest coordination, and polyhedral vertex atoms are numbered in a clockwise direction with the carbon atoms being given the lowest possible numbers.

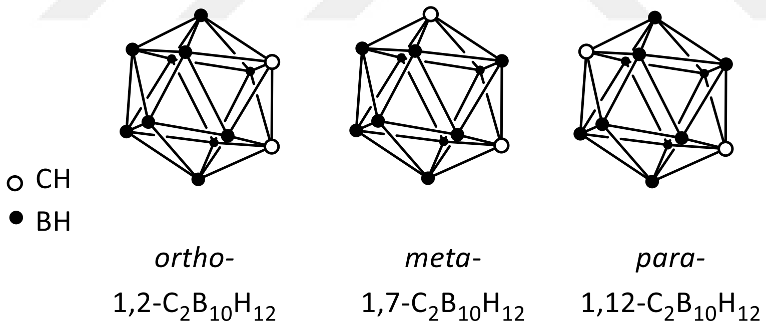

Figure 1.1 Icosahedral carborane isomers *ortho* (*o*-), *meta* (*m*-), *para* (*p*-) [26]

The growing interest in the properties of carboranes with high versatility, unique electronic properties and cage structure provides an opportunity to widen research across new applications. By an electron-counting scheme, thermodynamically stable structures of the cage can be estimated, while isomer stability is far from being predictable [27], [28]. Icosahedral $C_2B_{10}H_{12}$ can have extremely stable isomers according to early studies, for example, the stability of 1,7-$C_2B_{10}H_{12}$ is higher than 1,2-$C_2B_{10}H_{12}$ because of the rearrangement of the cage after heat treatment [27], [28]. Since the late 1950s, the $C_2B_{10}H_{12}$ isomers have been investigated not only theoretically but also experimentally, generating a vast literature that is just partially represented in a large number of compounds. Although their icosahedral geometry is not remarkable anymore, this geometry was quite impressive and novel at the time of discovery. This icosahedral system is highly stable due to the electro-delocalization of the cluster which consists of ten boron and two adjacent carbon atoms. Since 1,2-$C_2B_{10}H_{12}$ and its derivatives have the icosahedral cage structure, they are significantly stable against degradation under a broad range of conditions, such as strong acids and oxidative compounds [29], [30]. Carboranes have unique properties such as thermal resistivity [31], [32], neutron capture ability [33], [34], [35] and chemical stability [31], [32]. Furthermore, it has been shown that carborane-containing polymers have extreme thermo-oxidative durability in comparison with polymers without carborane cages in the backbone [36]. This can prove the significance of boron clusters for high temperature polymer applications. As an example for this concept, poly(carborane-siloxane-aryl acetylene) (PCSAA) isomers with *meta*- and *para*-Carborane, which are durable at high temperatures and under harsh oxidative conditions, have been synthesized by Kolel-Veetil et al. (Figure 1.2).

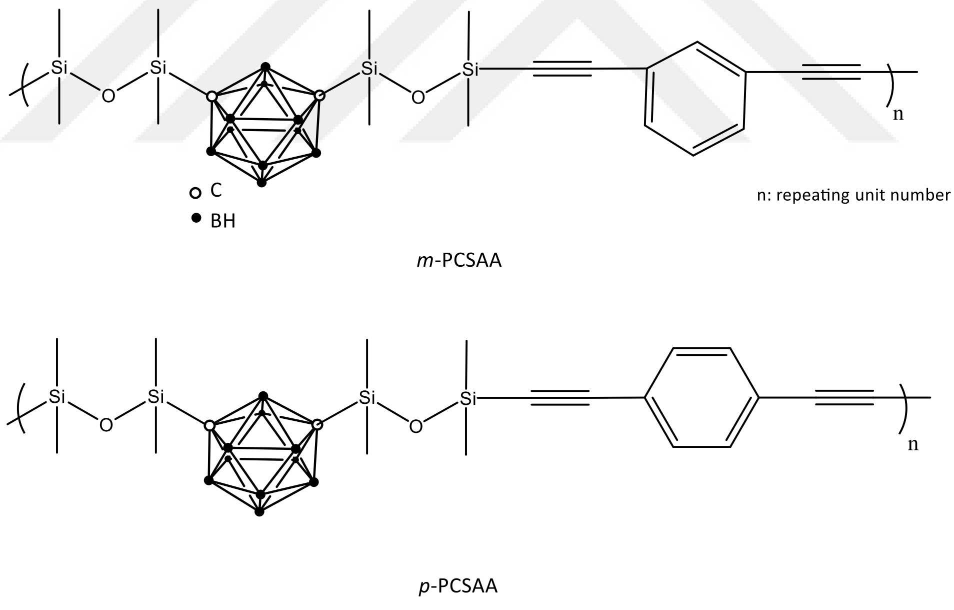

Figure 1.2 Aromatic group-containing carboranylenesiloxanes; poly(*m*-carborane-siloxane-arylacetylene) (*m*-PCSAA) and *p*-PCSAA

The carborane-based polymers do not show any weight losses at high temperatures. On the contrary, some amount of weight gain in air has been observed, which can be explained with the oxidation of boron to B_2O_3 and silicon to SiO_2 in the polymer chain [37]. The carborane-based polymers can be employed to prevent the oxidation of carbon fibres. The linear carborane-carbosilane-phenylacetylene copolymers were also used to develop thermoset systems [38]. As a result of the thermal stabilization in a temperature range from 600 to 900 °C in air, the ceramic-coated carbon fibres keep the weight stable in comparison to uncoated fibres.

For many years, scientists have predominantly centered research interests related to carboranes on the boron neutron capture therapy (BNCT) for cancer treatment in medical applications in which the unique character of the ^{10}B nucleus plays a significant role. This isotope (^{10}B) is nonradioactive and presents approximately 20 % of total boron in nature. As it is represented in Figure 1.3, α particles are generated by thermal irradiation of ^{10}B, and the cells are destroyed in parallel with the increasing energy [39]. Although, the activity of carborane derivatives in BNCT has been widely studied, carborane-based polymers are still in need to be deeply investigated for their medical application due to their promising properties in this field.

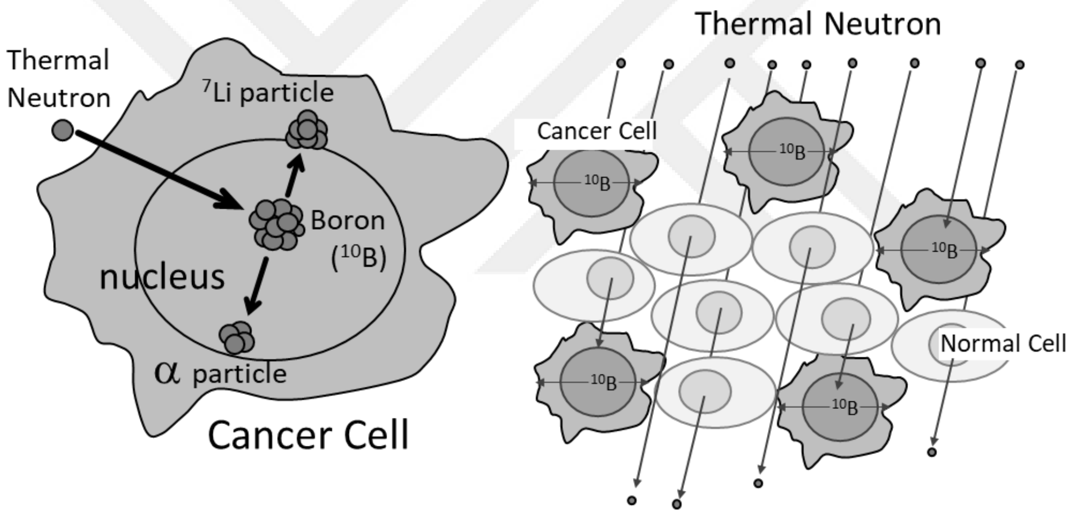

Figure 1.3 BNCT mechanism

Phosphorus, which was discovered by Hennig Brand in 1669, can be found as either white, black, red or violet phosphorus (among other forms), however, it does not exist as a pure element in nature due to its high reactivity. In place of this, phosphorus-containing minerals are mostly found in their maximally oxidized state, as in inorganic phosphate rocks. Phosphonates and phosphoric acids account for organophosphorus molecules. Their molecular formulas are respectively $R'PO(OH)_2$ and $R'PO(OR)_2$, here R and R' represent alkyl and/or aryl groups. In general alcohols and water can dissolve both phosphonate salts and phosphoric acids, whereas non-volatile forms are hardly soluble in organic solvents. Phosphonates are considered as herbicides in some important commercial applications such as plant regulation [40].

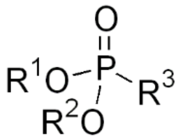

Figure 1.4 General ester of phosphoric acid

Phosphorus-containing flame retardant materials have been a wide interest in the field of polymeric materials for decades [41]. Many of the phosphorus compounds such as phosphonates, phosphine oxides, red phosphorus, phosphines and phosphates have a possible usage in heat resistant applications [40], [42], [43]. These flame retardants can be used as either additives or in the backbone of the polymer structure. The flame retardants that consist of phosphorus and its derivatives can be active both in condensed and gas phase [44]. In most of the reactions of phosphorus-containing flame retardants, phosphoric acid can be observed as a final product through thermal decomposition [45]. Phosphoric acid and phosphonate-based flame retardant polymers provide a remarkable char residue that can be determined by thermogravimetric analysis (TGA), especially phosphoric acid ones produce even higher amount of char than ester-based forms depending on the percentage of phosphorus in the polymer backbone [46].

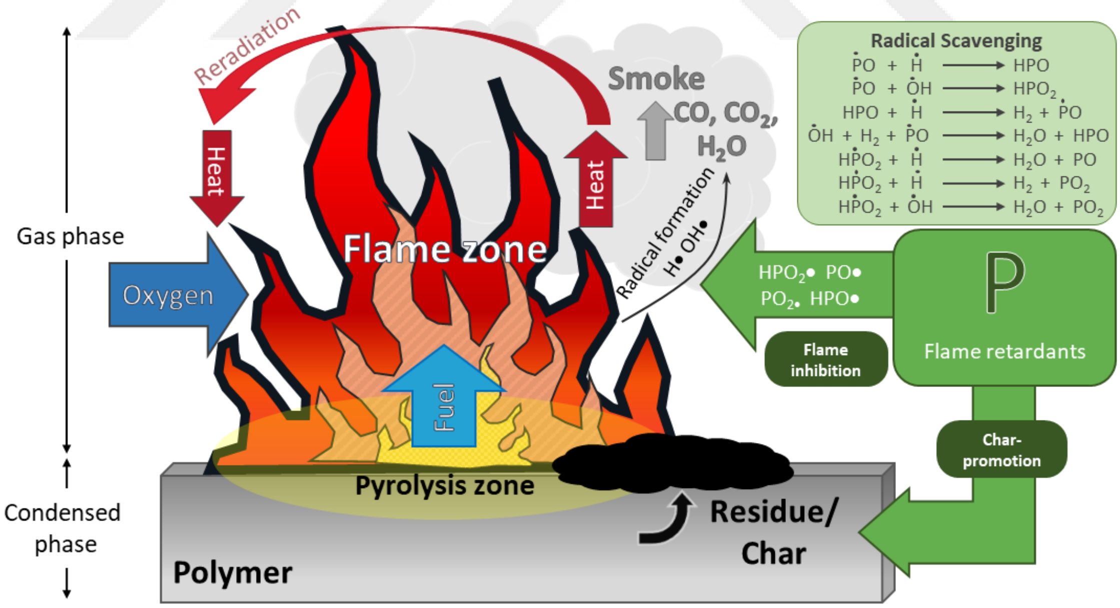

Figure 1.5 Fire behavior of a polymeric material and the role of phosphorus-containing heat resistants [46]

Pyrolysis and the behavior of the phosphorus-based flame retardants is shown in Figure 1.5. The mechanism of flame retardants in gas and condensed phase can be clearly observed. The decomposition temperature of fire resistant (FR) and the polymer matrix is highly critical for these mechanisms. It is important to have a high similarity of decomposition temperature of both the fire resistant and the polymer. FR should not decompose at low temperature to guarantee chemical interaction during pyrolysis. The decomposition property is even more critical for the high temperature thermoplastic processes such as compounding, extrusion, injection or blow molding, as well as vulcanization for rubbers, or curing thermosets. In addition to thermal stability, FR can be exposed to additional stress depending on the application area, e.g. FR must be stable during spinning, weaving and washing in fiber and textile industry [46].

Phosphoric acid-based polymers can be used as flame retardant additives in a polymer matrix for a wide variety of applications [47]. For example, 4,4'-bishydroxydeoxybenzoin-poly(arylate-*co*-phosphonate) BHDB-PAL-*co*-PPN) polymers and corresponding copolymers (PAL-*co*-PPN) were synthesized by Ranganathan and co-workers through polycondensation reaction in solution (Scheme 1.1). Thermal durability of the compounds in this study was investigated by PCFC (Pyrolysis Combustion Flow Calorimeter) test and TGA (Table 1.1) [48]. This study demonstrated that the HRC (Heat Release Capacity) of PAL-*co*-PPN copolymers was surprisingly lower than the corresponding homopolymers, e.g. the HRC of 1:1 (molar ratio) arylate- and phosphonate-containing copolymer was 36 J/(g·K), while the HRC of acrylate-based homopolymer and phosphonate-based homopolymer was 65 J/(g·K) and 81 J/(g·K), respectively. On the other hand, the copolymers showed higher char residue at 800 °C than each of the homopolymers. It was observed that the phosphorus functionality in PAL-*co*-PPN copolymers had an influence on both flammability and thermal durability of the polymers.

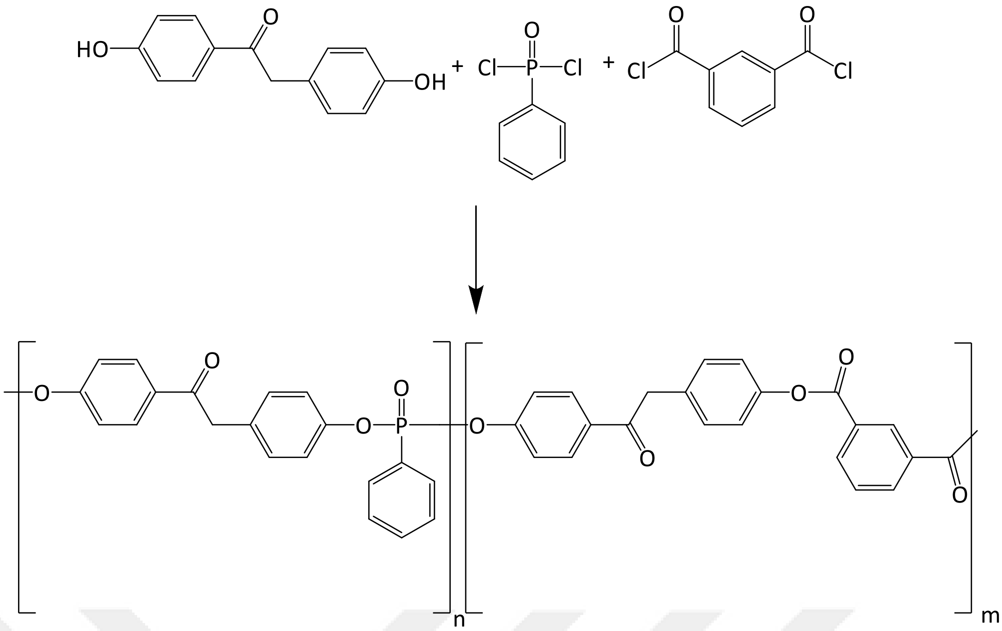

Scheme 1.1 Synthetic route of BHDB-poly(arylate-*co*-phosphonate) (PAL-*co*-PPN)[44]

Table 1.1 Flammability and thermal stability characterization of BHDB-poly (arylate-*co*-phosphonate) copolymers [44]

iPC:PPC (molar ratio)	Heat release capacity (J/(g·K))	5 wt% loss temperature (°C)	Char yield at 800 °C (wt%)
100:0	65±5	340	45
77:23	48±4	346	50
57:43	41±3	383	56
46:54	36±2	367	54
39:61	40±3	390	57
23:77	59±5	394	55
0:100	81±11	397	52

Another example of these polymers was reported by Wang and coworkers [49]. They synthesized a new aryl-phosphonate derivative from poly(sulfonyldiphenylene thiophenylphosphonate) (PSTPP) to investigate their flame-retardant effect on polyethylene terephthalate (PET) (Figure 1.6). The flame-retardant performance was negatively affected by substituting oxygen with sulfur, while an enhanced anti-dripping behavior was observed. In conclusion, they found that 2.5 wt% flame retardant addition to PET was enough to determine its fire-resistant effect.

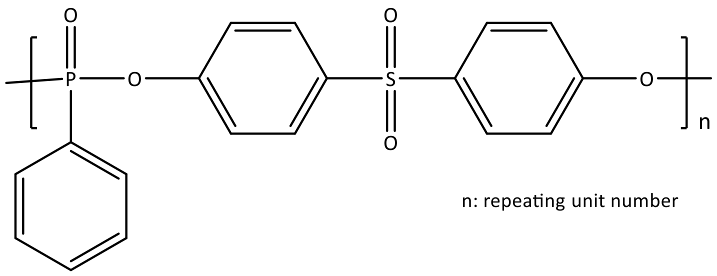

Figure 1.6 Chemical structure of poly(sulfonyldiphenylene thiophenylphosphonate) (PSTPP)

In addition to their flame-retardant applications, phosphoric acid-based polymers can also be used in various biomaterials, due to their capability of adhesion on bones and dentins [50], [51], [52]. However, biocompatibility of these polymers is crucial for dental applications. In this context, the combination of acrylic acid monomers and phosphoric acids allows to form a biocompatible polymer, that can adhere to the teeth, via generation of calcium phosphonates [53], [54], [55].

Furthermore, phosphoric acids are known as considerably efficient chelating agents for coating iron oxide nanoparticles [56]. Iron has been the most important metal in industry so far, and is the most abundant transition metal. The best-known iron oxides include FeO, Fe_2O_3 and Fe_3O_4. Natural mineral magnetite Fe_3O_4 includes some impurities such as α-Fe_2O_3. Moreover, a pure phase of Fe_3O_4 nanoparticles has been recently synthesized following various approaches. For instance, Alcala et al. have shown that the prolonged hydrothermal synthesis of iron nanoparticles (Fe_3O_4) reduces the α-Fe_2O_3 ratio. Zhang et al. employed heat treatment at 650 °C to form pure iron nanoparticles of Fe_3O_4 with 48 nm in diameter [57], [58]. The crystal structure of Fe_3O_4 generally contains octahedral and mixed octahedral/tetrahedral layers in the (111) direction; the tetrahedral sites are occupied by Fe(III), and the octahedral sites are occupied by both Fe(II) and Fe(III) [59], [60]. The studies on Fe_3O_4 have been continuously carried out in this regard, due to its superparamagnetism, low Curie temperature and coercivity of magnetism [61], [62], [63]. In recent years, many researchers have been working on the medical applications of iron nanoparticles, e.g. as *in vitro* diagnostic agents [61], [63].

Iron-based nanoparticles have been subject to intense research due to their distinguished properties such as catalytic performances, anti-microbial activities and magnetism [64], [65]. Iron oxide magnetic nanoparticles (Fe_3O_4-MNPs) with approximate size of 20–30 nm, can be magnetized by an external magnet; thus, they have been broadly used in varying bio-applications e.g. magnetic resonance imaging (MRI), drug delivery and magneto-thermal therapy [66]. Transmission electron microscopy (TEM) has extensively been used as a characterization tool to determine the size, morphology and size distribution of nanoparticles. By using this technique, Yang et al. have revealed that pure Fe_3O_4-MNPs are prone to aggregate and their sizes can be manipulated by grafting poly(GMA-MATAC) to the nanoparticles' surface [67]. Also noteworthy are the superparamagnetic nanoparticles modified via graft polymerization of glycidyl methacrylate (GMA) and methacryloxyethyl-trimethylammonium chloride (MATAC), used for immobilization of the lipase enzyme [68].

Price et al. have recently reported a series of Fe_3O_4-MNPs-functionalized with an amphiphilic polymer PEG600-*alt*-PTHF650 (PEG and PTHF refer to poly(ethylene glycol) and poly(tetrahydrofuran), respectively). They have demonstrated that magnetic nanoparticle clusters exhibit remarkable MRI performance and uptake/release performance within cell membranes, that is, they can be used for magnetically directed drug delivery applications [69].

Vanessa et al. have carried out a modification of multicore iron nanoparticles by coating with poly(4-vinylpyridine) polyethylenglycol copolymer. It has been clearly shown that a negative contrast of MR imaging in kidneys may occur because of the high PEG content in the copolymer coated iron oxide nanoparticles [70].

In order to modify the copolymer-coated nanoparticles, several conventional polymerization methods have been applied in the literature. These polymerization techniques have been also successfully used to obtain carborane- or phosphorus-containing polymers, as mentioned above. However, various significant controlled-polymerization techniques are getting more popular because of the increasing demand of customized polymer structures. Some of these controlled-polymerization methods are: atom transfer radical polymerization (ATRP) [71], nitroxide-mediated polymerization (NMP) [72], reversible addition-fragmentation chain transfer (RAFT) [73], [74] and ring-opening metathesis polymerization (ROMP) [75]. In order to functionalize linear polymers, there are several synthetic methods in the literature such as anionic, cationic and free radical polymerization of vinyl groups and group transfer polymerization techniques [76], [77], [78]. The ROMP method is straightforward and has become increasingly more popular, because it allows the controlled synthesis of polymers and copolymers, having various functionalities [79], [80]. This polymerization technique is a well-known reaction, which produces stereoregular polymers from cyclic olefins via [2+2] cycloaddition reaction (Scheme 1.2). The metallacyclobutane intermediate, which is crucial for the following steps, is formed in the propagation step of ROMP, followed by formation of a new double bond [75].

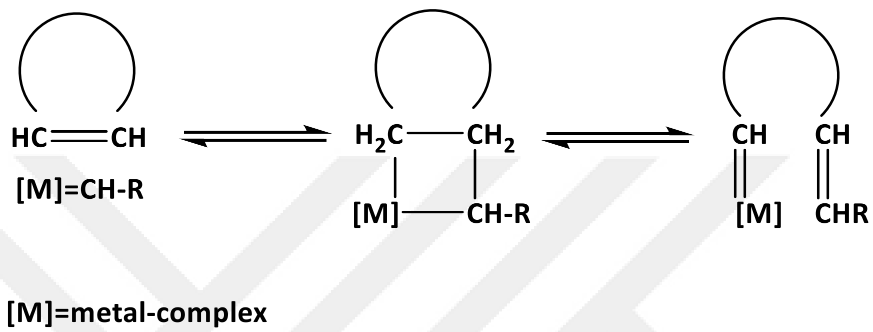

Scheme 1.2 The mechanism of ROMP including the metallacyclobutane intermediate

The selection of monomers is quite important for the synthesis of functional polymers, which can be linearly synthesized from cyclobutene and cyclooctene derivatives. In general, the control of regioregularity of the polymer backbone is not trivial [81], [82]. It is difficult to polymerize 5-, 6-, and 7-membered substituted cyclic alkenes via ROMP because of their reduced ring strain [83]. The reduced ring strain of cyclic olefin monomers (cyclopentene and norbornene) is essential in the polymerization [77]. Both monomer concentration and reaction temperature are intimately associated with the thermodynamics of ROMP [84], [85], [86]. The fundamental thermodynamic equation is:

$$\Delta G = \Delta H - T\Delta S$$

Each cyclic olefin monomer has a critical monomer concentration for the polymerization. The reaction cannot occur at a given temperature, in case the monomer concentration is less than the critical concentration. Table 1.2 indicates the thermodynamic parameters for the cyclic monomers.

Table 1.2 Thermodynamic parameters for the ROMP of a selection of liquid monomers to amorphous polymers at 25°C [87]

Monomer	Configuration of the double bond in the polymer	ΔH°/(kJ/mol)	ΔS°/(J/mol·K)	ΔG°/(kJ/mol)
Cyclopentene	*cis*	−15.4	−52	−0.3
	trans	−18	−52	−2.3
Cyclohexene	*cis*	−1−3	−31	6.2
	trans	1−3	−28	7.3
Cycloheptene	*cis*	−16	−20	−10.0
	trans	−20	−17	−15.0
Cyclooctene	*cis*	−20	−2	−19.4
	trans	−22	−2	−21.5
1,5-Cyclooctadiene	*cis*	−25	−5	−23.5
	trans	−33	−5	−31.5

High molecular weight polymers can be obtained via ROMP at low temperatures, and the catalyst provides high efficiency at low temperatures. These ruthenium-based catalysts shown in Figure 1.7, show less tolerance towards polar groups [77], [78], [80], [81], [84], [85], [88].

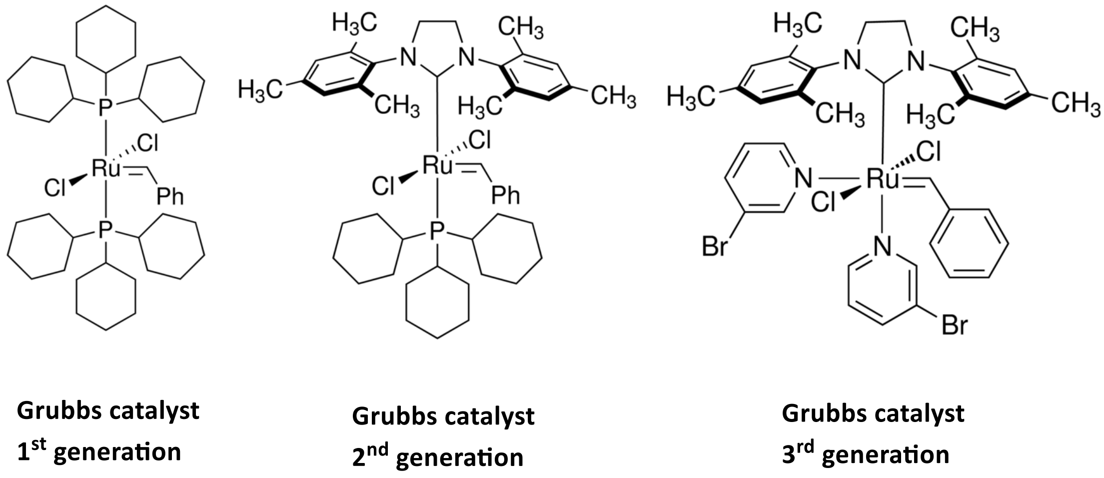

Figure 1.7 Ruthenium olefin metathesis catalysts [89]

The discovery and studies of such catalytic systems have resulted in the award of the Nobel Prize to Schrock, Grubbs and Chauvin in 2005 [89], [90], [91]. In the literature, the ROMP method has been used by many researchers, for example Yang et al. synthesized a novel shape memory polynorbornene-based polymer using this technique. Shape memory materials can "memorize" their previous form when subjected to certain stimuli such as thermomechanical or magnetic variations [92]. Polynorbornene has been functionalized with poly(ε-caprolactone) side chains and cyano groups via ROMP [93].

Random copolymers that contain phosphorus and anthracene have been synthesized via ROMP by Ecem et al., and these polymers are assumed to demonstrate shape memory effect due to the photo switchable property of anthracene units in their backbone [94]. Vernon proposed the term "shape–memory" first in 1941. However, after the use of cross-linked polyethylene (PE) for making heat-shrinkable tubes and films, the importance of shape memory polymers (SMPs) was realized in the 1960s. In the late 1980s, there were more efforts to develop SMPs. Then, these efforts speeded up in the 1990s and important improvements have been done in the past decade. Figure 1.8 indicates the shape memory behaviour of one of the PVDF (polyvinylidene fluoride) polymers under the influence of heat.

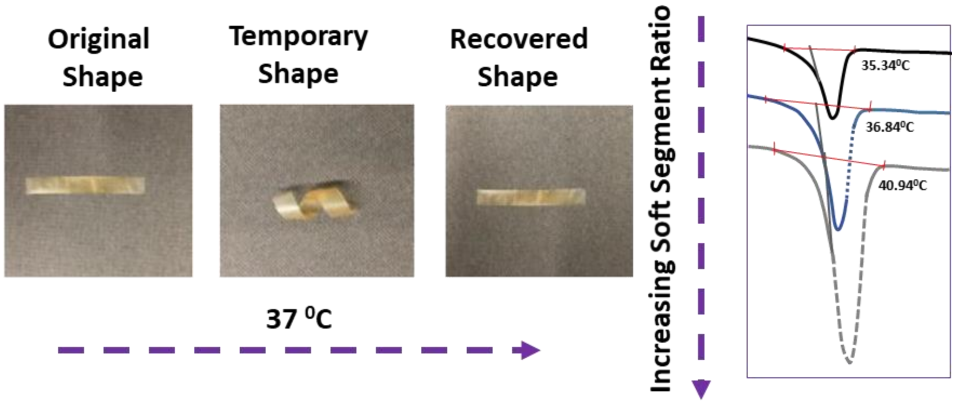

Figure 1.8 Shape memory properties via thermal relaxation [95]

SMPs are an important class of stimuli-responsive polymers with applications covering various fields of daily life [96], [97]. Smart fabrics, heat shrinkable tubes for electronics or films for packaging, intelligent medical devices or implants with minimally invasive surgery are examples for the application areas. Besides, applications of substrates for cell growth, biomedical devices such as stents and catheters, optically active materials, and flexible electronics demonstrate potential of shape-memory technology. Some typical commercially available examples are polyurethane (DIAPLEX, SMP Technologies Inc., originally from Mitsubishi Heavy Industries), polystyrene based SMP (Veriflex, Verilyte, Veritex, Cornerstone Research Group, Inc.), aliphatic polyurethane (tecoflex, Lubrizol Advanced Materials), epoxy-based SMP (TEMBO, Composite Technology Development, Inc.), and UV-curable polyurethane (NOA-63, Norland Products Inc.). Furthermore, SMPs somehow keep the given shape in their memory, and even after several successive deformations, they return to their former shape [96], [97]. A good definition of the possible shape memory mechanism is given by several reviews, moreover quite comprehensive classifications of such materials can be found in the literature [98], [99], [100], [101].

Even though most of the reported SMPs are thermally-induced shape memory polymers, there can be other paths to stimulate the shape memory effect. For example, light allows the materials to be activated remotely even at ambient temperature, and there have been several reports regarding this topic. Coupled with the placement of photosensitive groups in the polymer backbone, the transfer of movement from molecular to macroscopic level is necessary for the control of macromolecular architecture [96]. It is well-known that photoactive SMPs are based on reversible photochemical crosslinking. Photo-induced reversible covalent cross-linking in polymers can be formed by some photo-chemically reactive groups. Cinnamylidene acetic acid, anthracene, coumarin and their derivatives account for the species that are capable of photo-dimerization, and have been comprehensively investigated by adding to polymer structures for photo-switchable shape memory [102], [103], [104], [105]. Photo-reactive moieties exist in the dimer form with their inter-chain dimerization responsible for chain crosslinking, as photosensitive groups are used as crosslinkers in polymer networks. Anthracene has the ability to undergo a typical [4πs + 4πs] photo-dimerization reaction and is photo and thermally reversible. The typical photo-dimerization reaction of anthracene occurs favorably under UV light irradiations and can be employed for application in photo-responsive materials [106]. The dimers dissociate upon exposure to heat or light of less than 300 nm (E_a=111–160 kJ/mol) (Figure 1.9).

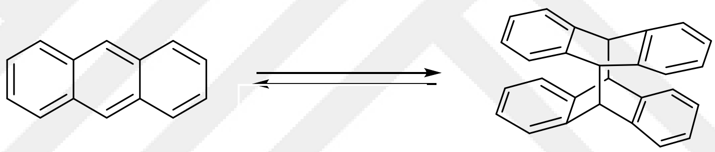

Figure 1.9 Conversion between anthracene and its dimer [107]

An interesting example of the application of anthracene photo-dimerization has been reported recently by Berda and coworkers [106]. They synthesized anthracene-based polymers and observed that the obtained polymers displayed photo-switch behavior (Figure 1.10) under UV light which was quenched at ≈ 350 nm. In that study, the photo-dimerization of pendant anthracene units as an effective intramolecular cross-linking feature was noted. On the other hand, photo dimers can be reversed if irradiated with light at $\lambda < 300$ nm, or if heated at temperatures greater than 180 °C [108], [109].

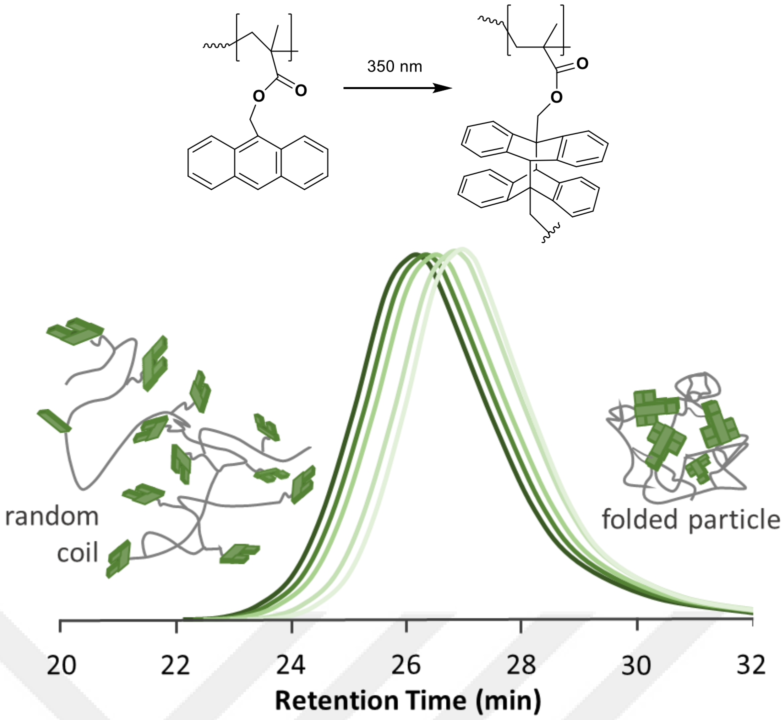

Figure 1.10 Observed photo-switch behavior of anthracene-based polymer [106]

Manufacturing flexible films that can be used in display devices, is of growing interest [110]. Generally, flexible films do not possess high mechanical stability, because of aggregation quenching in the solid state. It is reported in the literature that carborane-based luminescent molecules are used in optical materials to improve solid-state emissive properties of the materials [111]. Anthracene has unique properties, such as [4+4] photocycloadditions, and has been used in many varied application fields [88], [106]. Anthracene groups also have capabilities in energy and charge transfer, as well as photoswitchable effects, that can be applied in the synthesis of stimuli-responsive materials. Recent articles discuss the luminescence properties of anthracene- and carborane-containing molecules [112], including intramolecular charge transfer processes between the anthracene moiety and the carborane cluster in the crystalline state.

1.2 Objective of the Thesis

The interest on the hybrid materials consisting of both organic and inorganic parts have been increasing with each passing day. As examples of such hybrid materials, natural structures such as bone, crustacean shells and tooth tissues can be given. By controlled mimicking of hybrid biosystems, it can be designed and developed that novel and innovative polymeric materials that are intended to employ in industrial applications [1]. Preperation of nanoscale smart materials has been possible thanks to the self-organizing ability of specificly synthesized block copolymers [2], [3], [10], [12]. Recently, functional block copolymers including both hydrophilic and hydrophobic segments can form miscelles in certain solvents [6], [7], [11], [13]. The materials developed in this way can be applied in wide range of applications such as lithography, stabilization of magnetic nanoparticle, drug delivery and seperation systems [4], [5], [6], [7], [8], [9], [10], [11], [13], [14]. Controlled and living polymerization techniques allow to synthesize specially designed polymeric materials that have adjustable in polydispersity and molecular weight by demand. One of the well-known common tecniques among living polymerization methods is ring opening metathesis polymerization (ROMP) that can be used for well-defined block copolymer synthesis [113], [114]. ROMP provides oppurtunity to control polymer chain distribition precisizely and consequently obtained polymeric system can organize self-assembly by which it can be switching according to the hydrophilicity and hydrophobicity of the media [4], [16], [115], [116], [117]. As an example, researches on stimuli-responsive self-assembly structures (particularly pH-dependent) and its complex systems with metal ions (e.g. Cu(II) and Fe(II)) in the network have been studied [118].

Here, we used the synthetic approach phosphorus-carborane containing polymers and investigate their potential chelation efficiencies aginst iron nanoparticles and heat resistance properties. Synergistic effect of phosphorus and carborane functionality in air and under nitrogen atmosphere were studied. Besides that carborane-anthrecene bearing polymers were also synthesized and investigated their photo-switchable properties. Using controlled polymerization techniques enable to investigate the structure-property relationship of carborane-phosphorus and carborane-anthracene functional polymers. Carborane-phosphonate functional group possesing oligomers derived from condensation type polymers also used in epoxy resin formulation to increase thermo-mechanical properties.

1.3 Hypothesis

Developing inorganic-organic cluster is one of the main targeting approach for the mimic the nature. Block copolymers, two or more polymer segments covalently connected to each other, are one of the typical synthetic approach for the self-assemble of the macromolecules in nanoscale in solution as well as on the solid surface. There are many polymerization techniques are available to synthesize the block copolymers featuring narrow molecular weight distributions with controllable molecular weights and defined constitution. Anionic polymerization, ATRP, RAFT and nitroxide mediated polymerization techniques are typical examples for the living polymerization techniques and used for the synthesis of block copolymers. Ring opening metathesis polymerization (ROMP) is one of the living polymerization techniques and can be applied for the preparation of well-defined block copolymers as well. For a typical ROMP, initiation rates exceed propagation rates with the proper metathesis catalyst making the formation of polymers with a low polydispersity possible [113], [114]. Exploiting the precise control over the polymer chains, as offered by ROMP, obtained block copolymers can undergo self-assembly. Moreover, if functional moieties were incorporated into the block copolymer structure, reversible – and also block-selective - switching capabilities between hydrophobic and hydrophilic states are accessible [4], [16], [115], [116], [117]. Here, in the first part of this study we used the synthetic scheme for block copolymer synthesis of carborane functional block and phosphonate and/or phosphonic acid functionality at the same backbone through ROMP mediated polymerization method. Self-assemble of the block copolymers were investigated in water and solid surface. Thermal properties and chelation efficinecies to the iron nanoparticles were evaluated.

Today, halogenated compounds are predominantly preferred in flame retardant indsutry. Polybrominated diphenyl ethers (PBDEs) have mostly been consumed in plastic industry during early time of flame retardants until the European Court of Justice banned them, which pentaBDE together with octaBDE and decaBDE are banned in 2004 and 2008, respectively. DecaBDE can only be used in North America in mattress and furniture upholstery with the obligation of being sold in that state. Novel flame retardants are needed to develop because of that health issues, and growing interest for studies for new polymers exhibiting flame retardancy behaviour without using any additives will be important. At present the most promising use for the various carboranes and phosphorus functionalities is to incorporate them into polymers with the objective of building into the polymers special properties such as high temperature resistance and/or specialized chemical resistance. Copolymers possessing different carborane and phosphorus groups were synthesized and furthermore used to investigate the structure-thermal properties of the polymers. Potential application of carborane-phosphorus bearing polymers was also investigated in the epoxy formulations. In this part of the study, new phospho-boron containing oligomers synthesized via condensation of carborane diol and dichlorophosphine oxide to end up with hydroxyl terminated oligoester. Carborane-phosphorus functional oligomer was further used in epoxy formulation. Hence, the dual flame retardancy effect of boron and phosphorous group is investigated under air and nitrogen atmosphere using TGA and MCC analysis.

Final chapter of the thesis is to obtain well defined architecture bearing different loading antracene and carborane units at the backbone. Photo switching properties of block copolymers were investigated via anthracene functional groups concentrations at the polymer backbone. Aim of the study is to obtain stimuli responsive materials via light induce through anthracene groups.

CHAPTER 2

EXPERIMENTAL

2.1 Instruments and Chemicals

^{1}H NMR, ^{13}C NMR, ^{11}B {^{1}H} NMR and ^{31}P{^{1}H} NMR spectra were recorded using a Bruker Avance III 400 MHz spectrometer. GPC analyses were performed against polymethylmethacrylat (PMMA) with column at 50 °C. 0.01 M LiBr/DMF were used for the mobile phase and toluene was used for flow marker. Flow rate was 0.7 mL/min. A PerkinElmer Spectrum One spectrometer was used for attenuated total reflectance Fourier transform infrared (ATR-FTIR) spectroscopy. Microscale combustion calorimetry (MCC, Fire Testing Technology, UK) was used for the MCC measurement according to ASTM D7309. Size analysis of polymer-coated nanoparticles in their dry form was conducted by evaporating a drop of an aqueous solution of nanoparticles on a holey carbon film coated 300 mesh Cu grid (Pacific Grid Tech, USA). Images were acquired using transition electron microscopy (TEM) with an accelerating voltage of 5 kV on a LVEM5 Electron Microscope (Delong Instruments, USA). SII Nanotechnology, TG/DTA 6300 Series was used for thermal analysis. The thermal stability of polymers was investigated between room temperature and 900 °C under nitrogen and air with a heating rate of 25 °C/min. Shmadzu UV-vis spectrophotometer was performed for photo studies.

Furan, maleimide, diethyl (hydroxy methyl) phosphonate, triphenylphosphine, diisopropyl azodicarboxylate (DIAD), trimethylene oxide, *n*-butyllithium solution (2.5 M in *n*-hexane), *tert*-butyldimethylsilyl chloride, 3-bromopyridine, potassium carbonate, bromo trimethylsilane, (2-bromoethyl) benzene, diethyl hydroxy methyl phosphonate, ethyl vinyl ether, tetrahydrofuran (THF), petroleum ether, diethyl ether, dichloromethane, and methanol were purchased from Sigma Aldrich and used as received. Ethyl acetate, THF and *n*-hexane were distilled by conventional techniques. Grubbs' second generation catalyst was purchased from Sigma Aldrich. Grubbs' third generation catalyst [(H_2-Imes)(3-Br-py)$_2$(Cl)$_2$Ru=CHPh] was freshly prepared according to the previously reported procedure [119]. Epoxy resin was supplied by Fasrverbundwerkstoffe (EPC, epoxy equivalent, 0.54). All other reagents including buffers and salts were obtained from Sigma Aldrich. *o*-Carborane was obtained from Katchem, Prague.

2.2 Synthesis of Monomers

2.2.1 Synthesis of 5-norbornene-2,3-dicarboxylic imide (oxanorbornene imide)

Furan and maleimid Diels-Alder reaction was adapted from literature [120]. Exo-10-oxa-4-azatricyclo[5.2.1.02,6]dec-8-ene-3,5-dione was obtained 78% yield as pure exo isomer. In 250 ml schlenk flask, 5.0 g (51.5 mmol) of maleimide was firstly dissolved in 50 mL of ethyl acetate and then 3.85 g (4.1 mL, 56.5 mmol) of furan was added into the reaction flask. The solution was stirred at 90 ^{o}C for overnight under nitrogen atmosphere. The reaction mixture was then washed with excess amount of diethyl ether. After all, the product was filtered, and dried under vacuum overnight. 100% exo isomer was obtained as a white powder. NMR datas of the compound matched the previously reported ones. ^{1}H NMR ($CDCl_3$): δ (ppm) = 8.12 (1H,s), 6.55 (2H, s), 5.34 (2H, s), 2.92 (2H, s).

2.2.2 Synthesis of phosphonate-oxanorbornen {3,5-dioxo-10-dioxa-4-azotricyclo[5.2.1.02,6]dec-8-en-4-ylmethyl)-phosphonic acid diethyl ester} (monomer 1)

The literature was used to synthesize Monomer 1 [16].

In 250ml two-necked round bottom flask oxanorbornene-imide (3.01 g, 13.2 mmol) is added with 30 ml dry THF and triphenylphospine (4.75 g, 18.1 mmol). After stirring for 10 minutes, diethyl (hydroxymethyl) phosphonate (2.8 mL, 19.0 mmol) was added and the reactants were stirred under N_2 at room temperature for 15 minutes, then diisopropyl azodicarboxylate (3.8 mL, 19.4 mmol) was put into the flask slowly by syringe in 30 minutes at 0^{o}C. The flask was covered with aluminum then flask was brought to room temperature, it was stirred for 2 nights under N_2. Then, petroleum ether was added and the mixture was precipitated. Column chromatography on silica gel by methanol/ haxane/ ethyl acetate (1:1:4) solvent mixture was used in order to obtain white crystalline solid product with an yield of 62 %. ^{1}H NMR ($CDCl_3$): δ (ppm) = 6.52 (s, 2H),5. 26 (s, 2H), 4.10–4.20 (m, 4H), 3.90 (d, 2 H, J=11Hz),2.91 (s, 2H),1.32 (t, 6 H, J=7 Hz, CH_3). ^{13}C{^{1}H} NMR ($CDCl_3$): δ (ppm) = 174.7 (C=O), 136.5 (C=C), 80.9(C-O), 62.9 an 62.8 (O-CH_2-CH_3-phosphonate), 47.5 [CH-C(=O)], 35.09 and 35.03 (d, CH_2P) 16.32 and16.24 (CH_3-phosphonate). ^{31}P{^{1}H} NMR ($CDCl_3$): δ (ppm) =18.51.IR (cm^{-1}): 703 (s), 725 (s), 807 (m), 835 (s), 881 (s), 955(s), 1007 (s), 1053 (m), 1094 (m), 1241 (s), 1319 (s), 1378(m), 1399 (s), 1699 (s), 1769 (w), 2985 (w). HRMS (EI)calcd. for $C_{13}H_{18}NO_6P$: 315.26 Found: 315.24 [16].

2.2.3 Synthesis of the [2-(*tert*-butyl-dimethyl-silanyl)-1,2-dicarba-*closo*-dodecaboran(12)-1-yl]-propan-1-ol (Monomer 2)

Monomer 2 was prepared according to the literature [121].

First step of the synthesis is to obtain 1-(tert-butyl-dimethylsilanyl)-1,2-dicarba-*closo*dodecaborane(12) (Compound **A)**. In a round-bottom 250 mL Schlenk flask capped with a rubber septum and equipped with a magnetic stir bar under an argon atmosphere, *o*-carborane (5g, 34.7 mmol, 1 eq) dissolved in 20 mL diethyl ether was deprotonated by dropwise addition of *n*-butyllithium (26 mL, *n*-BuLi 1.6 M, 41.7 mmol, 1.2 eq) at 0 °C. After 1 h, *tert*-butyldimethylsilyl (TBDMS) chloride (6.8 g, 45 mmol, 1.3 eq) in 10 mL diethyl ether was added. Then the stopcock was closed and the septum removed. A rubber septum-capped condenser was fitted on top of the reaction flask with a nitrogen overpressure. The stopcock was then opened and the solution was brought to reflux overnight. The solution was quenched with a few drops of methanol to avoid an exothermic reaction upon addition of 30 mL of water. The layers were separated in a separatory funnel and the aqueous solution was extracted with additional diethyl ether (3 x 30 mL). The combined extracts were dried over Na_2SO_4 and concentrated *in vacuo* to give silyl-*o*-carborane **A** as a white powder (88% yield). ^{1}H NMR ($CDCl_3$): δ (ppm) = 3.46 (s, 1H, CH), 1.04 (s, 9H, CCH_3), 0.25 (s, 6H, $SiCH_3$); ^{13}C{^{1}H} NMR ($CDCl_3$): δ (ppm) = 66.03, 60.24, 26.97, 19.43, -4.55 ; ^{11}B{^{1}H} NMR ($CDCl_3$): δ (ppm) = 0.3 (1B), -1.8 (1B), -7.0 (2B), -10.7 (2B), -13.3 (2B); m.p. = 61 °C.

Second step of the synthesis is to obtain [2-(tert-butyl-dimethyl-silanyl)-1,2-dicarba-*closo*dodecaboran(12)-1-yl]-propan-1-ol (Compound **B)**. Under a nitrogen atmosphere, compound **A** (5 g, 19.3 mmol, 1 eq) dissolved in 30 mL diethyl ether was deprotonated by addition of *n*-BuLi (14.5 mL of a 1.6 M solution, 23.2 mmol, 1.2 eq) at 0 °C. Trimethylene oxide (1.63 mL, 25.13 mmol, 1.3 eq) was added after 1 h and the solution turned light yellow. The solution was refluxed overnight and turned orange. The reaction was quenched with a few drops of methanol and 30 mL of water. The layers were separated in a separatory funnel and the aqueous solution was extracted with additional diethyl ether (3 x 30 mL). The combined extracts were dried over Na_2SO_4 and concentrated *in vacuo* to give a sticky solid. The solid was then recrystallized from boiling hexanes followed by cooling at 0 °C. Thin fibrous white crystals were formed and isolated by filtration over sintered glass to obtain carboranylpropanol **B** (87% yield). ^{1}H NMR ($CDCl_3$): δ (ppm) = 3.62 (q, 2H, CH_2OH), 2.36 (q, 2H, C$H_2$$CH_2$OH), 1.78 (t, 2H, C$H_2$-Cage), 1.06 (s, 9H, CCH_3), 0.33 (s, 6H, $SiCH_3$);); ^{13}C{^{1}H} NMR ($CDCl_3$): δ (ppm) = 81.27, 76.46, 61.60, 34.72, 33.04, 27.54, 20.33, -2.49; ^{11}B{^{1}H} NMR ($CDCl_3$): δ (ppm) = 0.2 (1B), -4.0 (1B), -7.4 (2B), -10.4 (6B); m.p. = 83 °C.

For last step of the synthesis, in a dry 250 mL round bottom flask, [2-(*tert*-butyldimethyl- silanyl)-1,2-dicarba-*closo*-dodecaboran(12)-1-yl]-propan-1-ol **B** (4 g, 12.75 mmol, 1.1 eq), *exo*-7-oxonorbornene imide (1.9 g, 11.5 mmol, 1 eq) and triphenylphosphine (3.325 g, 12.75 mmol, 1.1 eq) were dissolved in 100 mL dry tetrahydrofuran (THF) under a nitrogen atmosphere. The flask was cooled to 0 °C by using an ice bath. After 10 minutes, diisopropylazodicarboxylate (DIAD) (2.5 mL, 12.75 mmol, 1.1 eq) was added and the solution turned yellow. The mixture was stirred overnight. The crude mixture was then concentrated *in vacuo* to obtain a sticky yellow paste. The solid was purified by column chromatography (2/1 ethyl acetate/petroleum ether) (88% yield).

^{1}H NMR ($CDCl_3$): δ (ppm) = 6.53 (s, 2H, C*H*=C*H*), 5.75 (s, 2H, bridgeheads), 3.47 (t, 2H, NCH_2), 2.84 (s, 2H, NC(O)C*H*), 2.14 (m, 2H, NC$H_2$$CH_2$), 1.81 (m, 2H, NCH_2CH_2CH_2), 1.07 (s, 9H, CCH_3) 0.32 (s, 6H, SiCH_3); ^{13}C{^{1}H}NMR (CDCl3): δ (ppm) = 176.10, 136.50, 80.95, 80.38, 70.18, 47.42, 38.06, 34.97, 28.29, 27.50, 20.38, -2.61; ^{11}B{^{1}H} NMR ($CDCl_3$): δ (ppm) = 0.4 (1B), -3.9 (1B), -7.5 (2B), -10.4 (6B); m.p. = 136 °C.

2.2.4 Synthesis of 2-(anthracen-9-ylmethyl)-3,4,7,7-tetrahydro-4,7-epoxyisoindole-1,3-dione (Monomer 3)

9-(chloromethyl)anthracene (2.77 g, 12.2 mmol) and oxanorbornene imide product (1.005 gr, 6.1 mmol) stirred for 5 minutes in dry DMF (70 mL) under nitrogen. K_2CO_3 (0.5 g, 3.6 mmol) was added to the mixture and the reaction mixture stirred for 5 hours at 50^{o}C. After cooling the reaction mixture to the room temperature, the solution was diluted with dichloromethane, then washed in brine and distilled water. Na_2SO_4 was used as drying agent. The product was filtered and evaporated under reduced pressure. It was washed in diethylether. At the end 43% yields of product was obtained. The structure of product was confirmed by ^{1}H NMR spectroscopy. ^{1}H NMR ($CDCl_3$): δ (ppm) = 8.55-7.3 (m, 9H), 6.39 (s, 2H), 5.59 (s, 2H), 5.18 (s, 2H), 2.68 (s, 2H).

^{13}C{^{1}H} NMR (CDCl3): δ (ppm) =176.11, 136.33, 131.09, 129.12, 126.03, 124.7, 80.96, 77.02, 47.31, 36.35.

2.2.5 Synthesis of 1,2-dicarba-*closo*-dodecaboran(12)-1-yl]-propan-1,2-ol (Monomer 4)

A 1.53 M solution of *n*-BuLi in n-hexane (10.43 mL, 5.96 mmol) was added dropwise to a solution of o-$C_2B_{10}H_{12}$ (1 g, 6.94 mmol) in a dry toluene/Et_2O mixture (2:1, 30 mL) with stirring at 0°C. The mixture was allowed to warm to room temperature and stirred for 90 min. The solution was then cooled to 0°C, and a solution of oxetane (1.03 ml, 15.96 mmol) in toluene/ Et_2O (2:1, 10 mL) was added with stirring. The reaction mixture was stirred at room temperature overnight and then quenched with 50 mL of water. The organic layer was separated, and the aqueous layer was extracted with Et_2O (30 mL x 2). The combined organic portions were dried over anhydrous Na_2SO_4. Removal of the solvents gave a white solid that was washed with n-hexane (10 mL x 2) and dried under vacuum to afford as a white powder (1.5 g, 83%). Recrystallization from dichloromethane yielded colorless crystals. ^{1}H NMR ($CDCl_3$): δ (ppm) = 3.67 (t, 4H, 3 J HH = 5.4 Hz, CH_2OH), 2.34 (m, 4H, CH_2 C_{cage}), 1.79 (m, 4H, CH_2CH_2 C_{cage}); ^{13}C{^{1}H} NMR (CDCl3): δ (ppm) =79.6 (C_{cage}), 61.3 (CH_2OH), 32.4 (CH_2 C_{cage}), 31.6 (CH_2CH_2 C_{cage}); ^{11}B{^{1}H} NMR ($CDCl_3$): δ (ppm) = −4.74 (s, 2B), −10.43 (s, 8B).

2.3 Synthesis of the Polymers

2.3.1 Carborane and Phosphorus Containing Polymers via ROMP

2.3.3.1 Carborane and Phosphonate Ester Containing ROMP (Ring Opening Metathesis Polymerization) Block Copolymers

Monomer **1** was dissolved in dry CH_2Cl_2 (DCM) under nitrogen atmosphere. The required amount of catalyst was calculated and dissolved in dry CH_2Cl_2 in a separate vial, and then added to the monomer solution in one pot with vigorous stirring. When the first block was completed (∼1 h), as determined via GPC, ^{1}H NMR spectroscopy or TLC, the required amount of monomer **2** previously dissolved in dry CH_2Cl_2 was added to the polymerization mixture. To reach completion, the mixture was allowed to stir for 1 h at room temperature. The reaction was stopped by addition of an excess amount of ethyl vinyl ether, while stirring for 30 min [121]. The polymer was precipitated and washed with petroleum ether, then dried in vacuum oven under nitrogen. NMR characterization of block copolymers was done in $CDCl_3$, and GPC was performed in THF. Phosphonate- and carborane-based block copolymers' weight ratio was: **P1**: 10 kDa : 40 kDa; **P2**: 40 kDa : 10 kDa; and **P3**: 25 kDa : 25 kDa. The required amount of monomer and catalyst for each polymerization was: 0.1274 g (0.4 mmol, 1.0 eq) of monomer **1**, 0.5 g of monomer **2** (1.1 mmol, 2.75 eq) and 0.0112 g (0.012 mmol, 0.3 eq) of Grubbs 3rd catalyst for **P1**. 0.5 g (1.59 mmol, 5.9 eq) of monomer **1**, 0.1252 g (0.27 mmol, 1.0 eq) of monomer **2** and 0.011 g (0.012 mmol, 0.04 eq) of Grubbs 3rd catalyst for **P2**. 0.5 g (1.59 mmol, 1.45 eq) of monomer **2** and 0.5 g (1.1 mmol, 1.0 eq) of Grubbs 3rd catalyst for **P3**.

P1: ^{1}H NMR ($CDCl_3$): δ (ppm)= 6.08 (s, 2H, PhCH−HC=C**H**$_{trans}$), 5.80 (s, 2H, PhCH−HC=C**H**$_{cis}$), 4.98 (m, 2H, HC=C**H**$_{cis}$), 4.47 (m, 2H, HC=C**H**$_{trans}$), 4.14 (m, 4H, PO−C**H**$_2$), 3.90 (t, 2H, $(C{=}O)_2$N−C**H**$_2$−P), 3.44-3.37 (m, 6H, $(C{=}O)_2$N−C**H**$_2$−CH_2), 2.20 (m, 2H, CH_2C**H**$_2$$CH_2$−C$_{cluster}$), 1.80 (br t, 2H, CH_2C**H**$_2$−C$_{cluster}$), 1.28 (t, 6H, PO−CH_2C**H**$_3$), 1.07 (s, 9H, C(C**H**$_3$)$_3$), 0.33 (s, 6H, Si−C**H**$_3$).

^{13}C{^{1}H} NMR ($CDCl_3$): δ (ppm) = 174.2 (**C**=O), 131.6 (**C**=C), 70.3 (**C**−O), 62.5 (**C**−O), 53.4 (CH_3**C**H_2−OP), 52.3 (**C**H_2−N), 38.1 (P−**C**H_2−N), 31.8 (CH−**C**H−CO), 28.5 (CH_3−**C**H_2), 23.1 (**C**H_3−CH_2), 21.9 (**C**H_3−C(CH_3)), 20.5 (**C**H_2−C$_{cluster}$), 16.3 (**C**−Si), 14.1 (**C**−Si), 11.6 (**C**$_{cluster}$).

$^{31}P\{^1H\}$ NMR ($CDCl_3$): δ (ppm) = 18.4 (s, (**P**=O)).

$^{11}B\{^1H\}$ NMR ($CDCl_3$): δ (ppm) = 0.1 (br s, 2B), −7.6 (br s, 8B).

P2: ^1H NMR ($CDCl_3$): δ (ppm)= 6.08 (s, 2H, PhCH−HC=C**H**$_{trans}$), 5.79 (s, 2H, PhCH−HC=C**H**$_{cis}$), 4.96 (m, 2H, HC=C**H**$_{cis}$), 4.48 (m, 2H, HC=C**H**$_{trans}$), 4.15 (m, 4H, PO−C**H**$_2$), 3.90 (t, 2H, (C=O)$_2$N−C**H**$_2$−P), 3.44-3.37 (m, 6H, (C=O)$_2$N−C**H**$_2$−CH$_2$), 2.18 (m, 2H, CH$_2$C**H**$_2$CH$_2$−C$_{cluster}$), 2.01 (br t, 2H, CH$_2$C**H**$_2$−C$_{cluster}$), 1.34 (t, 6H, PO−CH$_2$C**H**$_3$), 1.07 (s, 9H, C(C**H**$_3$)$_3$), 0.32 (s, 6H, Si−C**H**$_3$).

$^{13}C\{^1H\}$ NMR ($CDCl_3$): δ (ppm) = 173.9 (**C**=O), 131.6 (**C**=C), 80.4 (**C**−O), 63.2 (**C**−O), 53.2 (CH$_3$**C**H$_2$−OP), 52.0 (**C**H$_2$−N), 38.8 (P−**C**H$_2$−N), 35.6 (CH−**C**H−CO), 31.7 (CH$_3$−**C**H$_2$), 29.2 (**C**H$_3$−CH$_2$), 26.9 (**C**H$_3$−C(CH$_3$)), 18.1 (**C**H$_2$−C$_{cluster}$), 16.2 (**C**−Si), 13.6 (**C**−Si), 11.3 (**C**$_{cluster}$).

$^{31}P\{^1H\}$ NMR ($CDCl_3$): δ (ppm) = 19.2 (s, (**P**=O)).

$^{11}B\{^1H\}$ NMR ($CDCl_3$): δ (ppm) = 23.8 (br s, 2B, **B**−C$_{cluster}$), −7.9 (br s, 8B, **B**−B$_{cluster}$).

P3: ^1H NMR ($CDCl_3$): δ (ppm)= 6.08 (s, 2H, PhCH−HC=C**H**$_{trans}$), 5.79 (br s, 2H, PhCH−HC=C**H**$_{cis}$), 4.98 (m, 2H, HC=C**H**$_{cis}$), 4.47 (br s, 2H, HC=C**H**$_{trans}$), 4.13 (m, 4H, PO−C**H**$_2$), 3.87 (t, 2H, (C=O)$_2$N−C**H**$_2$−P), 3.44-3.37 (m, 6H, (C=O)$_2$N−C**H**$_2$−CH$_2$), 2.20 (br s, 2H, CH$_2$C**H**$_2$CH$_2$−C$_{cluster}$), 1.90 (br t, 2H, CH$_2$C**H**$_2$−C$_{cluster}$), 1.33 (t, 6H, PO−CH$_2$C**H**$_3$), 1.06 (s, 9H, C(C**H**$_3$)$_3$), 0.33 (s, 6H, Si−C**H**$_3$).

$^{13}C\{^1H\}$ NMR ($CDCl_3$): δ (ppm) = 173.8 (**C**=O), 131.1 (**C**=C), 80.4 (**C**−O), 69.7 (**C**−O), 62.5 (CH$_3$**C**H$_2$−OP), 53.2 (**C**H$_2$−N), 38.6 (P−**C**H$_2$−N), 35.2 (CH−**C**H−CO), 33.7 (CH$_3$−**C**H$_2$), 31.7 (**C**H$_3$−CH$_2$), 27.3 (**C**H$_3$−CH$_2$), 21.7 (**C**H$_3$−C(CH$_3$)), 15.8 (**C**H$_2$−C$_{cluster}$), 13.9 (**C**−Si), 10.9 (**C**$_{cluster}$).

$^{31}P\{^1H\}$ NMR ($CDCl_3$): δ (ppm) = 18.5 (s, (**P**=O)).

$^{11}B\{^1H\}$ NMR ($CDCl_3$): δ (ppm) = 0.4 (br s, 2B, **B**−C$_{cluster}$), −10.3 (br s, 8B, **B**−B$_{cluster}$).

2.3.3.2 Carborane and Phosphonic Acid Containing ROMP (Ring Opening Metathesis Polymerization) Block Copolymers

A literature procedure was followed for this synthesis [16]. Three polymers (**P1**, **P2** and **P3**), which obtained in the previous step, were separately used for each synthesis. The polymer (100 mg, 0.002 mmol) was dissolved in 8 mL dry dichloromethane. Excess bromo trimethyl silane (2 mL, 15.3 mmol) was added the polymer solution at room temperature, then the reaction mixture was stirred under nitrogen at 40 °C for 3 h. The reaction was cooled down to the room temperature, then the solution was purged nitrogen. Excess amount of methanol was added and the reaction was stirred at room temperature for 3 days. Methanol solvent was removed under reduced pressure and resulting product was washed with excess diethyl ether. It was kept in a desiccator after having been dried.

P1A: ^{1}H NMR (DMSO-d_6): δ (ppm)= 5.96 (s, 2H, PhCH−HC=C$\mathbf{H}_{trans}$), 5.76 (s, 2H, PhCH−HC=C$\mathbf{H}_{cis}$), 4.76 (m, 2H, HC=C$\mathbf{H}_{cis}$), 4.39 (m, 2H, HC=C$\mathbf{H}_{trans}$), 2.21 (br s, 2H, $CH_2C\mathbf{H}_2CH_2$−$C_{cluster}$), 1.67 (br s, 2H, $CH_2C\mathbf{H}_2$−$C_{cluster}$), 1.01 (s, 9H, $C(C\mathbf{H}_3)_3$), 0.30 (s, 6H, Si−C$\mathbf{H}_3$).

^{31}P{^{1}H} NMR ($CDCl_3$): δ (ppm) = 14.1 (s, (**P**−OH)).

P2A: ^{1}H NMR (DMSO-d_6): δ (ppm)= 5.96 (s, 2H, PhCH−HC=C$\mathbf{H}_{trans}$), 5.74 (s, 2H, PhCH−HC=C$\mathbf{H}_{cis}$), 4.79 (m, 2H, HC=C$\mathbf{H}_{cis}$), 4.37 (m, 2H, HC=C$\mathbf{H}_{trans}$), 2.20 (br s, 2H, $CH_2C\mathbf{H}_2CH_2$−$C_{cluster}$), 1.68 (br s, 2H, $CH_2C\mathbf{H}_2$−$C_{cluster}$), 1.01 (s, 9H, $C(C\mathbf{H}_3)_3$), 0.30 (s, 6H, Si−C$\mathbf{H}_3$).

^{31}P{^{1}H} NMR ($CDCl_3$): δ (ppm) = 14.4 (s, (**P**−OH)).

P3A: ^{1}H NMR (DMSO-d_6): δ (ppm)= 5.96 (s, 2H, PhCH−HC=C$\mathbf{H}_{trans}$), 5.75 (s, 2H, PhCH−HC=C$\mathbf{H}_{cis}$), 4.81 (m, 2H, HC=C$\mathbf{H}_{cis}$), 4.55 (m, 2H, HC=C$\mathbf{H}_{trans}$), 2.20 (br s, 2H, $CH_2C\mathbf{H}_2CH_2$−$C_{cluster}$), 1.67 (br s, 2H, $CH_2C\mathbf{H}_2$−$C_{cluster}$), 1.01 (s, 9H, $C(C\mathbf{H}_3)_3$), 0.29 (s, 6H, Si−C$\mathbf{H}_3$).

^{31}P{^{1}H} NMR ($CDCl_3$): δ (ppm) = 13.3 (s, (**P**−OH)).

2.3.3.3 Incorporation of Iron Naoparticles with Deprotected Carborane and Phosphonate Ester Containing ROMP (Ring Opening Metathesis Polymerization) Block Copolymers

In the first part of the study, bare iron nanoparticles were synthesized using the co-precipitation method. Eighty milliliters of distilled water was placed into a jacketed glass reactor and degassed using nitrogen gas for 30 min while stirring with a mechanical stirrer (200 rpm) at 60 °C. Then, 0.28 g of $FeCl_3$ and 0.24 g of $FeSO_4 \cdot 7H_2O$ was added to the reactor and left stirring for 15 min. Then, NaOH solution (0.51 g dissolved in distilled H_2O) was added to the reactor and nitrogen gas was stopped. The solution turned black immediately after base addition and stirring was continued for 30 min. Then the reaction mixture was transferred into a falcon tube and centrifuged at 5000 rpm for 5 min. The obtained bare iron oxide nanoparticles were washed with acetone three times and dried using a lyophilizer.

In a typical example, **P2A** was dissolved in 3 ml DMSO and 1-5% (by weight) iron oxide nanoparticles were added to the scintillation vial and sonicated for 6 h. After membrane dialysis, the polymer-uncoated iron oxide nanoparticles were separated and the polymer-coated nanoparticles were characterized via TEM, ICP-OES techniques. The same procedure was also applied for **P1A** and **P3A**.

2.3.3.4 Carborane and Phosphonate Ester Containing ROMP (Ring Opening Metathesis Polymerization) Random Copolymers

Monomer **1** and **2** were dissolved in the presence of 1 mL dry CH_2Cl_2. The required amount of catalyst was dissolved by dry CH_2Cl_2 in another flask, and then added into the dissolved monomers´ solution with vigorous stirring. The reaction mixture was stirred for 2.5 h at room temperature. The reaction was stopped by addition of excess amount of ethyl vinyl ether (dissolved in dry dichloromethane). The polymer was purified by petroleum ether and dried under nitrogen. Polymers were dissolved in $CDCl_3$ for NMR measurement. Phosphonate- and carborane- containing random copolymers' weight ratio was: **P4**: 10 kDa: 40 kDa; **P5**: 40 kDa : 10 kDa; and **P6**: 25 kDa : 25 kDa.

The required amount of monomer and catalyst for each polymerization was: 0.1274 g (0.4 mmol, 1.0 eq) of monomer **1**, 0.5 g of monomer **2** (1.1 mmol, 2.75 eq) and 0.0112 g (0.012 mmol) of Grubbs 3rd catalyst for **P1**. 0.5 g (1.59 mmol, 5.9 eq) of monomer **1**, 0.1252 g (0.27 mmol, 1.0 eq) of monomer **2** and 0.011 g (0.012 mmol) of Grubbs 3rd catalyst for **P2**. 0.5 g (1.59 mmol, 1.45 eq) of monomer **2** and 0.5 g (1.1 mmol, 1.0 eq) of Grubbs 3rd catalyst for **P3**.

P4: ^{1}H NMR ($CDCl_3$): δ (ppm)= 6.08 (s, 2H, PhCH−HC=C**H**$_{trans}$), 5.80 (s, 2H, PhCH−HC=C**H**$_{cis}$), 4.98 (m, 2H, HC=C**H**$_{cis}$), 4.47 (m, 2H, HC=C**H**$_{trans}$), 4.14 (m, 4H, PO−C**H**$_2$), 3.90 (t, 2H, (C=O)$_2$N−C**H**$_2$−P), 3.44-3.37 (m, 6H, (C=O)$_2$N−C**H**$_2$−CH_2), 2.20 (m, 2H, CH_2C**H**$_2$$CH_2$−C$_{cluster}$), 1.80 (br t, 2H, CH_2C**H**$_2$−C$_{cluster}$), 1.28 (t, 6H, PO−CH_2C**H**$_3$), 1.07 (s, 9H, C(C**H**$_3$)$_3$), 0.33 (s, 6H, Si−C**H**$_3$).

$^{13}C\{^{1}H\}$ NMR ($CDCl_3$): δ (ppm) = 156.1 (**C**=O), 132.3 (**C**=C), 69.9 (**C**−O), 48.2 (**C**−O), 38.8 (CH_3**C**H_2−OP), 30.7 (**C**H_2−N), 27.3 (P−**C**H_2−N), 26.4 (CH−**C**H−CO), 21.9 (CH_3−**C**H_2), 21.2 (**C**H_3−CH_2), 19.0 (**C**H_3−C(CH_3)), 18.8 (**C**H_2−$C_{cluster}$), 15.4 (**C**−Si), 14.3 (**C**−Si), 11.4 (**C**$_{cluster}$).

$^{31}P\{^{1}H\}$ NMR ($CDCl_3$): δ (ppm) = 18.4 (s, (**P**=O)).

$^{11}B\{^{1}H\}$ NMR ($CDCl_3$): δ (ppm) = 24.1 (br s, 2B, **B**−$C_{cluster}$), −19.9 (br s, 8B, **B**−$B_{cluster}$).

P5: ^{1}H NMR ($CDCl_3$): δ (ppm)= 6.08 (s, 2H, PhCH−HC=C**H**$_{trans}$), 5.79 (s, 2H, PhCH−HC=C**H**$_{cis}$), 4.96 (m, 2H, HC=C**H**$_{cis}$), 4.48 (m, 2H, HC=C**H**$_{trans}$), 4.15 (m, 4H, PO−C**H**$_2$), 3.90 (t, 2H, $(C=O)_2$N−C**H**$_2$−P), 3.44-3.37 (m, 6H, $(C=O)_2$N−C**H**$_2$−CH_2), 2.18 (m, 2H, CH_2C**H**$_2$$CH_2$−$C_{cluster}$), 2.01 (br t, 2H, CH_2C**H**$_2$−$C_{cluster}$), 1.34 (t, 6H, PO−CH_2C**H**$_3$), 1.07 (s, 9H, C(C**H**$_3$)$_3$), 0.32 (s, 6H, Si−C**H**$_3$).

$^{13}C\{^{1}H\}$ NMR ($CDCl_3$): δ (ppm) = 174.2 (**C**=O), 132.3 (**C**=C), 62.9 (**C**−O), 41.2 (**C**−O), 39.8 (CH_3**C**H_2−OP), 33.6 (**C**H_2−N), 29.1 (P−**C**H_2−N), 27.3 (CH−**C**H−CO), 22.3 (CH_3−**C**H_2), 22.1 (**C**H_3−CH_2), 20.0 (**C**H_3−C(CH_3)), 19.4 (**C**H_2−$C_{cluster}$), 16.4 (**C**−Si), 14.3 (**C**−Si), 11.4 (**C**$_{cluster}$).

$^{31}P\{^{1}H\}$ NMR ($CDCl_3$): δ (ppm) = 18.1 (s, (**P**=O)).

$^{11}B\{^{1}H\}$ NMR ($CDCl_3$): δ (ppm) = 28.7 (br s, 2B, **B**−$C_{cluster}$), −19.5 (br s, 8B, **B**−$B_{cluster}$).

P6: ^{1}H NMR ($CDCl_3$): δ (ppm)= 6.08 (s, 2H, PhCH−HC=C**H**$_{trans}$), 5.79 (br s, 2H, PhCH−HC=C**H**$_{cis}$), 4.98 (m, 2H, HC=C**H**$_{cis}$), 4.47 (br s, 2H, HC=C**H**$_{trans}$), 4.13 (m, 4H, PO−C**H**$_2$), 3.87 (t, 2H, $(C=O)_2$N−C**H**$_2$−P), 3.44-3.37 (m, 6H, $(C=O)_2$N−C**H**$_2$−CH_2), 2.20 (br s, 2H, CH_2C**H**$_2$$CH_2$−$C_{cluster}$), 1.90 (br t, 2H, CH_2C**H**$_2$−$C_{cluster}$), 1.33 (t, 6H, PO−CH_2C**H**$_3$), 1.06 (s, 9H, C(C**H**$_3$)$_3$), 0.33 (s, 6H, Si−C**H**$_3$).

$^{13}C\{^{1}H\}$ NMR ($CDCl_3$): δ (ppm) = 174.6 (**C**=O), 132.3 (**C**=C), 70.1 (**C**−O), 62.9 (**C**−O), 53.4 (CH_3**C**H_2−OP), 41.4 (**C**H_2−N), 35.2 (P−**C**H_2−N), 29.1 (CH−**C**H−CO), 22.6 (CH_3−**C**H_2), 21.9 (**C**H_3−CH_2), 20.4 (**C**H_3−C(CH_3)), 19.5 (**C**H_2−$C_{cluster}$), 16.4 (**C**−Si), 14.1 (**C**−Si), 11.4 (**C**$_{cluster}$).

$^{31}P\{^{1}H\}$ NMR ($CDCl_3$): δ (ppm) = 18.7 (s, (**P**=O)).

$^{11}B\{^{1}H\}$ NMR ($CDCl_3$): δ (ppm) = 25.3 (br s, 2B, **B**−$C_{cluster}$), 11.0 (br s, 8B, **B**−$B_{cluster}$).

2.3.2 Synthesis of Carborane and Phosphorus Containing Polymers via Condensation Route and Application in Epoxy Resin Formulation

In a flame-dried 2-neck round-bottom flask connected to a dropping funnel, 1,2-$(HOCH_2CH_2CH_2)_2$-1,2-$C_2B_{10}H_{10}$ (Monomer **4**) (0.572 g, 2.42 mmol, 1.1 eq) was dissolved in 15 mL of anhydrous toluene and 0.3 mL (2.2 mmol, 1.0 eq) of anhydrous triethylamine. Then 4-dimethylaminopyridine (DMAP) (15 mg, 0.01 mmol, 0.005 eq) was added and the flask was cooled to 0 °C. Phenyl phosphonic dichloride (PPDC) (0.33 mL, 2.2 mmol, 1 eq) in 3 mL of anhydrous toluene was added drop-wise over ca. 15 min with vigorous stirring. The reaction mixture was then warmed up to room temperature, stirred for 3 h, and then for 4 h at 110 °C. The end-capping agent, 1,2-$(HOCH_2CH_2CH_2)_2$-1,2-$C_2B_{10}H_{10}$ (monomer **4**) (0.05 mg, 0.25 mmol, 0.11 eq) was then added, and stirred for an additional hour. After that, the reaction mixture was diluted with 250 mL of dichloromethane. The dichloromethane solution was washed with cold water (5 x 30 mL), and the organic phase was dried over anhydrous magnesium sulphate. The organic phase was then concentrated to 20 mL, then precipitated into a stirred solution of cold hexane (~100 mL), yielding a white sticky product (92%). The product was dried in vacuum oven for 24 h under nitrogen. The structure of **P7** was analyzed via NMR spectroscopy.

P7: ^{1}H NMR ($CDCl_3$): δ (ppm)= 9.34 (s, −O**H**), 7.70-7.09 (m, 5H, Ar−**H**), 3.46-3.37 (m, 4H, O−C**H**$_2$), 2.32-2.17 (m, 4H, $CH_2C\mathbf{H}_2CH_2$), 1.92-1.78 (m, 4H, C**H**$_2$−$C_{cluster}$).

$^{31}P\{^{1}H\}$ NMR (CDCl3): δ (ppm) = 17.5 (s, (**P**=O)).

$^{11}B\{^{1}H\}$ NMR ($CDCl_3$): δ (ppm) = −4.6 (br s, 2B, **B**−$C_{cluster}$), −10.3 (br s, 8B, **B**−$B_{cluster}$).

In order to investigate the flame-retardant properties of the polymer (**P7**), it was used in epoxy resin with the varied ratios such as 5%, 7.5%, 12.5% and 20% by weight. This oligomer (**P7**) can be introduced into the epoxy polymer system by physical mixing of the resin with the flame retardant before adding an accelerator and hardener. In a 25 ml flask, 1.1 g epoxy resin and accordingly calculated amount of **P7** were mixed at 100 °C for 1 h. After curing, the thermal properties of the samples were studied using TGA and MCC analysis. The reaction between epoxy bond and -OH bond in the polymer structure was monitored by DSC (Differential Scanning Calorimetry).

2.3.3 Carborane and Anthracene Containing Random Copolymers via ROMP

Carborane-based monomer (monomer **2**) and anthracene-based monomer (monomer **3**) were dissolved in 1 mL dry CH_2Cl_2 (2 mL dichloromethane was used for synthesis of **P10**). The required amount of catalyst was dissolved in dry CH_2Cl_2 (0.5 mL) in another flask and then the catalyst solution was added in one shot to the monomer solution while the reaction mixture was stirring. Then it kept being stirred at room temperature for 1 h under nitrogen. The reaction was terminated by an injection of 0.5 mL 30% ethyl vinyl ether (in dry dichloromethane). The polymer was precipitated and washed with excess petroleum ether, then dried under inert atmosphere. The structures of products were confirmed by NMR spectroscopy. Anthracene- and carborane-containing random copolymers are given as; **P8:** 10 kDa:70 kDa, **P9:** 20 kDa:60kDa and **P10:** 30kDa:50kDa g/mol, respectively.

P8: ^{1}H NMR ($CDCl_3$): δ (ppm)= 8.35-7.38 (m, 9H, Ar−**H**), 5.99 (br t, 2H, PhCH−HC=C**H**$_{trans}$), 5.68 (br s, 2H, PhCH−HC=C**H**$_{cis}$), 4.88 (br t, 2H, HC=C**H**$_{cis}$), 4.31 (br s, 2H, HC=C**H**$_{trans}$), 3.36-3.23 (m, 8H, $(C{=}O)_2N{-}C\mathbf{H}_2{-}CH_2$), 2.10 (br s, 2H, $CH_2C\mathbf{H}_2CH_2{-}C_{cage}$), 1.71 (t, 2H, $C\mathbf{H}_2{-}C_{cluster}$), 0.99 (s, 9H, $C(C\mathbf{H}_3)_3$), 0.24 (s, 6H, $Si{-}C\mathbf{H}_3$).

P9: ^{1}H NMR ($CDCl_3$): δ (ppm)= 8.32-7.33 (m, 9H, Ar−**H**), 5.84 (br t, 2H, PhCH−HC=C**H**$_{trans}$), 5.46 (br s, 2H, PhCH−HC=C**H**$_{cis}$), 4.80 (br t, 2H, HC=C**H**$_{cis}$), 4.28 (br s, 2H, HC=C**H**$_{trans}$), 3.28-2.96 (m, 8H, $(C{=}O)_2N{-}C\mathbf{H}_2{-}CH_2$), 2.10 (br s, 2H), 1.68 (t, 2H), 0.95 (s, 9H, $C(C\mathbf{H}_3)_3$), 0.21(s, 6H, $Si{-}C\mathbf{H}_3$).

P10: ^{1}H NMR ($CDCl_3$): δ (ppm)= 8.27-7.33 (m, 9H, Ar−**H**), 5.78 (br t, 2H, PhCH−HC=C**H**$_{trans}$), 5.40 (br s, 2H, PhCH−HC=C**H**$_{cis}$), 4.81 (br t, 2H, HC=C**H**$_{cis}$), 4.17 (br s, 2H, HC=C**H**$_{trans}$), 3.27-2.91(m, 8H, $(C{=}O)_2N{-}C\mathbf{H}_2{-}CH_2$), 2.10 (br s, 2H, $CH_2C\mathbf{H}_2CH_2{-}C_{cluster}$), 1.66 (t, 2H, $C\mathbf{H}_2{-}C_{cluster}$), 0.92 (s, 9H, $C(C\mathbf{H}_3)_3$), 0.19 (s, 6H, $Si{-}C\mathbf{H}_3$).

2.3.3.1 Hydrogenation of Carborane and Anthracene Containing ROMP (Ring Opening Metathesis Polymerization) Random Copolymer (P10)

According to the literature [116], 330 mg *p*-toluenesulfonyl hydrazide (1.78 mmol) was added to a solution of 110 mg (0.001 mmol) polymer (**P10**) in 25 ml *o*-xylene. After stirring under reflux for 2 h, the product was precipitated by using an excess amount of petroleum ether and washed with methanol. It was then dried in vacuum oven.

P11: ^{1}H NMR ($CDCl_3$): δ (ppm)= 8.38-7.35 (m, 9H, Ar−**H**), 3.32-2.85(m, 8H, $(C{=}O)_2N{-}C\mathbf{H}_2{-}CH_2$), 2.20 (br s, 2H, $CH_2C\mathbf{H}_2CH_2{-}C_{cluster}$), 1.76 (t, 2H, $C\mathbf{H}_2{-}C_{cluster}$), 0.93 (s, 9H, $C(C\mathbf{H}_3)_3$), 0.17 (s, 6H, $Si{-}C\mathbf{H}_3$).

2.3.3.2 Photocharacterization of Carborane and Anthracene Containing ROMP (Ring Opening Metathesis Polymerization) Random Copolymers

Photodimerization: The quartz cuvette containing the polymer sample was irradiated with light at 350 nm for 10 seconds intervals, after each interval, UV-vis spectrum was recorded. This process was repeated until no changes in the UV-vis spectra were detectable, signifying that the sample has reached its dimerization limit.

Photo Cleavage: The cuvette containing the completely dimerized block copolymer solution was irradiated with light at 254 nm for 10 second intervals, after each interval a UV-vis spectrum was recorded. This was repeated until no changes in the UV-vis spectra were detectable, signifying that the limit of photo-cleavage of the dimer was reached.

A stock solution of block copolymer at 0.16 mg/mL concentration was prepared by dissolving the polymer (1.6 mg) in tetrahydrofuran (10 mL) under N_2 atmosphere in a scintillation vial. The vial containing the solution was covered with septum cap and sonicated for 15 minutes. After using tetrahydrofuran (3.5 mL) in a quartz cuvette as a blank, the cuvette was emptied and dried before an aliquot (3.5 mL) the stock solution of polymer was added. By using the UV-vis spectrophotometer, the absorption spectrum of the sample was recorded.

CHAPTER 3

RESULT AND DISCUSSION

3.1 Synthesis and Characterization of Carborane and Phosphorus-containing Polymer

3.1.1 Synthesis of Phosphorus Functional Monomer (monomer 1)

In this part of the study, furan and maleimide were reacted in the presence of hot ethyl acetate to obtain the oxanorbornene structure (**1**) via Diels-Alder mechanism (Scheme 3.1).

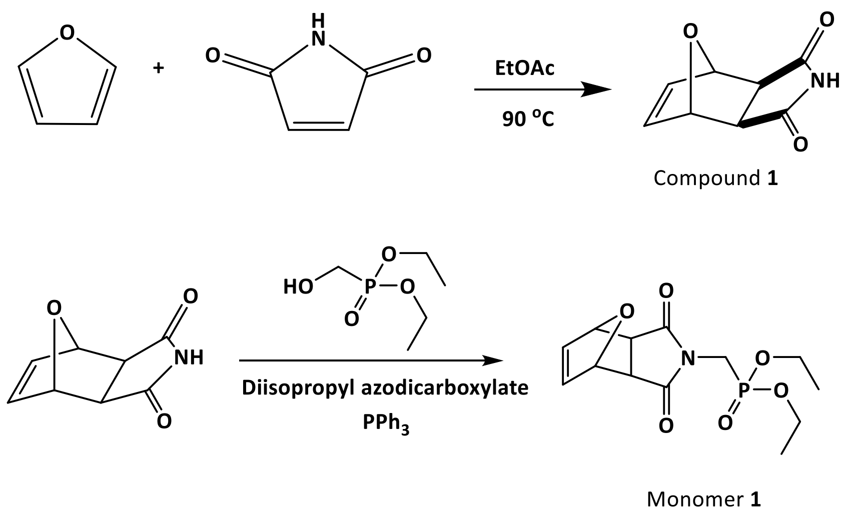

Scheme 3.1 Synthetic pathway to compound **1** and monomer **1** used in the study

In addition to the Diels-Alder reaction, compound **1** and hydroxyethyl phosphonate were synthesized by Mitsunobu coupling. In the field of organic chemistry, the Mitsunobu reaction has been widely used because it is a highly versatile and effective synthesis method [122], [123], [124]. This mild synthetic reaction was discovered in 1967. During the process, a hydroxyl group is converted into a potent leaving group, which can be replaced with a wide variety of nucleophiles [125]. For C−O, C−N, C−C and C−X bond formation, the Mitsunobu reaction is a practical, useful and diverse method, with the additional advantages of requiring mild reaction conditions and having excellent stereoselectivity. Obviously it will keep being a very important synthetic pathway in organic chemistry [126].

The phosphonate-functionalized oxanorbornene monomer **1** was prepared according to the general synthetic route shown in Scheme 3.1. A key feature of the synthesis was the Mitsunobu coupling of hydroxymethylphosphonate and compound **1**. Monomer **1** was characterized by ^{1}H NMR and $^{13}C\{^{1}H\}$ NMR spectroscopy (Figure 3.2, 3.3). The data were in accordance with the reported literature values [127]. Characteristic signals appeared at 1.3 and 4.1 ppm in the ^{1}H NMR spectrum and 16.3 and 62.9 ppm in the $^{13}C\{^{1}H\}$ NMR spectrum, which can be assigned to the new aliphatic bonds. In addition, $^{13}C\{^{1}H\}$ NMR showed the characteristic doublet shifts from 33.0 to 35.1 ppm due to the hetero-coupling between the C-nucleus and the P-nucleus [128].

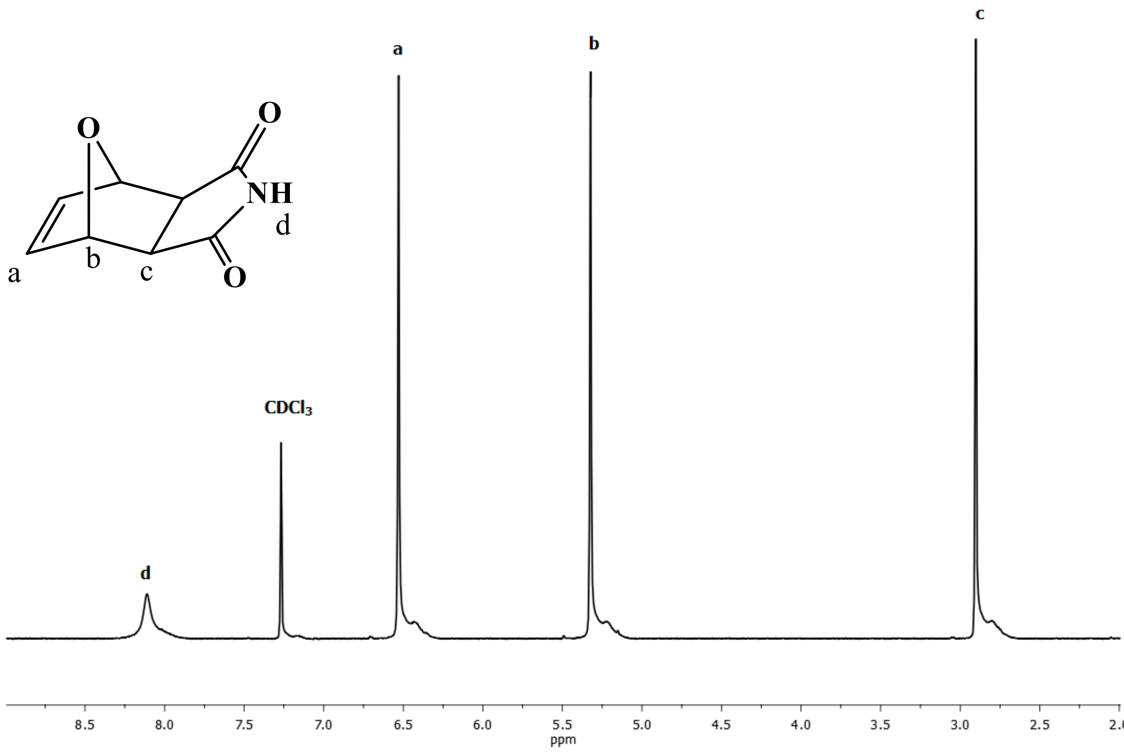

Figure 3.1 ^{1}H NMR (400.13 MHz) spectrum in $CDCl_3$ of compound **1**

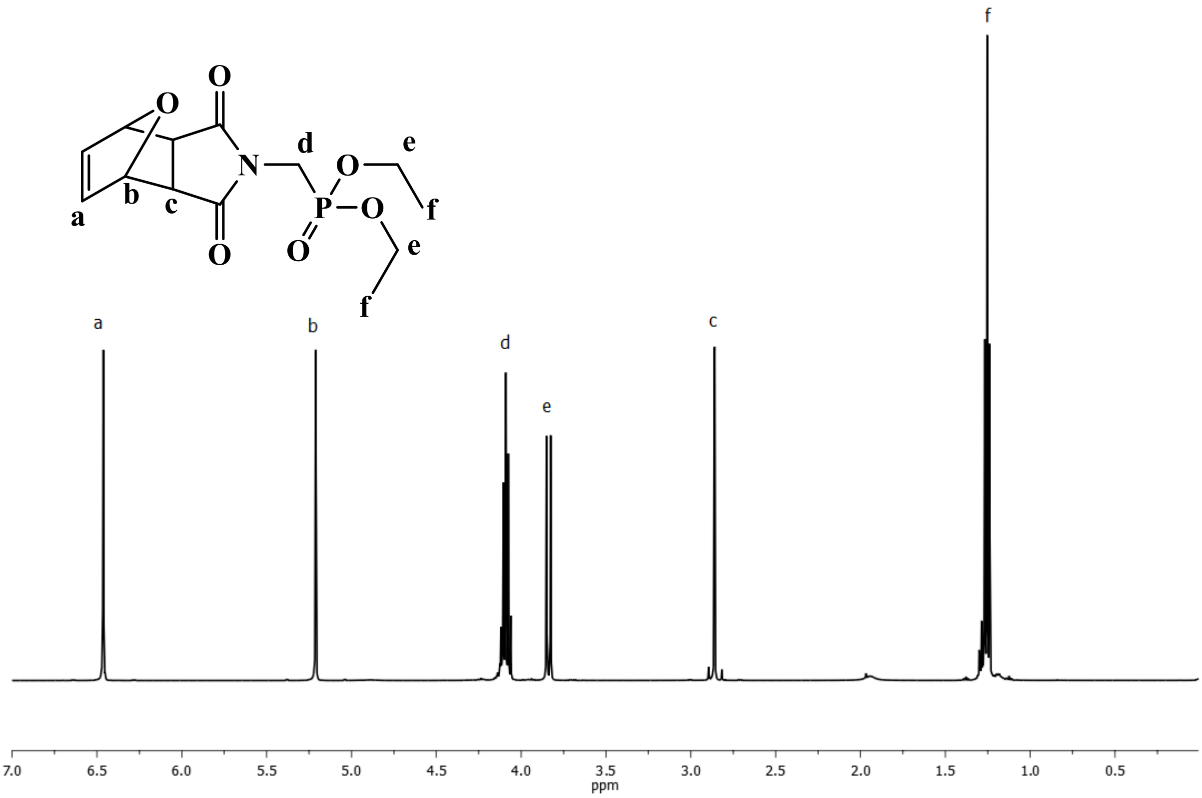

Figure 3.2 ^{1}H NMR (400.13 MHz) spectrum in $CDCl_3$ of monomer **1**

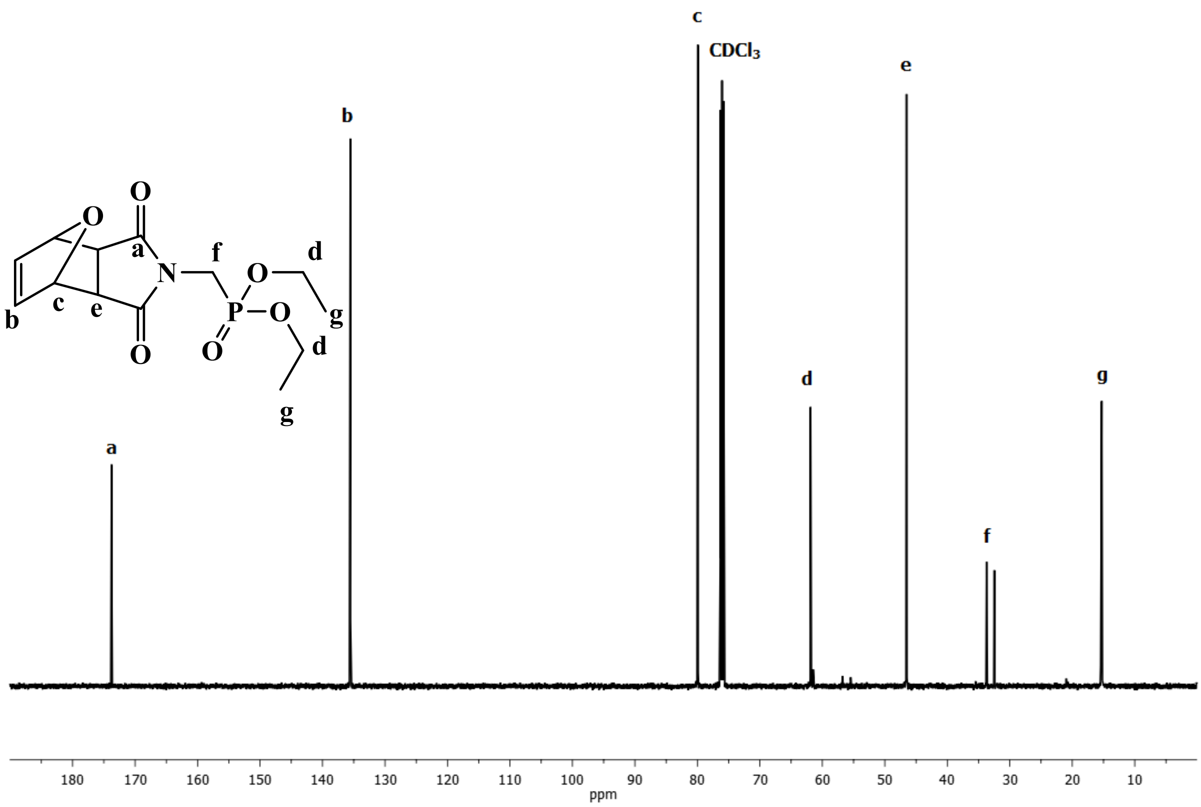

Figure 3.3 ^{13}C {^{1}H} NMR (100.16 MHz) spectrum in $CDCl_3$ of monomer **1**

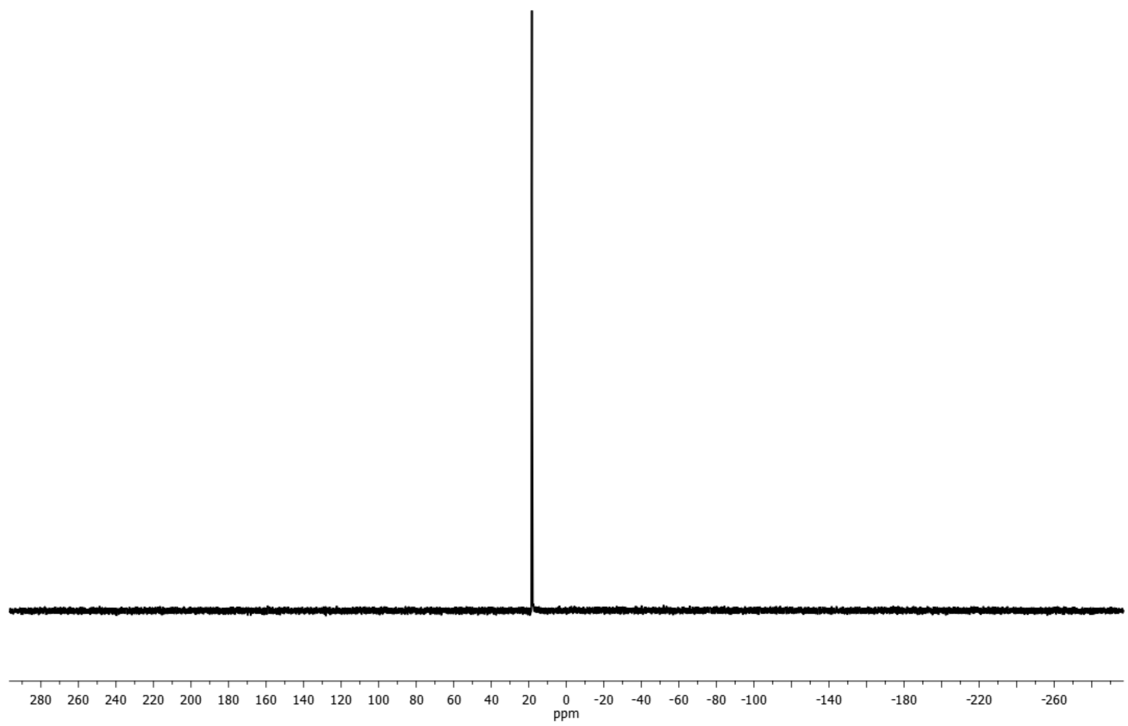

Figure 3.4 ^{31}P{^{1}H} NMR (161.97 MHz)) spectrum in $CDCl_3$ of monomer **1**

3.1.2 Carborane functional Monomer (Monomer 2)

A literature procedure was used for the synthesis of the carborane-containing oxanorbornene unit, monomer **2** [121]. The final product (monomer **2**) was obtained with a 3-steps reaction, which is given in Scheme 3.2.

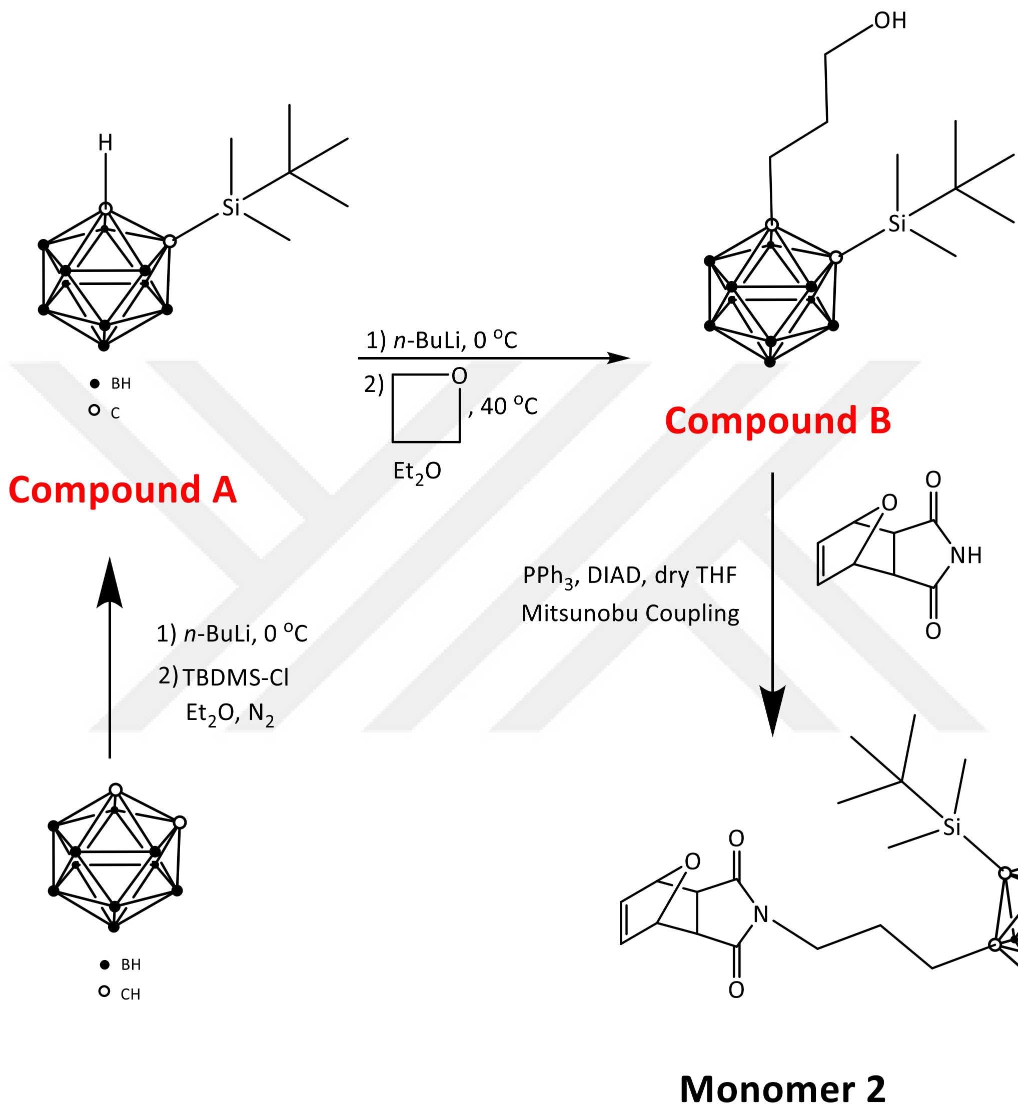

Scheme 3.2 Synthetic pathway to monomer **2**

In the first step, one of the carbon atoms in *o*-carborane was protected by using *tert*-butyldimethylsilyl chloride (compound **A**) to obtain a monosubstituted carborane derivative. After purification and characterization, the intermediate compound **A** was used for the second step, to obtain the propan-1-ol derivative of the silyl protected carborane (compound **B**). In the last step, monomer **2** was obtained as a pure white powder via Mitsunobu coupling between compound **B** and oxanorbornene (**1**). All the compounds in each step were purified and then characterized by ^{1}H, ^{13}C and ^{11}B NMR spectroscopy. The ^{1}H NMR spectrum of monomer **2** (Figure 3.5) shows characteristic signals at 0.32 and 1.07 ppm for 15 protons, which belong to the protons of the *tert*-butyl and methyl groups, respectively, and a peak at 3.47 ppm for the protons in alpha position to the nitrogen atom. Moreover, the protons of the double bond (H^{a}) are found at 6.53 ppm. Based on the $^{13}C\{^{1}H\}$. NMR spectrum (Figure 3.6), specific peaks at –2.6, 20.3 and 27.5 ppm belong to carbon atoms next to the silicon atom, the peak at 34.9 ppm shows the carbon atom next to the nitrogen atom, and the peak at 136.5 ppm belongs to the double bond. The $^{11}B\{^{1}H\}$ NMR spectrum shows four peaks with relative intensities 1:1:2:6, as expected (Figure 3.7) [121]. The $^{11}B\{^{1}H\}$ NMR spectrum of monomer **2**, shown in Figure 3.7, illustrates broad peaks due to ^{11}B being a quadrupole; therefore, it is normal that signals overlap, even though it is expected to see more signals in the spectrum due to asymmetric substitution at the cluster.

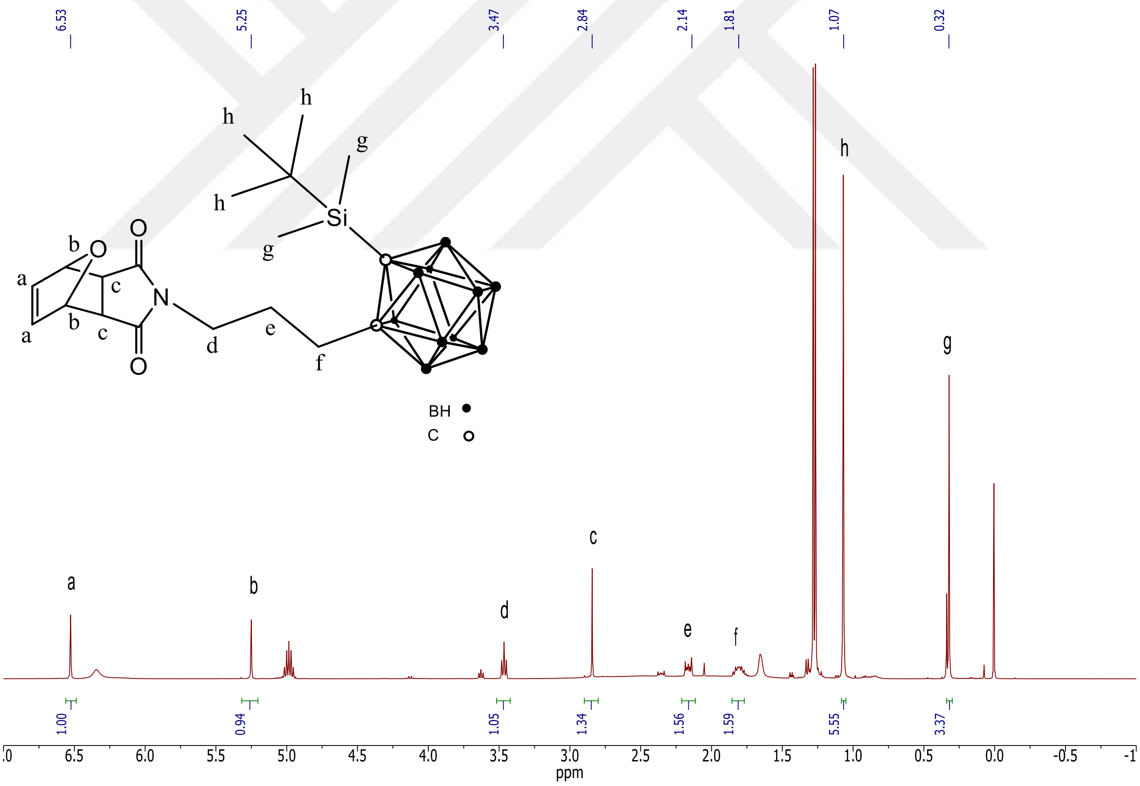

Figure 3.5 ^{1}H NMR (400.13 MHz) spectrum in $CDCl_3$ of monomer **2**

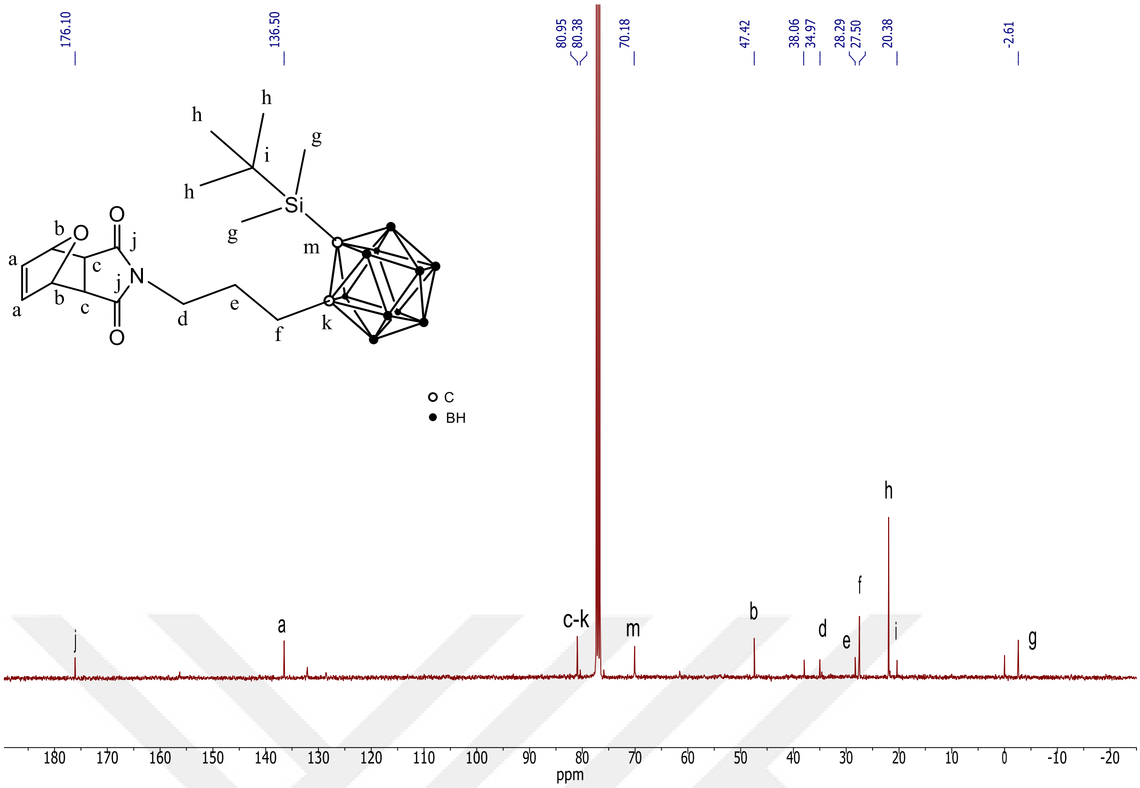

Figure 3.6 $^{13}C\{^{1}H\}$ NMR (100.16 MHz) spectrum in $CDCl_3$ of monomer **2**

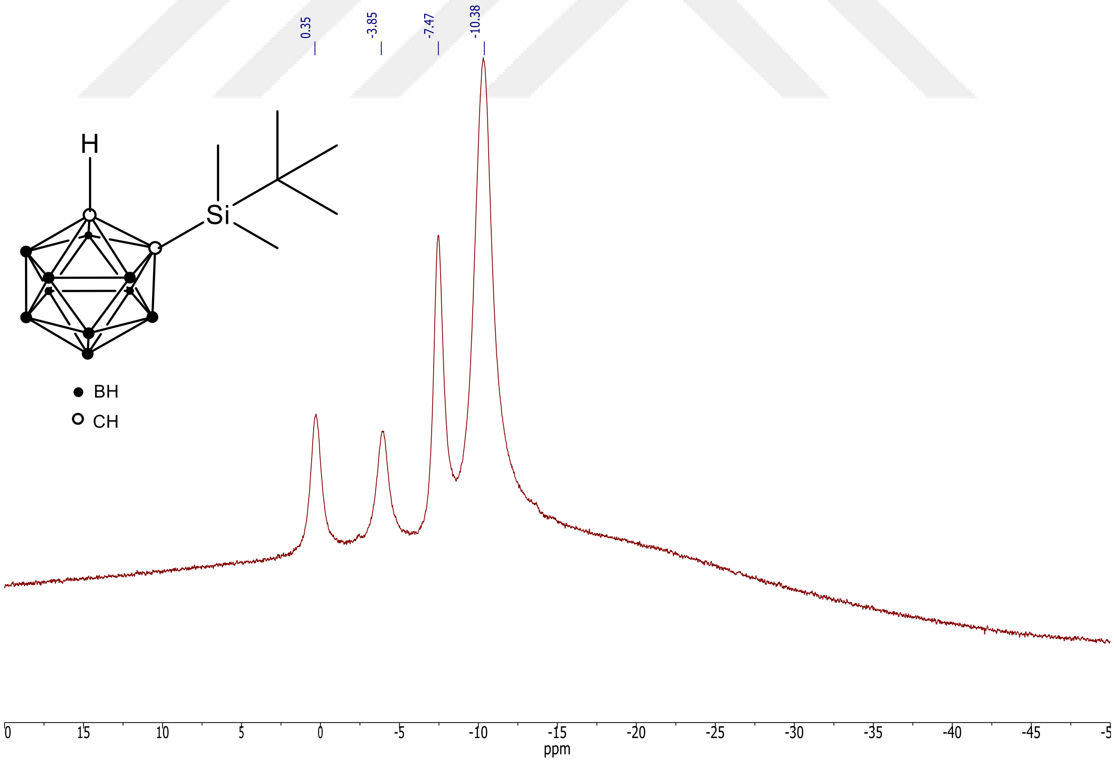

Figure 3.7 $^{11}B\{^{1}H\}$ NMR (128.37 MHz) spectrum in $CDCl_3$ of monomer **2**

3.1.3 Synthesis of Carborane- and Phosphonate Ester-containing ROMP-type Block Copolymers (P1, P2, P3)

The synthesis of ROMP block copolymers is shown in Scheme 3.3. The first monomer (monomer **1**) was homopolymerized at room temperature in dry dichloromethane under nitrogen atmosphere, until complete conversion occurred (typically in 30 minutes), as observed by TLC, ^{1}H NMR spectroscopy, or Gel Permeation Chromatography (GPC). After building the first block, the second monomer (monomer **2**) was added to the reaction flask, yielding the copolymer. The polymerization was finalised by addition of ethyl vinyl ether, and then an excess amount of petroleum ether was used for washing the final product. The polymers were dried in vacuum under nitrogen for 24 h. The ratio of blocks was designed as 1:4, 4:1 and 1:1 by weight, with the same molecular weight in total of 50 kDa. The block copolymers were obtained with low polydispersity, and the molecular weight of the polymers matched the theoretical values. Thermomechanical behaviour of all polymers was determined by TGA (Thermogravimetric Analysis) and DSC (Differential Scanning Calorimetry); furthermore, their flame-retardant effect was investigated by MCC (Micro Combustion Calorimetry).

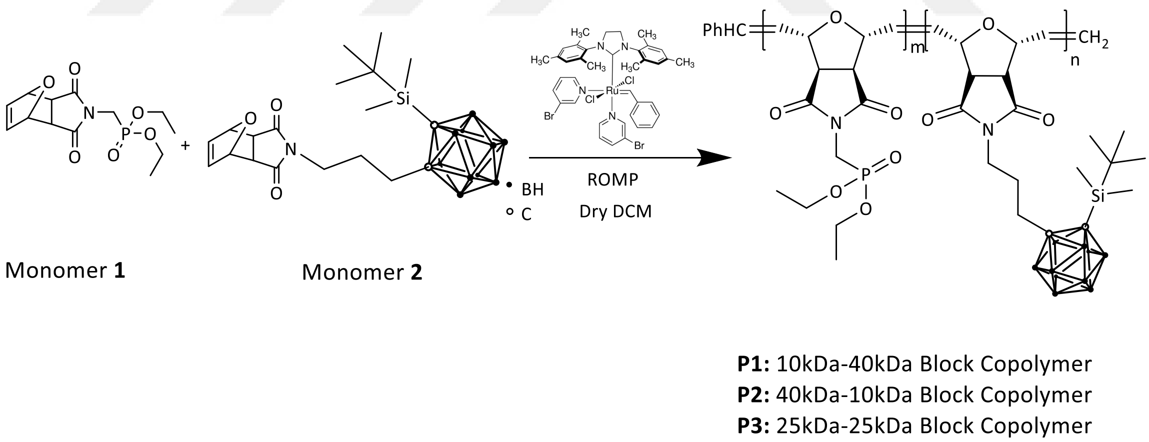

Scheme 3.3 The synthetic pathway for ROMP block copolymers

Figure 3.8, 3.13 and 3.18 (^{1}H NMR) show that polymerization was completed when olefin protons at 6.5 ppm of the monomer were completely gone, and new signals between 5.8 and 6.1 ppm for the double bond (*cis*/*trans*) in the polymer backbone appeared. Relative ratio of stereoisomers (*cis*/*trans*) was determined by comparing peaks at 6.1 ppm and 5.8 ppm in the ^{1}H NMR spectrum. It was observed that the ratio of *cis*/*trans* stereoisomers is around 60:40 in favor of the *cis* isomer. The polydispersity index ($Đ$) and the molecular weight distribution of the block copolymers were analyzed by SEC (Size Exclusion Chromatography) in DMF, using poly(methyl methacrylate) (PMMA) as standard.

Table 3.1 Summary of characterization of the carborane- and phosphonate ester-containing ROMP-type block copolymers (**P1**, **P2** and **P3**)

Polymer	m[a]	n[b]	Mol Ratio th (m/n)[c]	Mol Ratio obs (m/n)[d]	$M_{n/block}$ Th (g/mol)[e]	$M_{n/block}$ NMR (g/mol)[f]	$Đ$[g]	cis/trans Ratio[h]
P1	31.75	86.33	0.37	0.42	50 000	56 756	1.06	1.48
P2	127	21.59	5.88	6.48	50 000	55 102	1.09	1.43
P3	79.365	53.95	1.47	1.59	50 000	54 081	1.03	1.44

a: Theoretical degree of polymerization (DP) of monomer **1**.

b: Theoretical DP of monomer **2**.

c: Theoretical molar ratio of monomers.

d: Calculated molar ratio using NMR.

e: Theoretical number-average molecular weight.

f: M_n calculated by NMR.

g: Polydispersity index (Đ) determined by SEC.

h: cis/trans ratio in the polymer backbone observed by ^{1}H NMR spectroscopy.

Based on the SEC results, the polydispersity index of the polymers is between 1.03 and 1.09, which is generally considered as narrow weight distribution. End group analysis method was applied to calculate the molecular weight of the polymers (M_n). Styrene end group protons stem from the carbene moiety of the Grubbs catalyst [76], [89], [90] and appear at ca. $\delta \sim 7.20$-7.50 ppm; the degree of polymerization was calculated based on these protons. The results, summarized in Table 3.1, clearly indicate that the observed molecular weight of the polymers is close to the theoretical one.

The ratio of the number of carborane repeating units (n, Table 3.1) to the number of phosphonate repeat units (m, Table 3.1) was determined by ^{1}H NMR spectroscopy. NMR samples were prepared and measured in $CDCl_3$. For instance, the peak at 4.13 ppm represents four protons for the phosphonate group (−P−OC**H**$_2$−), and the signal at 0.33 ppm shows six protons for the $SiMe_2$ group (the ^{1}H NMR spectra of **P1**, **P2** and **P3** in Figure 3.8, 3.13 and 3.18, respectively). The feed ratios of other copolymers, targeted and observed molecular weight analyzed by SEC and also found by NMR [16] are presented in Table 3.1. The molecular weights of the first repeating units (phosphonate part) in **P3** was 315 g/mol and second repeating units (carborane part) in **P3** was 463 g/mol; moreover, the ratio of the target repeating units was known as 79.4:53.9 (polymer **P3**, Table 3.1), then the theoretical number average molecular weight was ($M_{n,th}$) = (315 x 79.4) + (436 x 53.9) = 50 000 g/mol. The calculated molecular weight of **P3** based on styrenic end group analysis via NMR was 54 081 g/mol.

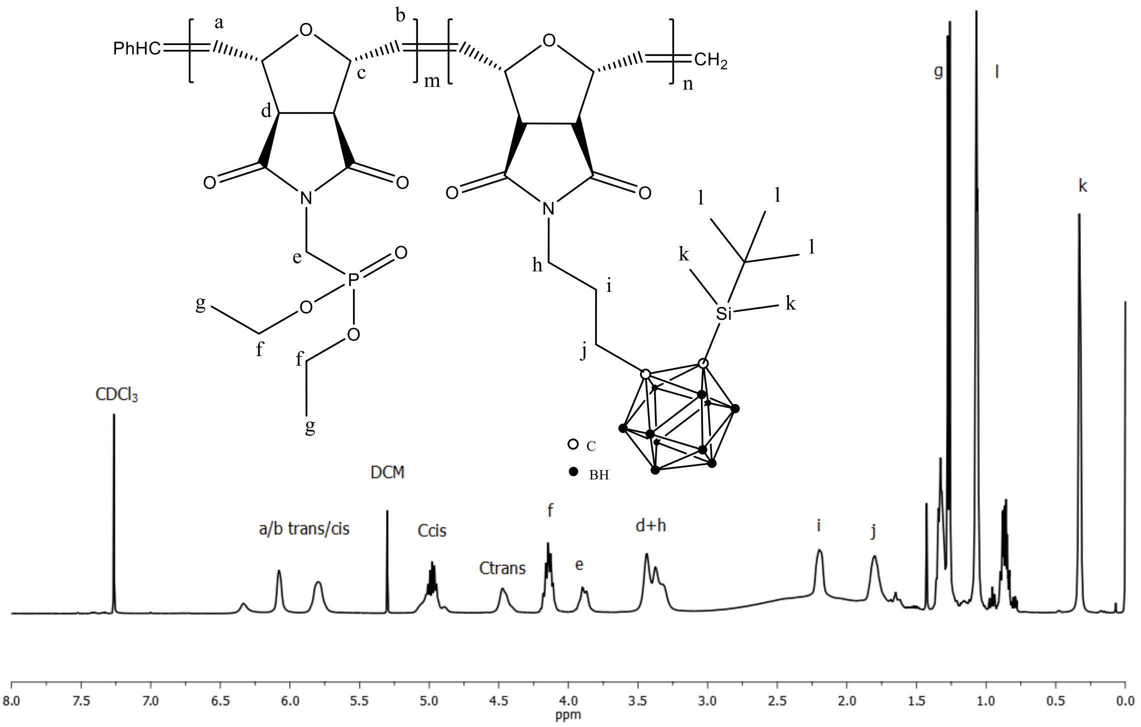

Figure 3.8 ^1H NMR (400.13 MHz) spectrum in $CDCl_3$ of ROMP block copolymer (**P1**)

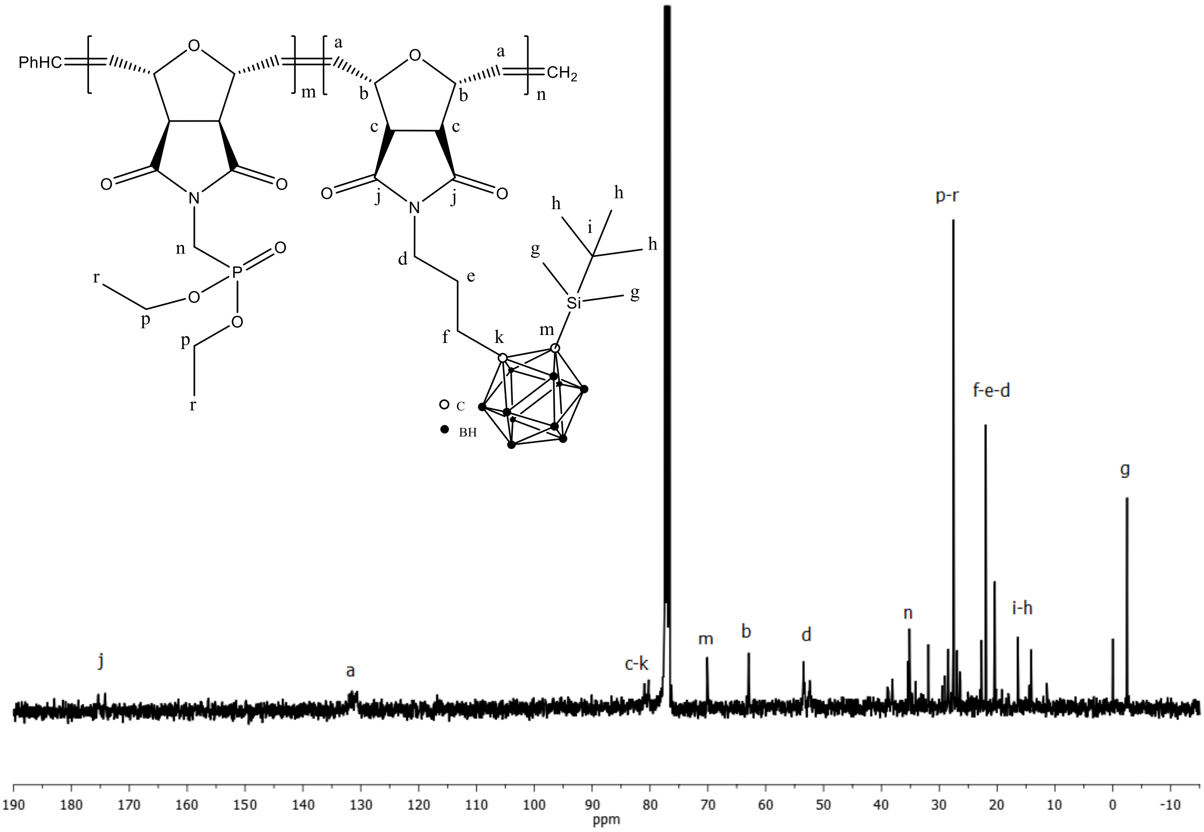

Figure 3.9 $^{13}C\{^{1}H\}$ NMR (100.16 MHz) spectrum in $CDCl_3$ of ROMP block copolymer (**P1**)

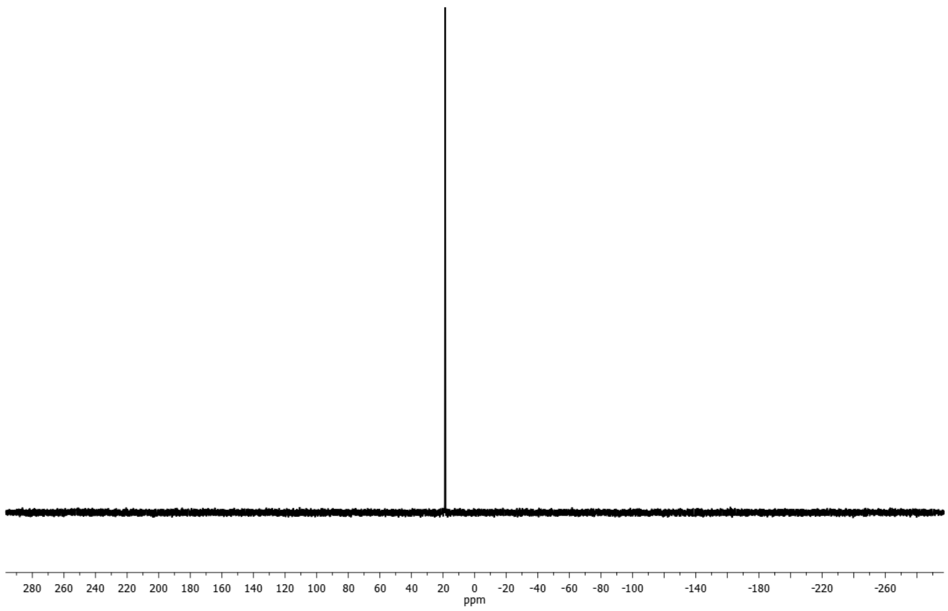

Figure 3.10 $^{31}P\{^{1}H\}$ NMR (161.97 MHz) spectrum in $CDCl_3$ of ROMP block copolymer (**P1**)

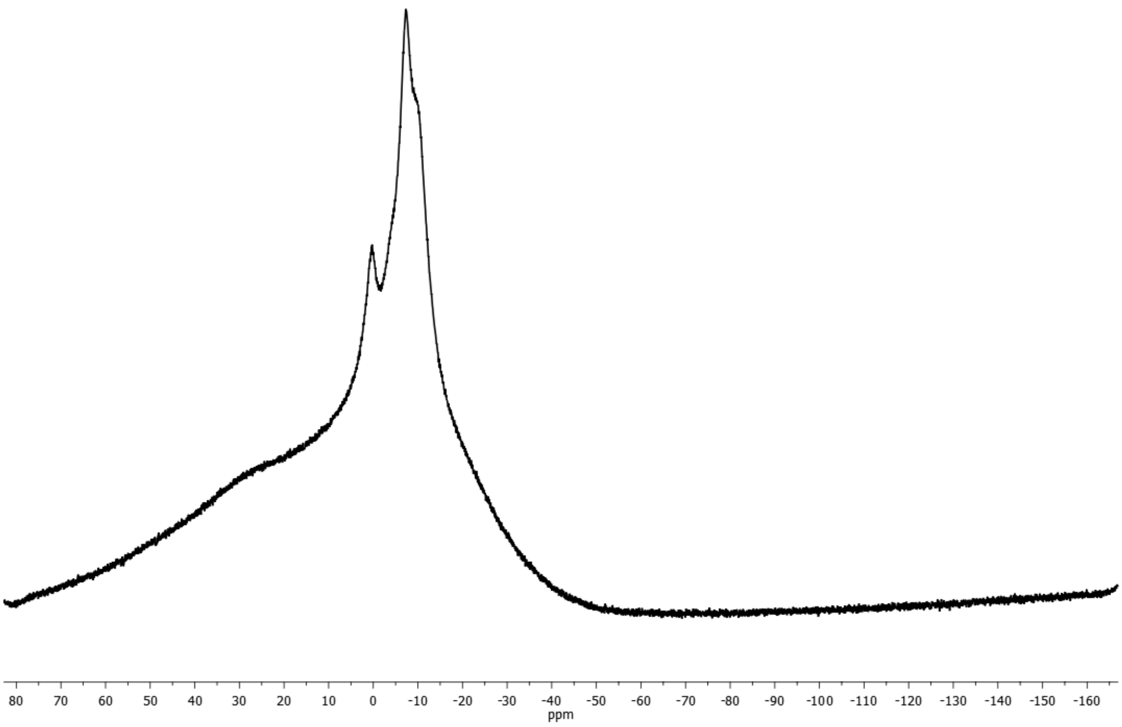

Figure 3.11 $^{11}B\{^{1}H\}$ NMR (128.37 MHz) spectrum in $CDCl_3$ of ROMP block copolymer (**P1**)

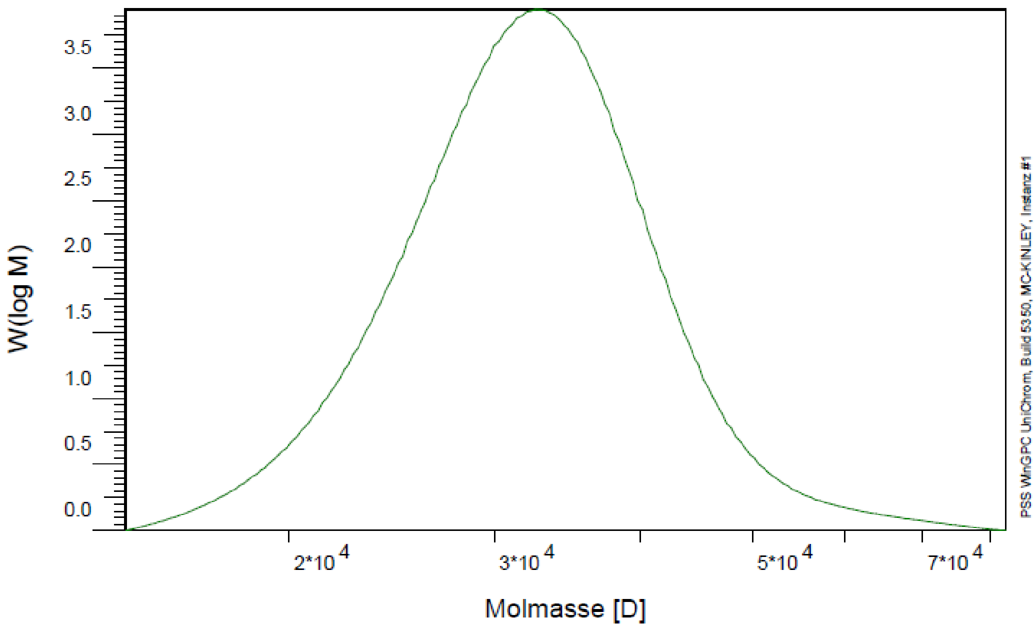

Figure 3.12 GPC spectrum of ROMP block copolymer (**P1**) (W (log M): molar mass distribution).

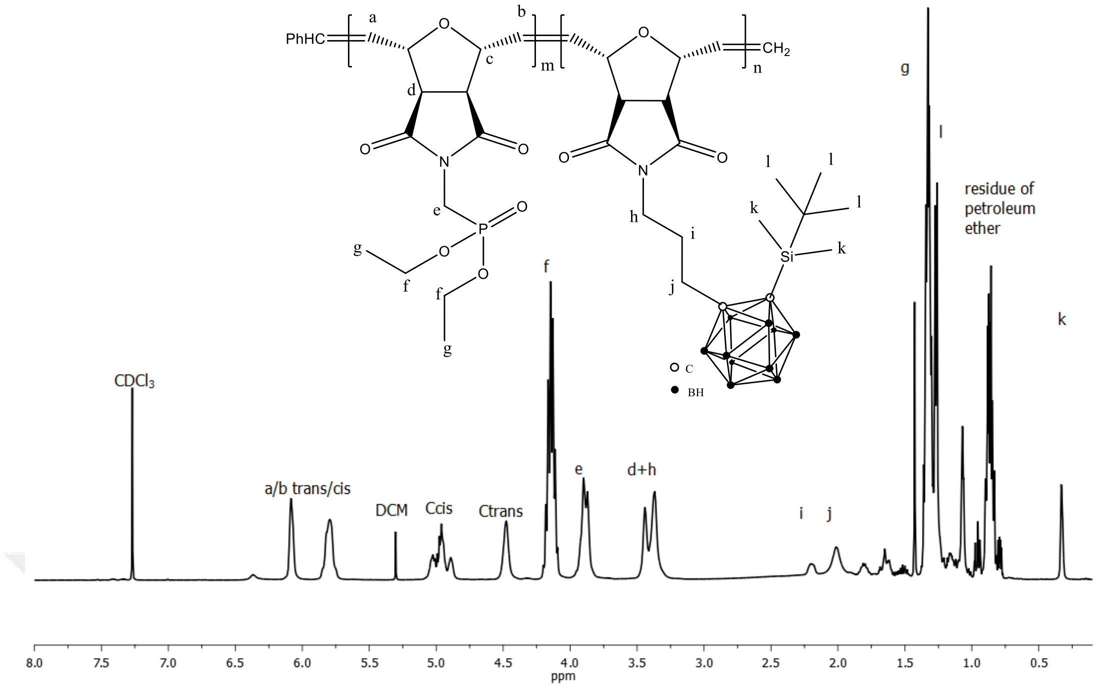

Figure 3.13 ^{1}H NMR (400.13 MHz) spectrum in $CDCl_3$ of ROMP block copolymer (**P2**)

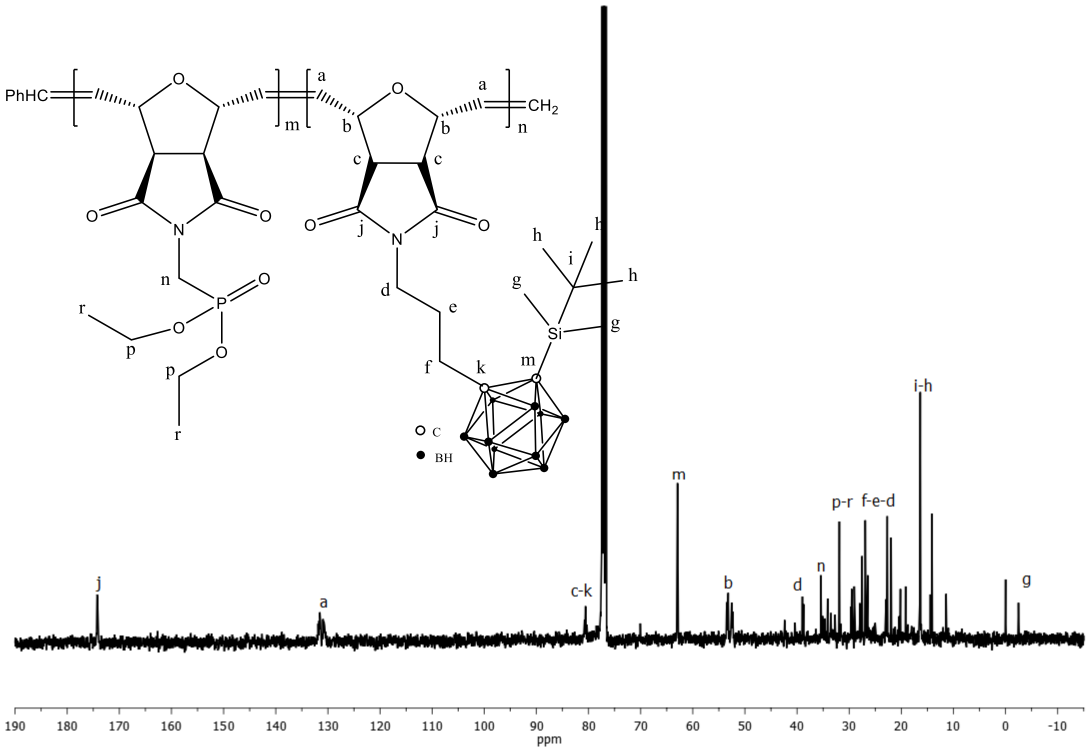

Figure 3.14 $^{13}C\{^{1}H\}$ NMR (100.16 MHz) spectrum in $CDCl_3$ of ROMP block copolymer (**P2**)

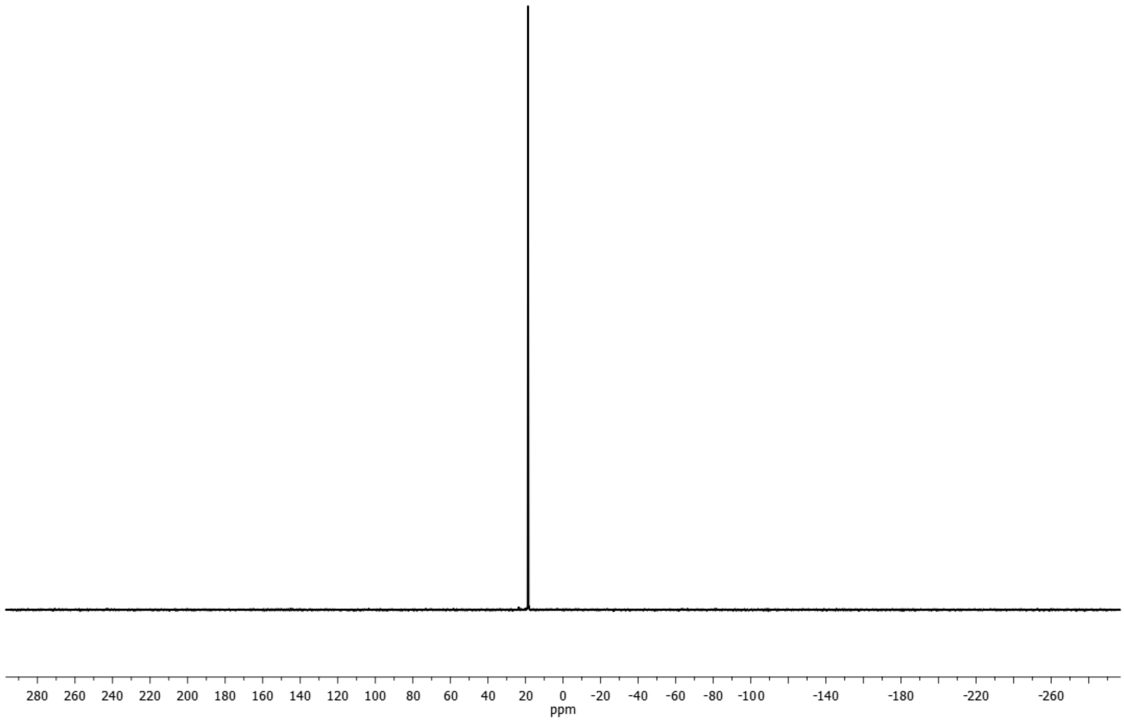

Figure 3.1 $^{31}P\{^1H\}$ NMR (161.97 MHz) spectrum in $CDCl_3$ of ROMP block copolymer (**P2**)

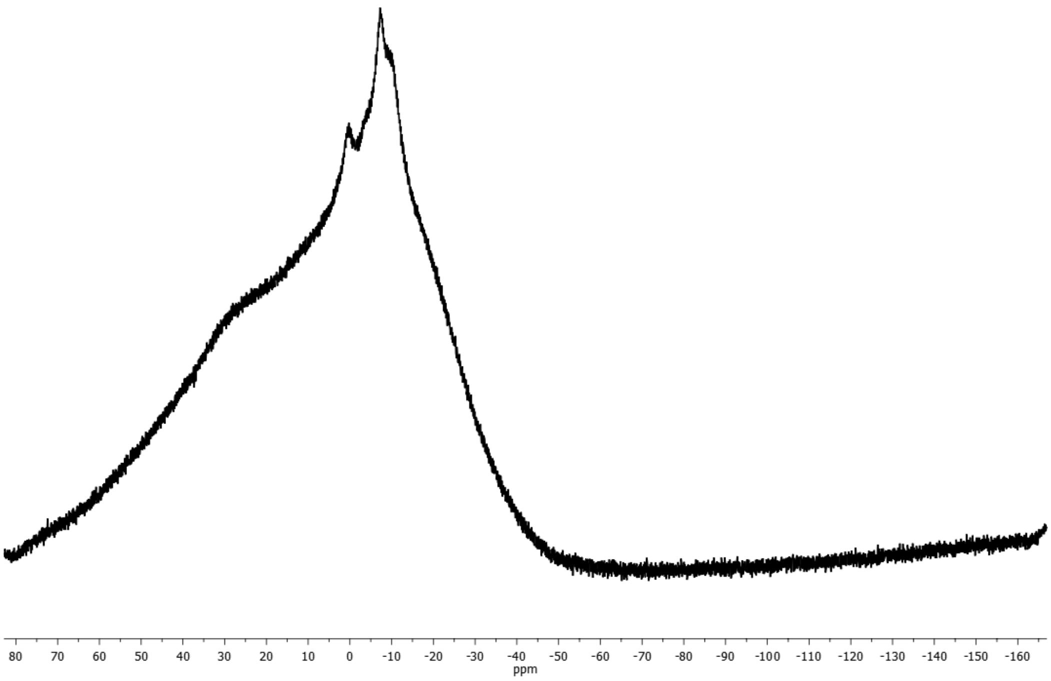

Figure 3.16 $^{11}B\{^1H\}$ NMR (128.37 MHz) spectrum in $CDCl_3$ of ROMP block copolymer (**P2**)

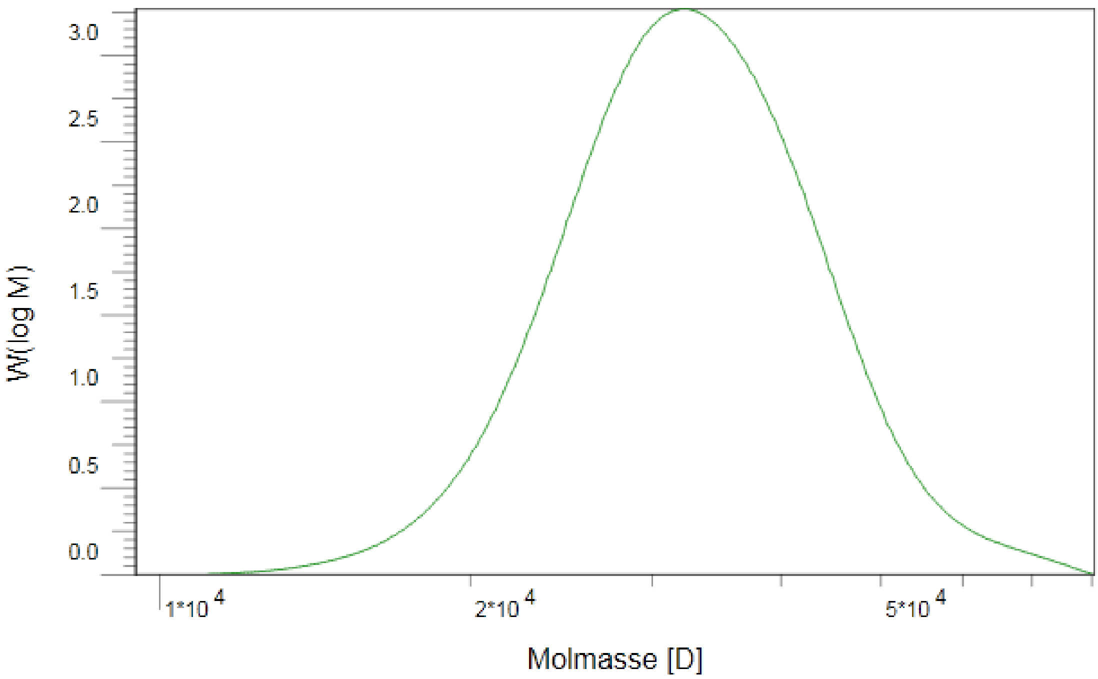

Figure 3.17 GPC spectrum of ROMP block copolymer (**P2**) (W (log M): molar mass distribution)

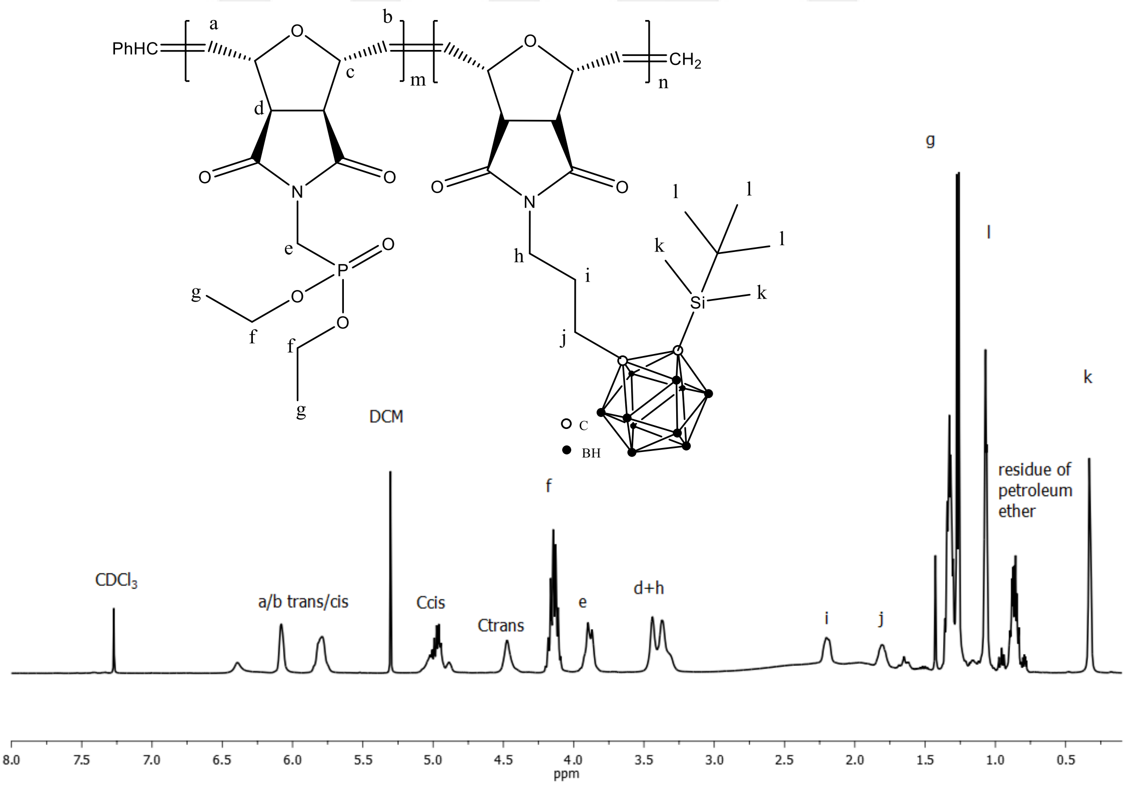

Figure 3.18 ^{1}H NMR (400.13 MHz) spectrum in $CDCl_3$ of ROMP block copolymer (**P3**)

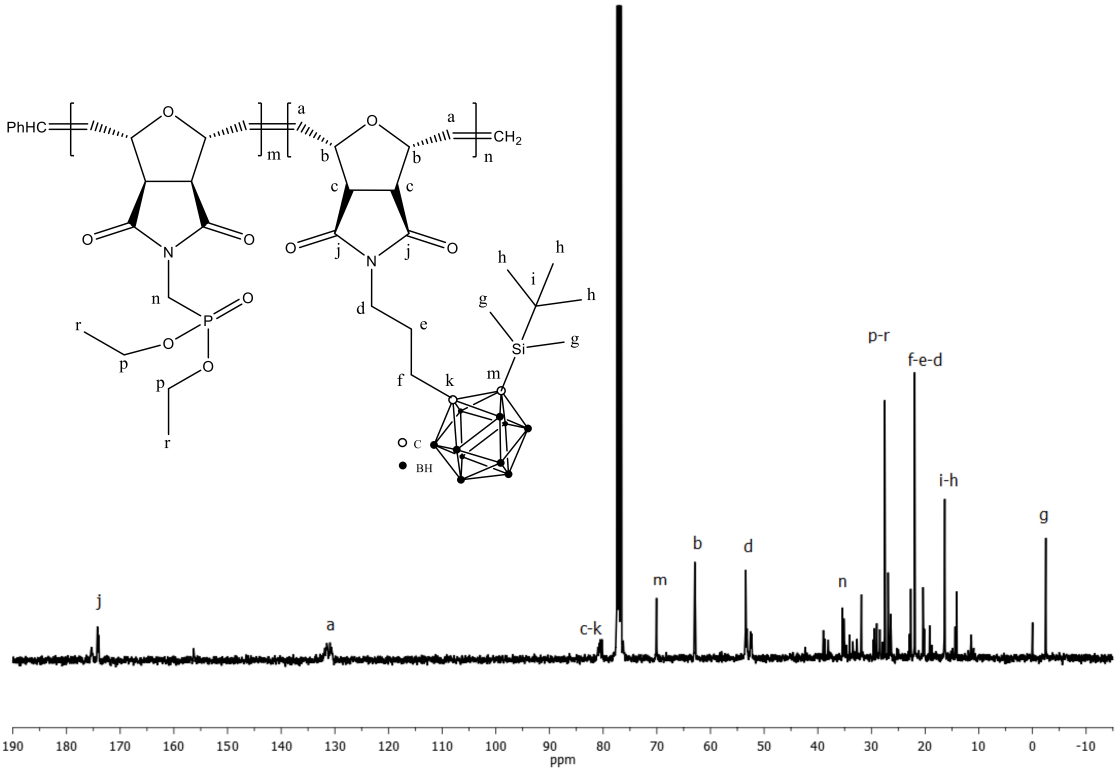

Figure 3.19 $^{13}C\{^{1}H\}$ NMR (100.16 MHz) spectrum in $CDCl_3$ of ROMP block copolymer (P3)

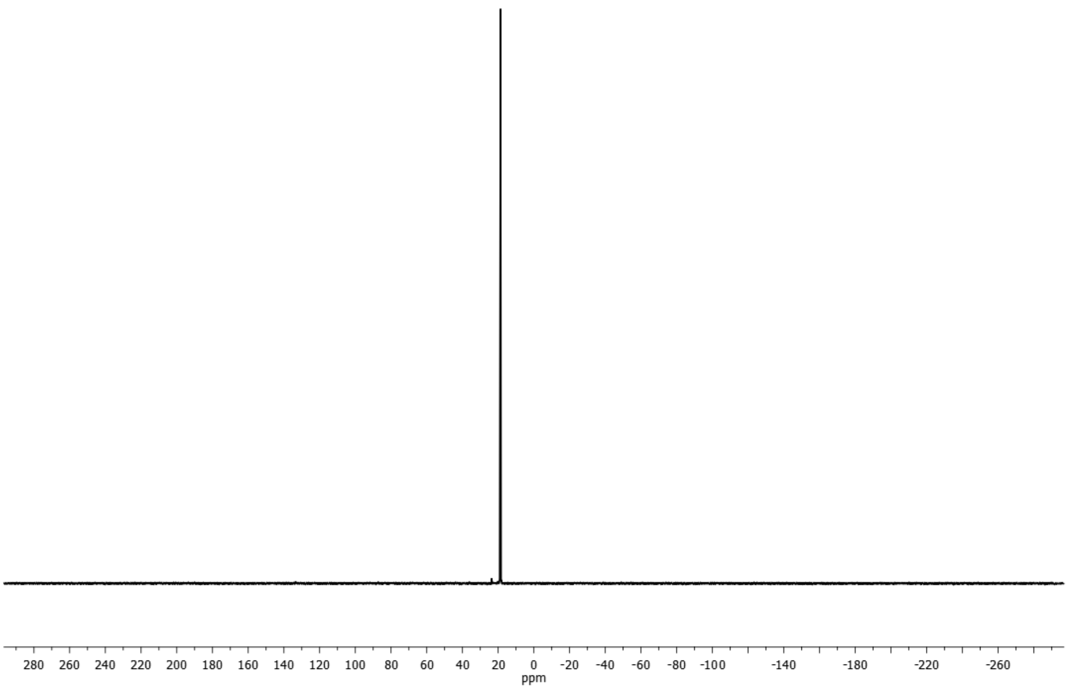

Figure 3.20 $^{31}P\{^{1}H\}$ NMR (161.97 MHz) spectrum in $CDCl_3$ of ROMP block copolymer (**P3**).

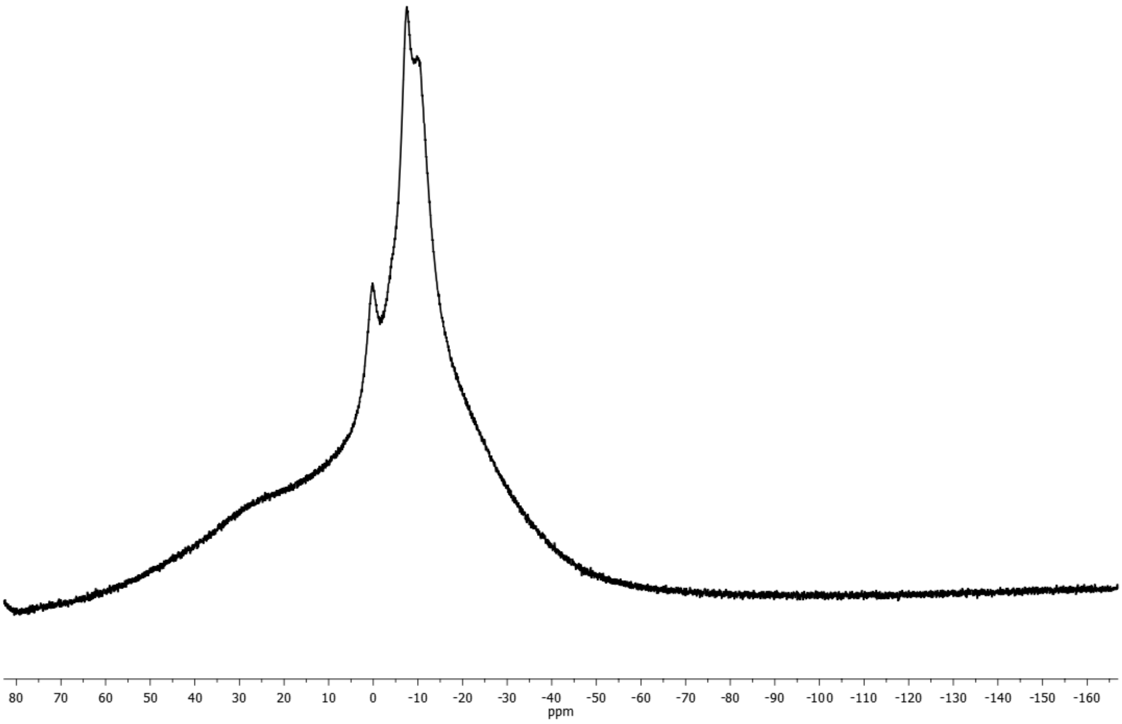

Figure 3.21 $^{11}B\{^1H\}$ NMR (128.37 MHz) spectrum in $CDCl_3$ of ROMP block copolymer (**P3**)

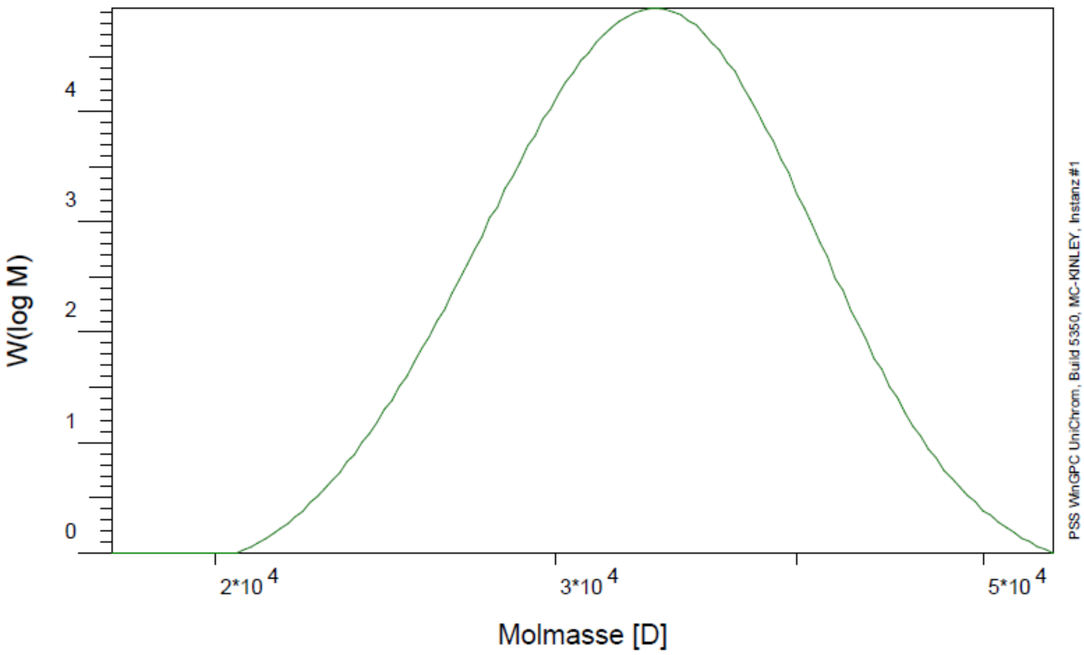

Figure 3.22 GPC spectrum of ROMP block copolymer (**P3**) (W (log M): molar mass distribution)

3.1.4 Carborane- and Phosphonic Acid-containing ROMP-type Block Copolymers

Phosphoric acid derivatives can be useful in chemical industry thanks to their properties as, for example, metal ion chelators or proton conductors for fuel cell membranes under anhydrous conditions [129]. Furthermore, they typically enhance the fire-retardant performance of a material and have found application in the biomedical area, such as in dental composites, with a good chelation efficiency to dentin [50].

In this study, the phosphonate ester groups of the block ROMP polymers **P1**, **P2** and **P3** were hydrolyzed in methanol/dichloromethane (3:1, (v/v)) in the presence of trimethylsilylbromide, yielding the respective phosphoric acid-containing polymers **P1A**, **P2A** and **P3A** (Scheme 3.4).

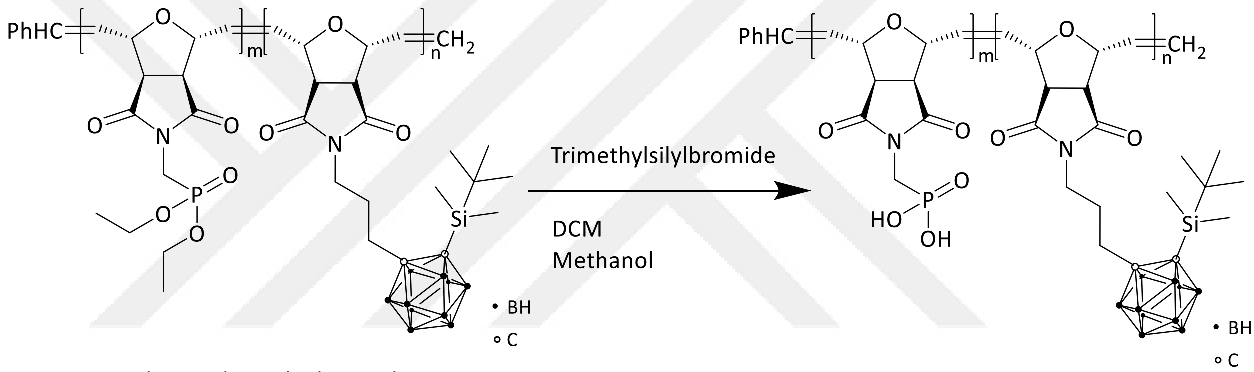

Scheme 3.4 The synthetic pathway for hydrolyzed ROMP-based block copolymers

The products were obtained as rubbery soft solids after purification. **P1A**, **P2A** and **P3A** were characterized by NMR spectroscopy (Figure 3.23, 3.25, 3.27). NMR samples for each polymer were prepared and measured in DMSO-d_6. The peak at 4.13 ppm, which represents four protons for the phosphonate group (−P−OC**H**$_2$−), in the ^{1}H NMR spectrum disappeared after cleavage. Furthermore, ^{31}P{^{1}H} NMR spectroscopy was the most informative to analyse the conversion. The ^{31}P{^{1}H} NMR spectrum of **P1A**, **P2A** and **P3A** confirmed a replacement by shifts from 18.4 to 14.1 ppm for **P1A** (Figure 3.24), from 19.2 to 14.1 ppm for **P2A** (Figure 3.26), and from 18.5 to 14.1 ppm for **P3A** (Figure 3.28) referring to the phosphonate ester and phosphoric acid, respectively.

In a typical example, Figure 3.27 shows the FT-IR spectrum of ROMP block copolymer **P2** with the strong stretching vibration at 1260 cm^{-1} indicating the phosphonate group (P=O) which disappeared after conversion to the corresponding phosphoric acid (**P2A**).

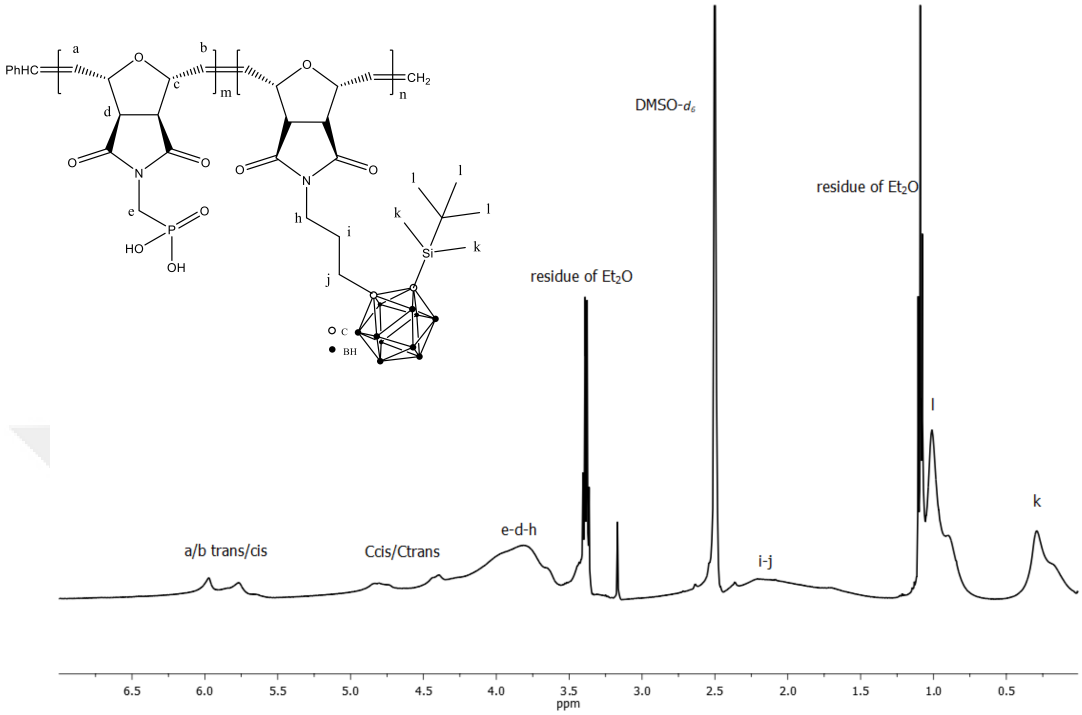

Figure 3.23 ^{1}H NMR (400.13 MHz) spectrum in DMSO-d_6 of hydrolyzed ROMP block copolymer (**P1A**)

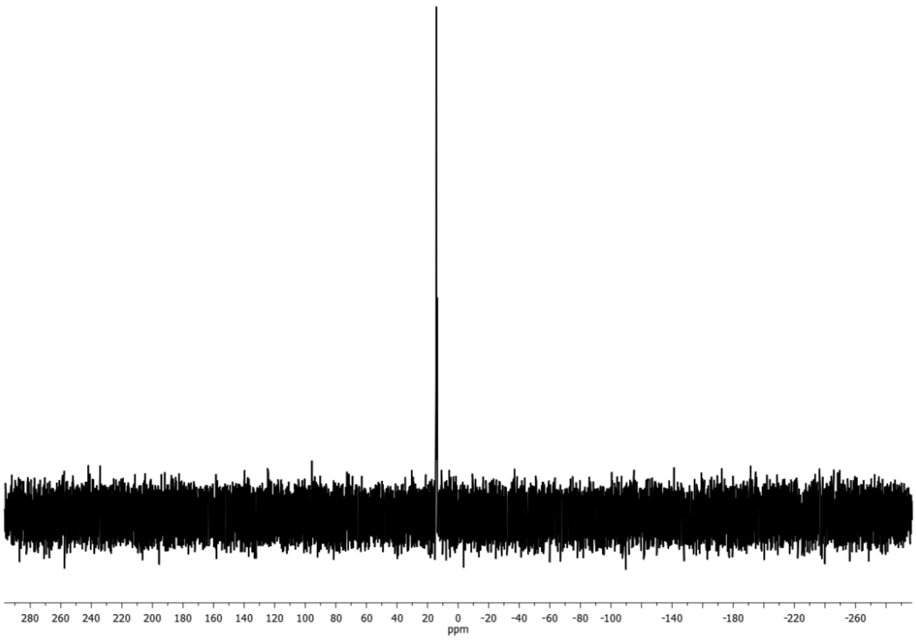

Figure 3.24 $^{31}P\{^{1}H\}$ NMR (161.97 MHz) spectrum in DMSO-d_6 of hydrolyzed ROMP block copolymer (**P1A**)

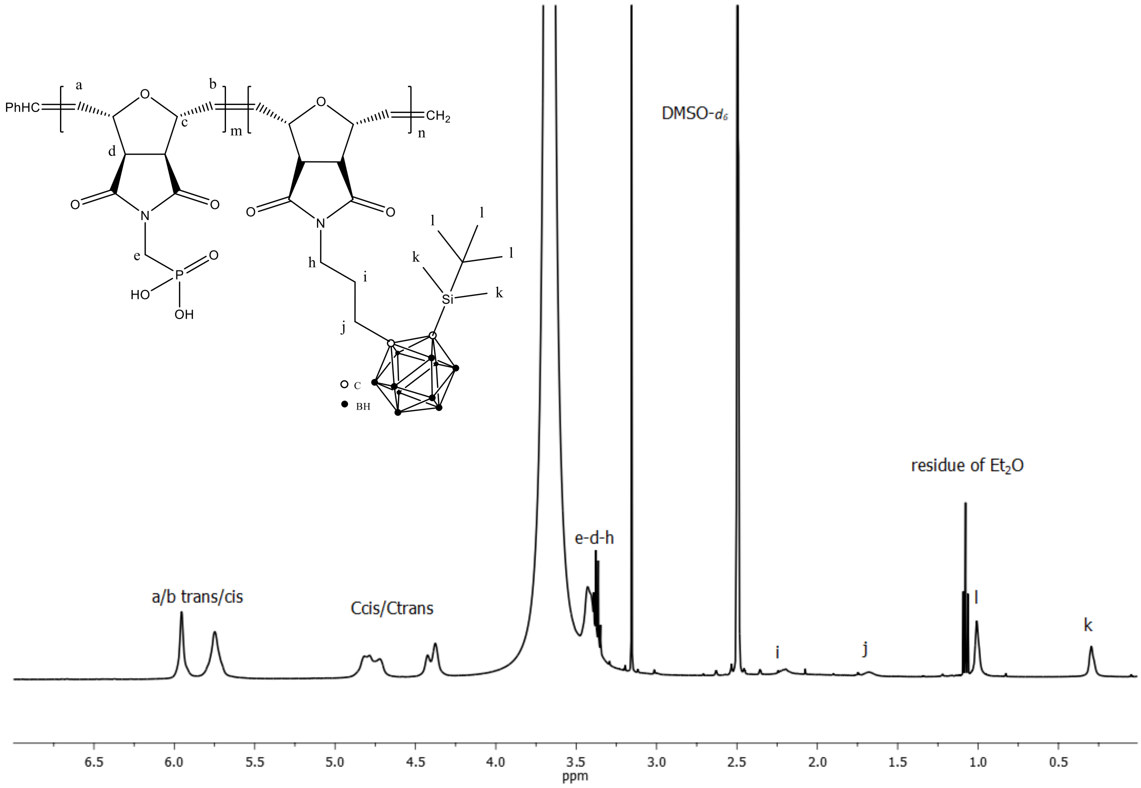

Figure 3.25 ^{1}H NMR (400.13 MHz) spectrum in DMSO-d_6 of hydrolyzed ROMP block copolymer (**P2A**)

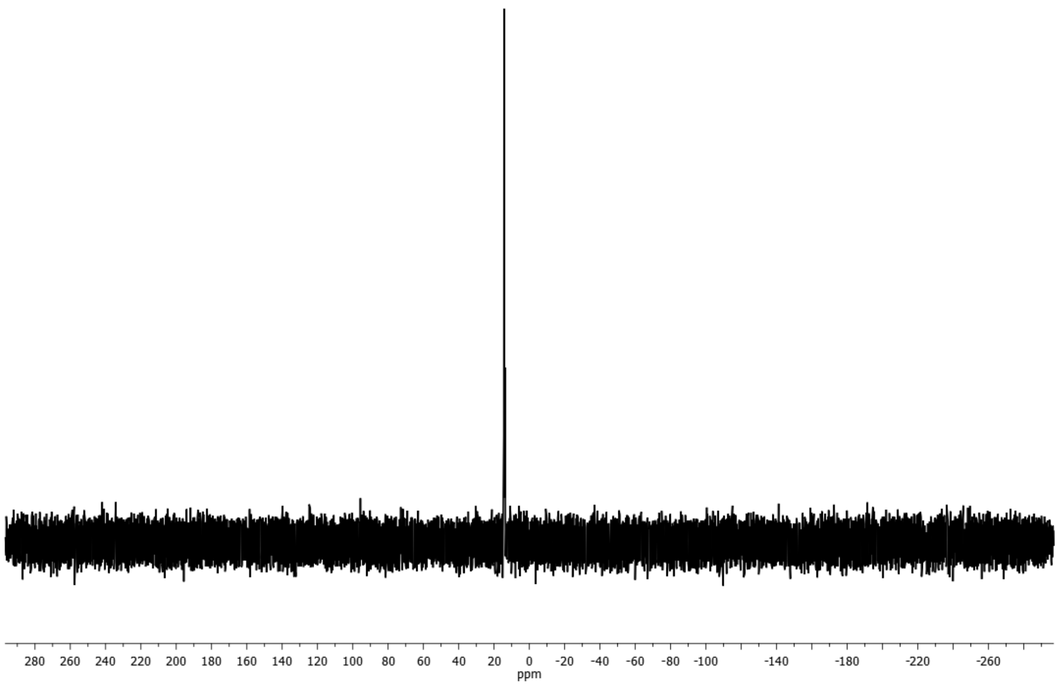

Figure 3.26 ^{31}P{^{1}H} NMR (161.97 MHz) spectrum in DMSO-d_6 of hydrolyzed ROMP block copolymer (**P2A**)

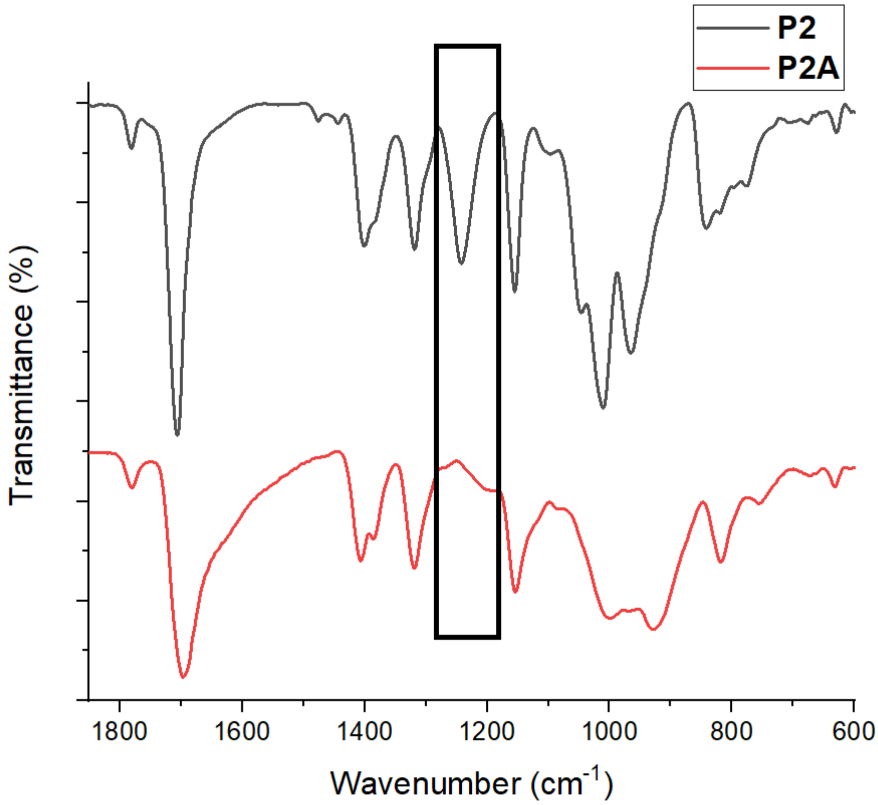

Figure 3.27 FT-IR spectra of ROMP block copolymer (**P2**) and hydrolyzed ROMP block copolymer (**P2A**)

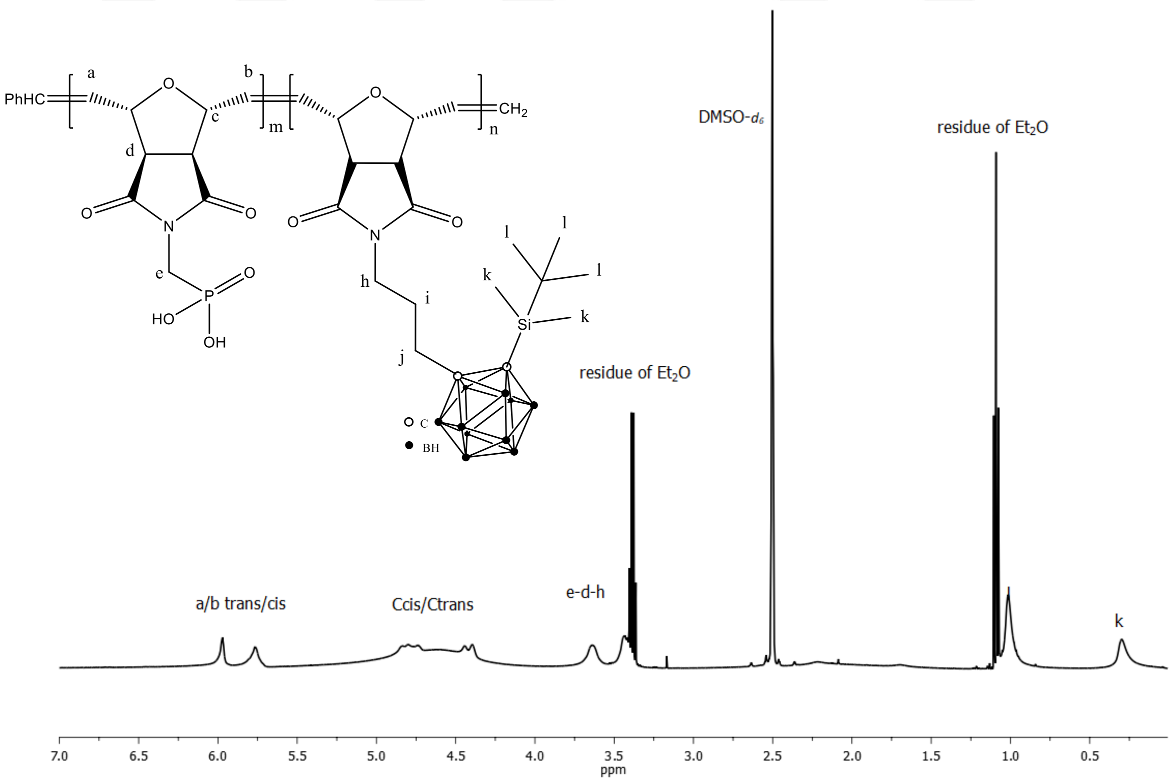

Figure 3.28 ^{1}H NMR (400.13 MHz) spectrum in DMSO-d_6 of hydrolyzed ROMP block copolymer (**P3A**)

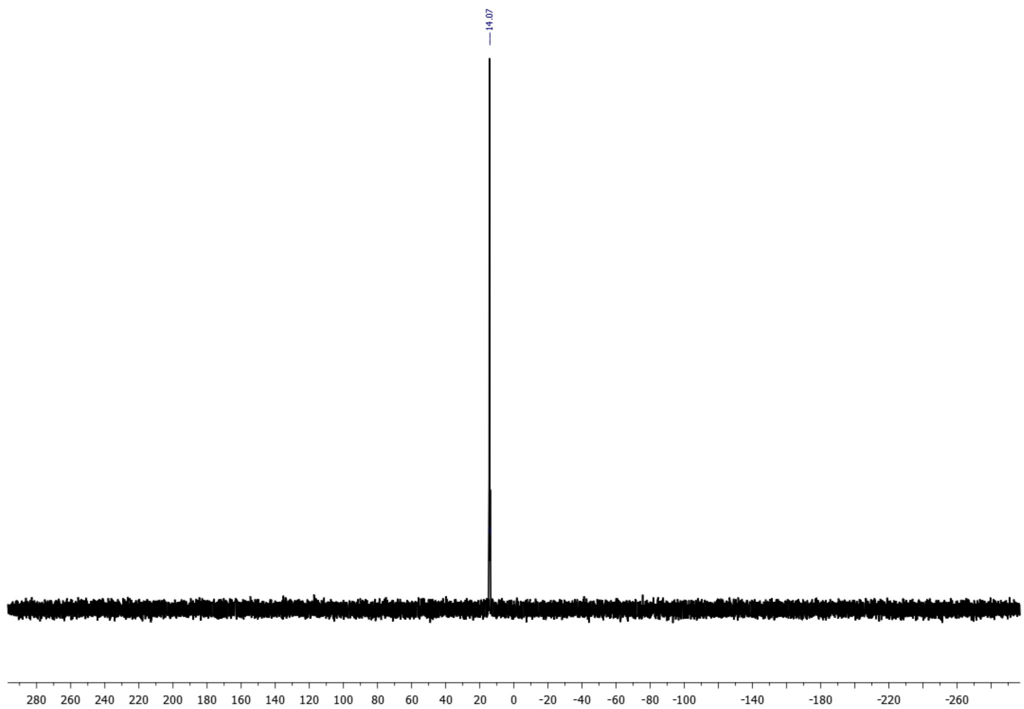

Figure 3.29 $^{31}P\{^{1}H\}$ NMR (161.97 MHz) spectrum in DMSO-d_6 of hydrolyzed ROMP block copolymer (**P3A**)

3.1.5 Carborane and Phosphonate Ester-containing ROMP Random Copolymers

Monomer **1** and monomer **2** were polymerized in dry dichloromethane at room temperature with Grubbs 3rd generation catalyst, via ROMP method. Polymerization was terminated by the addition of an excess amount of ethyl vinyl ether (in dry dichloromethane), and then the product was immediately precipitated with excess petroleum ether. The reaction progress was monitored via TLC (4:1 ethyl acetate/*n*-hexane (v/v)). The polymer was washed with petroleum ether and dried under nitrogen. Polymers were dissolved in $CDCl_3$ for NMR measurements and Table 3.2 summarizes the composition of copolymers, as obtained from NMR data.

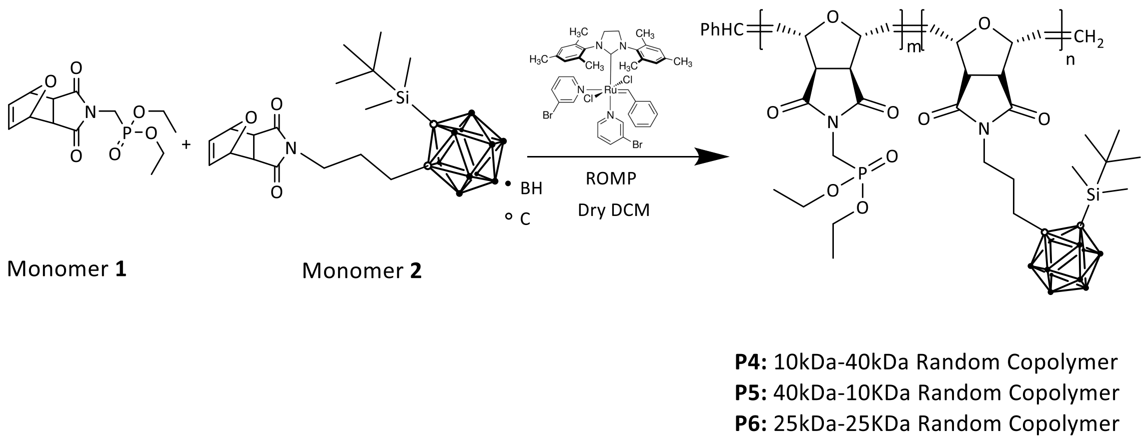

Scheme 3.5 The synthetic pathway for ROMP random copolymers

The appearance of the signals at 6.08–5.79 ppm, concomitant with the disappearance of the characteristic olefinic signals of the monomers at 5.50–6.50 ppm, proved that polymerization had occurred with high conversion. In order to evaluate the stereochemistry of the double bonds, the ratios of the signals c_{cis} and c_{trans} has been compared, as indicated in the ^{1}H NMR spectra. The signal of *cis* protons belonging to the polymers **P5** and **P6** is much greater than the signal of *trans* protons, namely c_{cis}/c_{trans} = 1.44/1.00 for **P5**, and c_{cis}/c_{trans} = 1.32/1.00 for **P6**. On the other hand, for **P4** the c_{cis}/c_{trans} ratio is 1:1.

Table 3.2 Characterization data for the random copolymers **P4–P6**.

Polymer	m[a]	n[b]	Mol Ratio Th (m/n)[c]	Mol Ratio Obs (m/n)[d]	$M_{n/block}$ Th (g/mol)[e]	$M_{n/block}$ NMR (g/mol)[f]	$M_{n/random}$ GPC (g/mol)[g]	PDI[g]	Cis/trans Ratio[h]	P % [i]
P4	31.75	86.33	0.37	0.7	50 000	56 756	24,465	1.11	1.00	4.12
P5	127	21.59	5.88	8.5	50 000	55 102	37,689	1.44	1.41	8.8
P6	79.365	53.95	1.47	2.18	50 000	54 081	14,605	1.16	1.32	21.54

a: Theoretical degree of polymerization (DP) of monomer **1**.

b: Theoretical DP of monomer **2**.

c: Theoretical molar ratio of monomers.

d: Calculated molar ratio using NMR.

e: Theoritical number-average molecular weight.

f: M_n calculated by NMR.

g: M_n and polydispersity index (PDI) are determined by GPC.

h: cis/trans ratio in the polymer backbone observed by ^{1}H-NMR.

i: Phosphorous percentage in the polymer backbone.

The ratio of repeating unit numbers of the copolymer **P5**, phosphorus-based (m, Scheme 3.5) to the repeat unit numbers of the carborane-based (n, Scheme 3.5) moiety were calculated by the observation of coincident ^{1}H NMR peaks. As an example, the phosphonate ester protons (−P−OC**H**$_2$−) indicated by *f* (Figure 3.30) at 4.18 ppm refer to four protons in one polymer unit, while the signal at 0.32 ppm (*k* in Figure 3.30) indicates six protons in the carborane-based backbone. Thus, the ratio of proton signal for the phosphonate ester-based unit to the proton signal for the carborane-based unit according to the NMR spectrum was found as 1.1 (m_{obs}) to 0.13 (n_{obs}), resulting in the ratio m:n ~1:0.12.

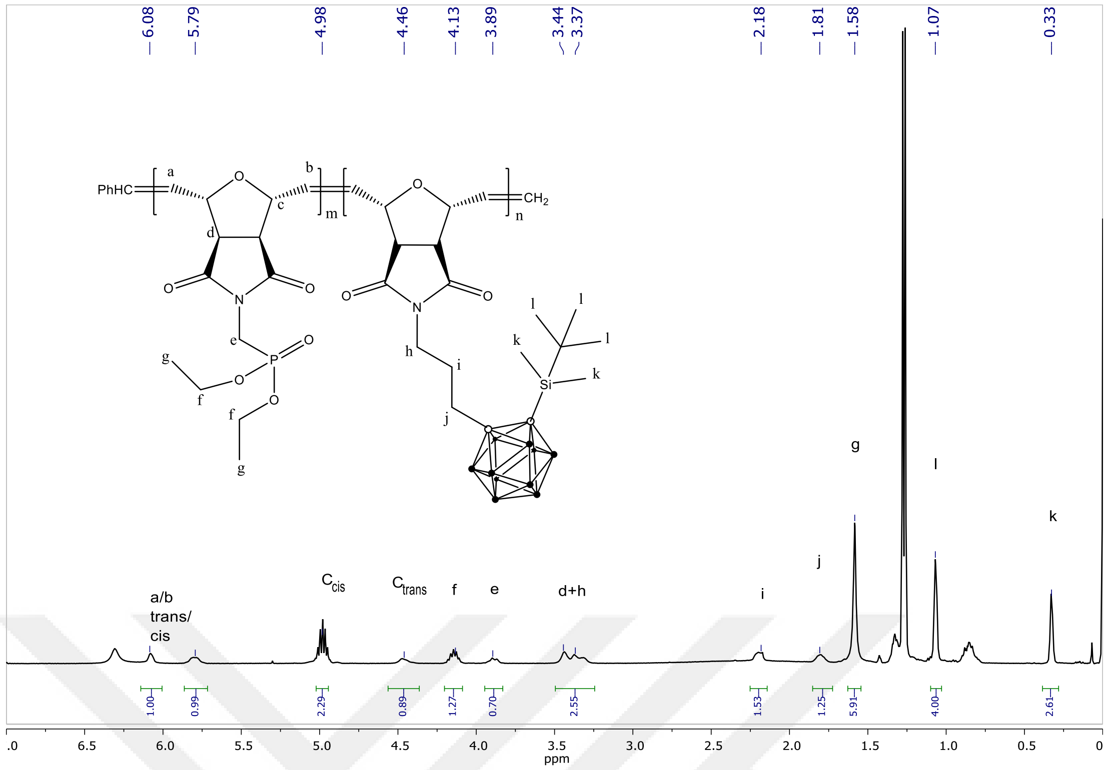

Figure 3.30 ^{1}H NMR (400.13 MHz) spectrum in $CDCl_3$ of ROMP random copolymer (**P4**)

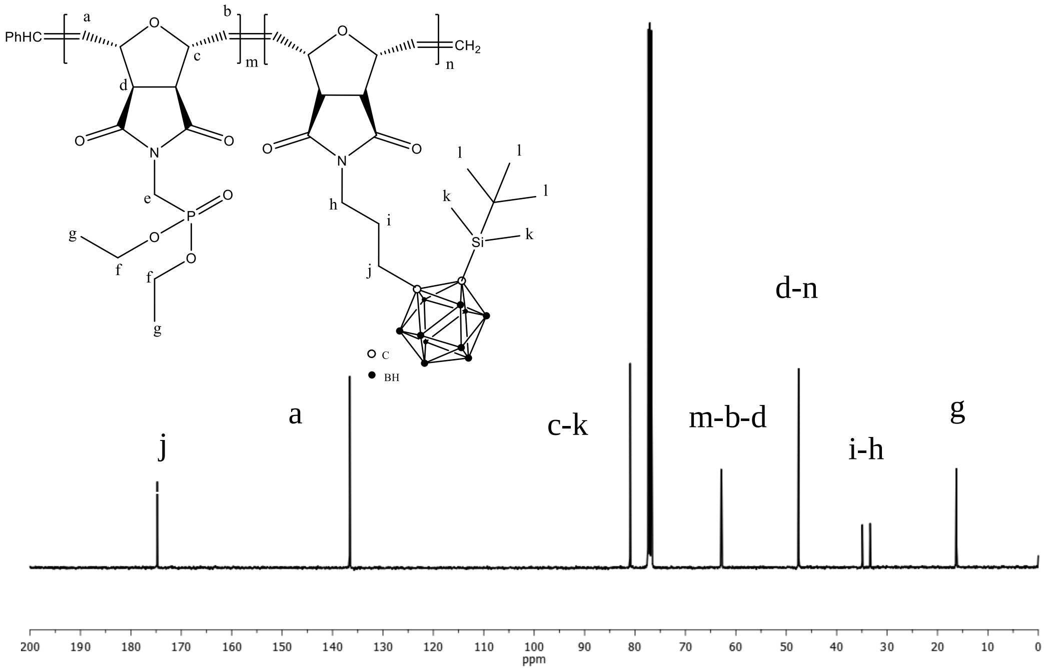

Figure 3.31 $^{13}C\{^{1}H\}$ NMR (100.16 MHz) spectrum in $CDCl_3$ of ROMP random copolymer (**P4**)

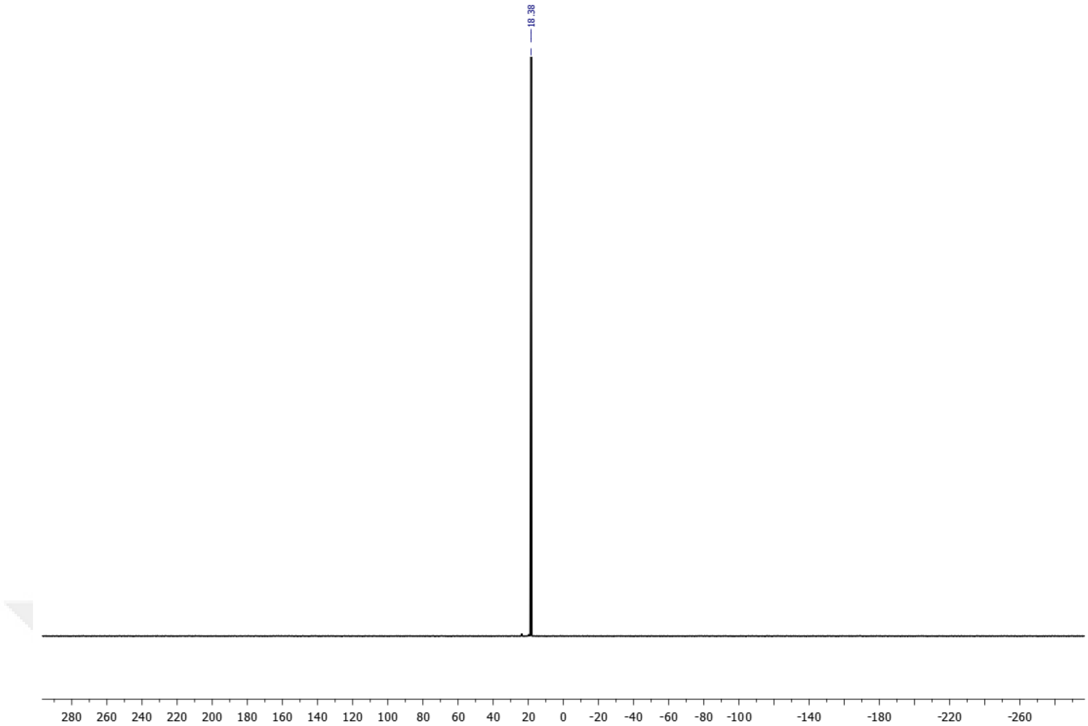

Figure 3.32 $^{31}P\{^1H\}$ NMR (161.97 MHz) spectrum in $CDCl_3$ of ROMP random copolymer (**P4**)

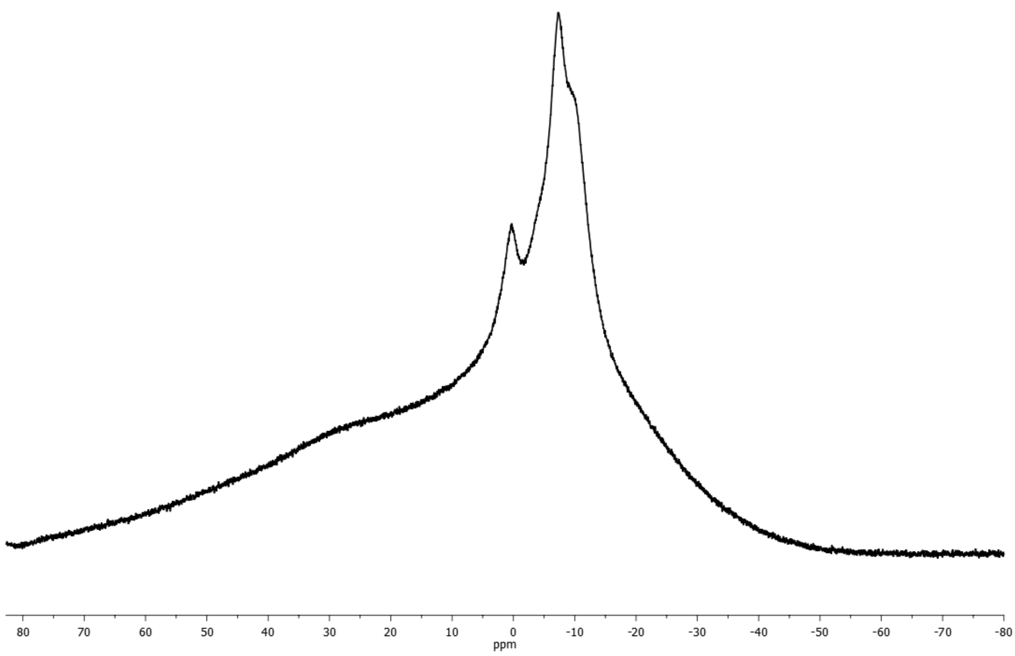

Figure 3.33 $^{11}B\{^1H\}$ NMR (128.37 MHz) spectrum in $CDCl_3$ of ROMP random copolymer (**P4**)

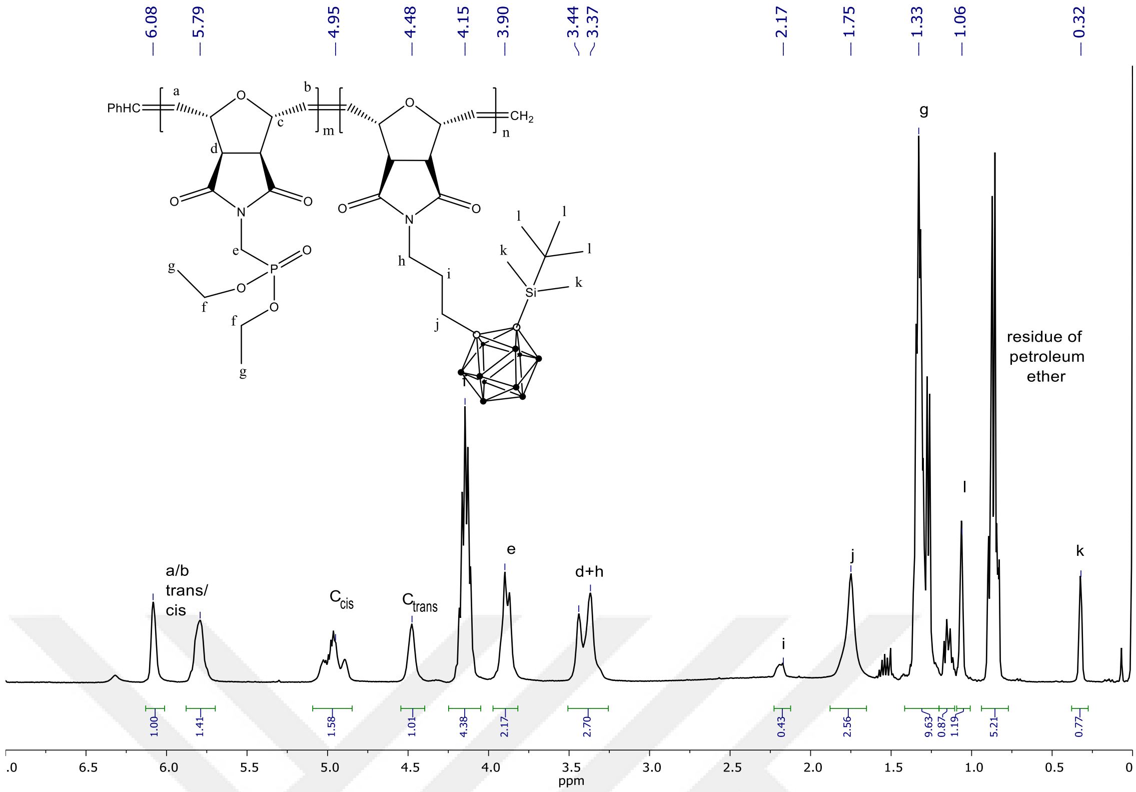

Figure 3.34 ^{1}H NMR (400.13 MHz) spectrum in $CDCl_3$ of ROMP random copolymer (**P5**)

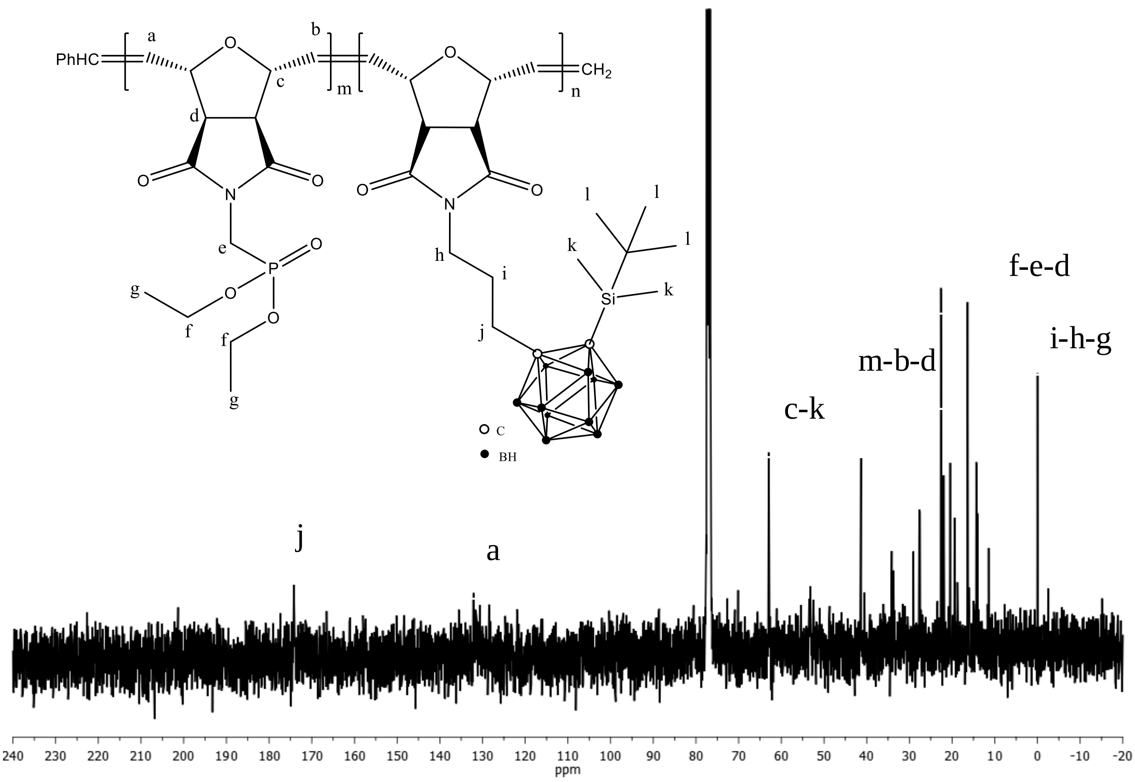

Figure 3.35 $^{13}C\{^{1}H\}$ NMR (100.16 MHz) spectrum in $CDCl_3$ of ROMP random copolymer (**P5**)

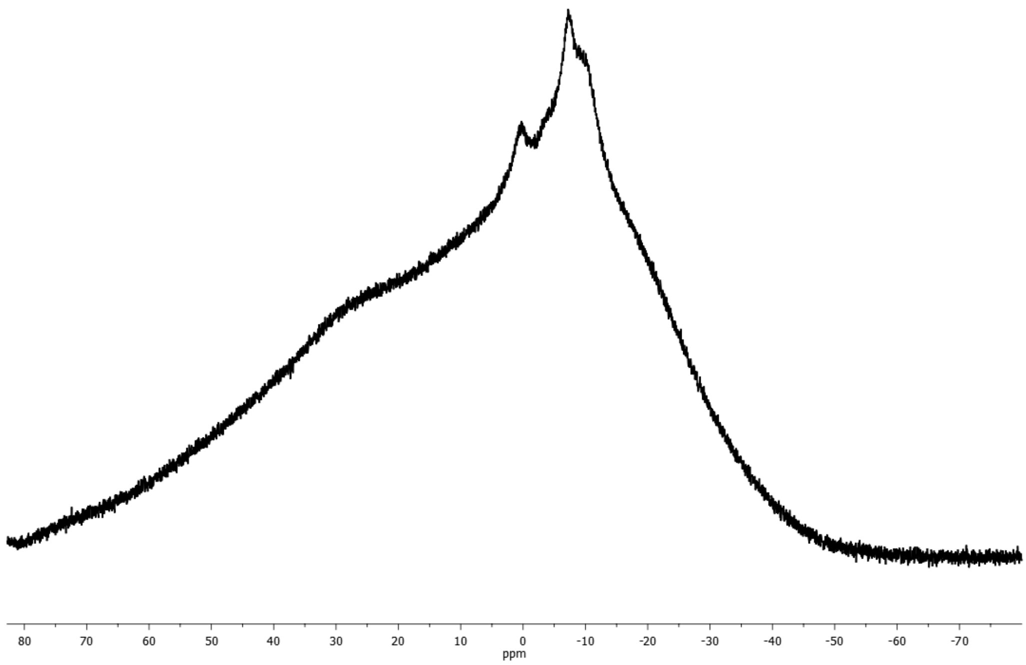

Figure 3.36 $^{11}B\{^{1}H\}$ NMR (128.37 MHz) spectrum in $CDCl_3$ of ROMP random copolymer (**P5**)

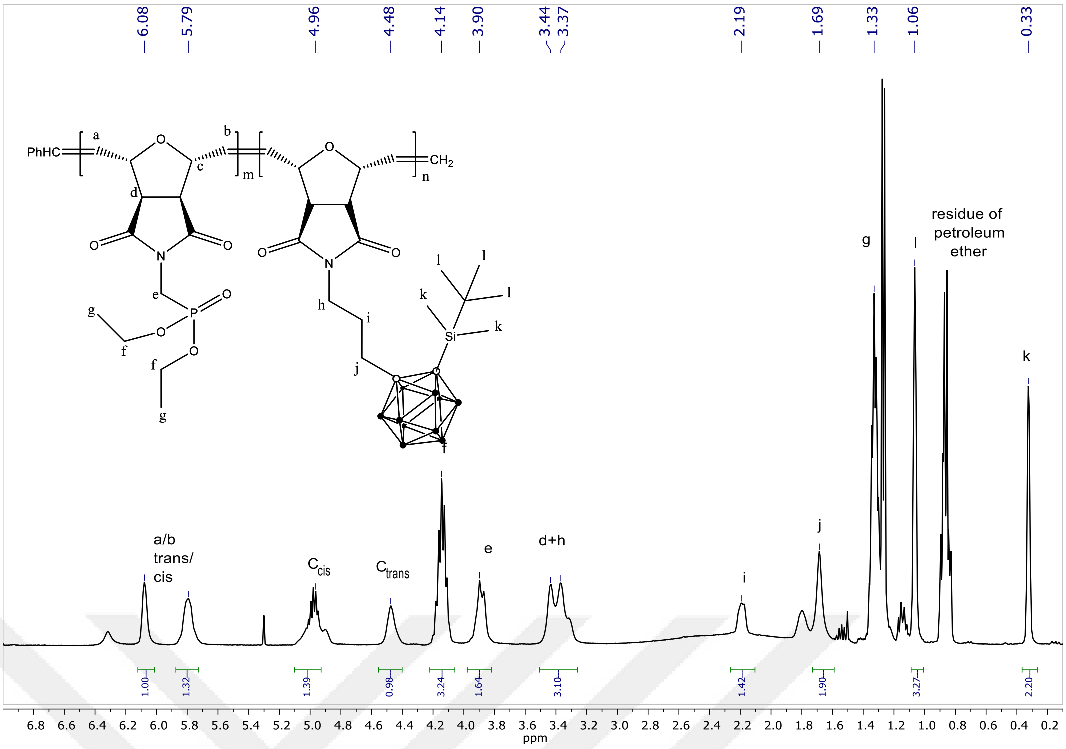

Figure 3.37 ^{1}H NMR (400.13 MHz) spectrum in $CDCl_3$ of ROMP random copolymer (**P6**)

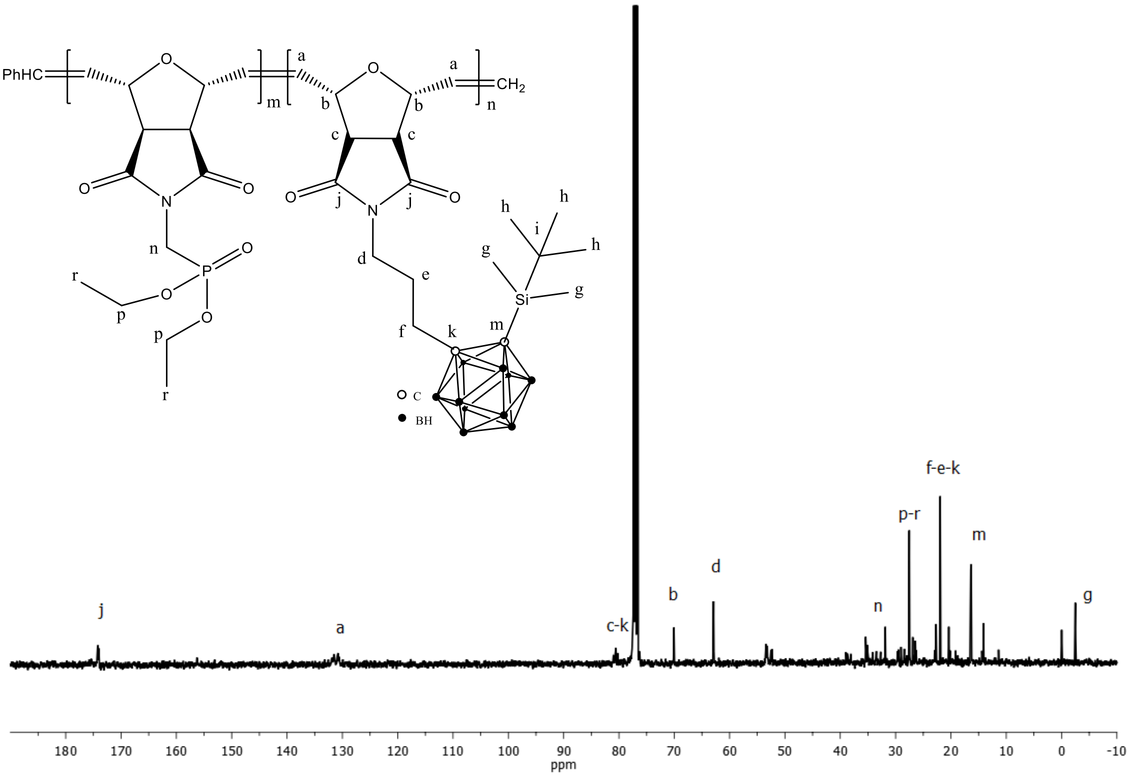

Figure 3.38 $^{13}C\{^{1}H\}$ NMR (100.16 MHz) spectrum in $CDCl_3$ of ROMP random copolymer (**P6**)

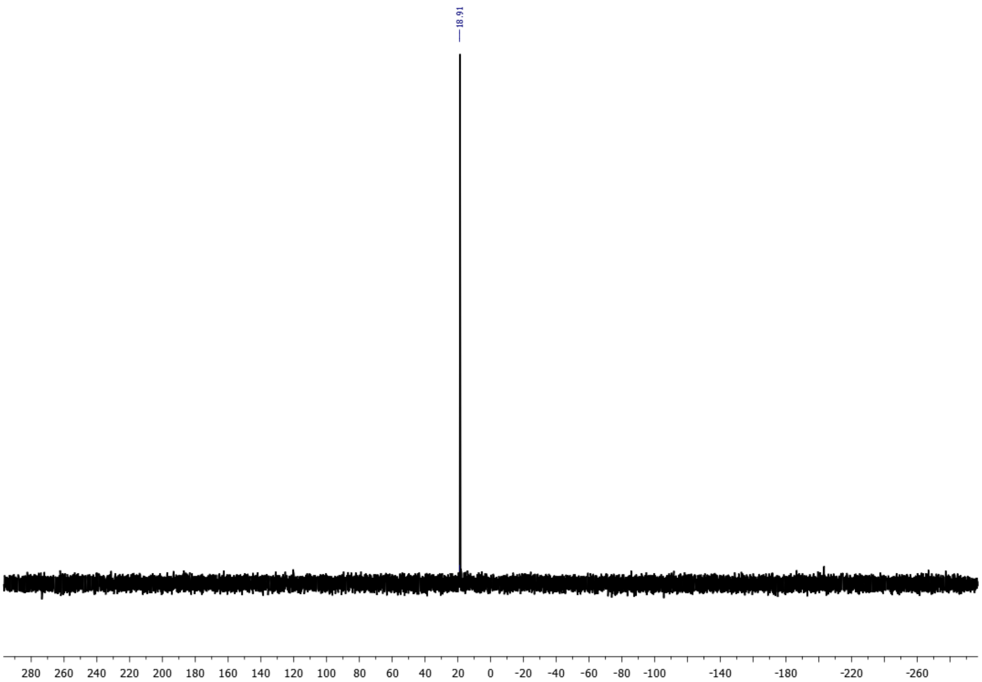

Figure 3.39 $^{31}P\{^{1}H\}$ NMR (161.97 MHz) spectrum in $CDCl_3$ of ROMP random copolymer (**P6**)

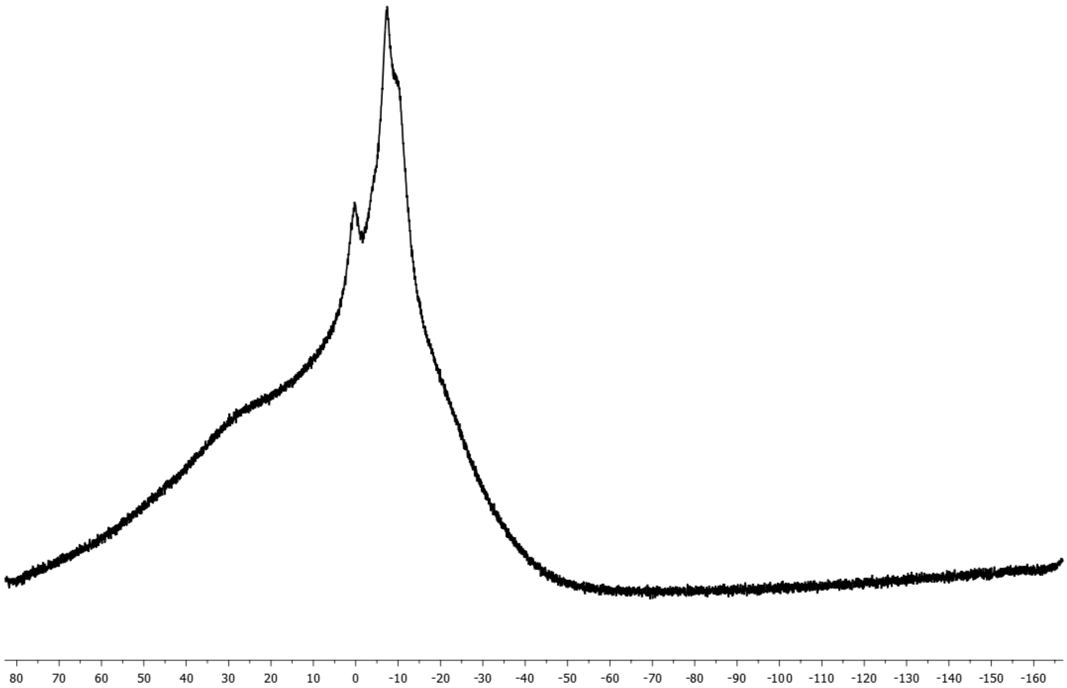

Figure 3.40 $^{11}B\{^{1}H\}$ NMR spectrum of ROMP random copolymer (**P6**)

3.1.6 Stabilization of Magnetic Fe_3O_4 Nanoparticles with ROMP Type Block Copolymers P1A, P2A, P3A

In order to prevent further agglomeration and phase separation, a suitable way has to be applied for stabilization of nanoparticles. In this study, phosphoric acid-containing ROMP block copolymers **P1A**, **P2A** and **P3A** were used for the coating of iron oxide nanoparticles. Phosphoric acid groups are known to attach to the iron oxide surface as ligands [130], [131].

Typically, the polymer (**P1A**, **P2A**, **P3A**) was dissolved in DMSO, 5% (by weight) bare iron oxide nanoparticles were added to the reaction vial and sonicated for 7 h. Scheme 3.6 indicates the synthetic pathway for the coating process.

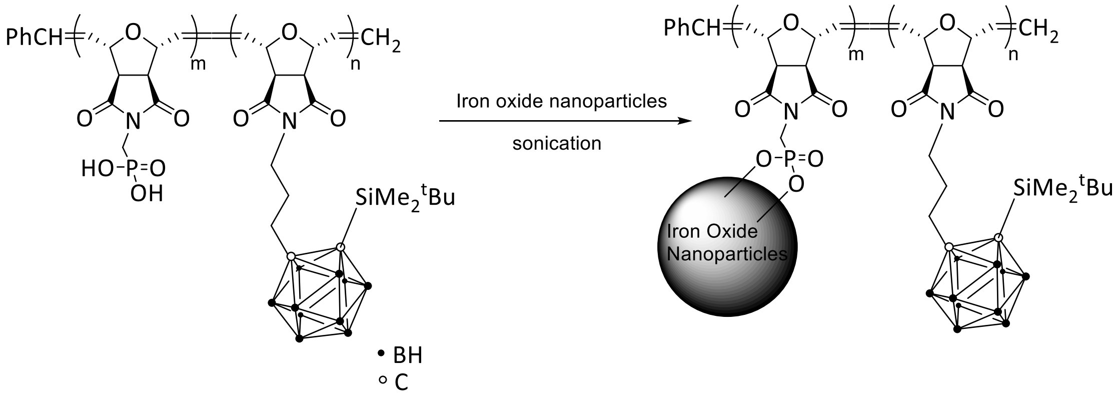

Scheme 3.6 Phosphoric acid-bearing ROMP block copolymers coordinate iron oxide nanoparticles

Some precipitated aggregates were removed by centrifugation at 2500 rpm for 5 min. The membrane dialysis purification method was applied for a week to get rid of uncoated iron nanoparticles. Once the polymer was grafted on the surface of the iron oxide nanoparticles, the color of the suspension turned brown. After dialysis against water (Figure 3.41), the color of the DMSO solution turned pale yellow. The final product was collected from the dialysis membrane, which consists of regenerated cellulose made from virgin wood pulp with 14 kDa molecular weight, then characterized by inductively-coupled plasma mass spectrometry (ICP-MS) and transmission electron microscopy (TEM).

	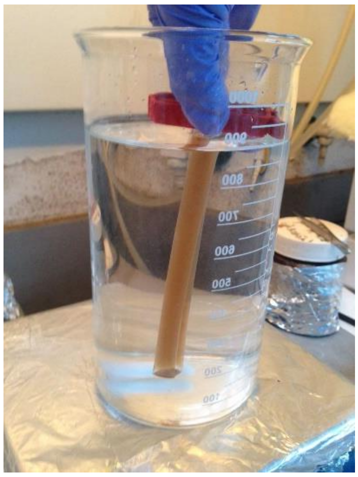
P2A-iron oxide nanoparticles in DMSO, before dialysis	**P2A**-iron oxide nanoparticle in water, after dialysis

Figure 3.41 Dialysis membrane application against water

In the literature, the use of phosphonates as ligands for the construction of metal-based polymeric networks has been mentioned [132]. The block copolymer **P2**, which bears the phosphonate ester groups, was also grafted on the iron oxide nanoparticles, using the same procedure as described above for **P2A**, for direct comparison of the binding efficiency of phosphonate ester and phosphoric acid. As indicated in Table 3.3, **P2A** seems to be a better ligand. Measurement was conducted using the Shimadzu ICPE900 ICP atomic emission spectrometer with 10 L/min plasma gas flowrate. It was observed that phosphonate ester-bearing polymer **P2** contained 61 ppm iron, and its phosphoric acid analog **P2A** 338 ppm iron (as determined with ICP–MS). On the other hand, ICP-MS results for the iron oxide nanoparticles coated with phosphoric acid-containing polymers (**P1A**, **P2A** and **P3A**) show 6.46 ppm, 338 ppm and 18.9 ppm iron after dialysis, respectively. These data indicate that increased phosphorus content in the backbone leads to higher binding efficiencies to iron oxide nanoparticles (NP). Phosphonate- and carborane-based block copolymers' weight ratio was: **P1**: 10 kDa:40 kDa; **P2**: 40 kDa:10 kDa; and **P3**: 25 kDa:25 kDa.

Table 3.3 Iron concentration obtained from the polymer samples[a]

Polymer	Fe amount before dialysis	Fe amount after dialysis
P1A	191.1ppm	6.46ppm
P2	858 ppm	61 ppm
P2A	758 ppm	338 ppm
P3A	98.5ppm	18.9ppm

[a] ICP MS result. Fe LOQ : SHIMADZU ICPE900; 0.1 mg/L , method; 0.5 with 2.6977% relative standard deviation

Morphology of the polymer-coated NP was investigated via TEM, after the application of dialysis against water. The coated nanoparticles were simply dropped on a carbon-coated copper grid and then left to dry overnight. Aggregation of nanoparticles was observed (Figure 3.42). Polymer-coated nanoparticles also aggregate in aqueous environment forming spherical micelles. The size distribution of the nanoparticles is not homogeneous, and the sample showed particle coalescence in the TEM micrographs. Magnetic interaction between nanoparticles and self-assembly via the phosphoric acid groups can result in vesicles or micelles and cause the observed large aggregates in aqueous environments. Iron oxide NP can practically be modified with surface-active compounds such as phosphonates for fine-tuning of the surface charges. Although it is well-known that block copolymers having phosphonate esters or phosphoric acids

(**P2A**) lead to surface coating on iron nanoparticles, the detailed mechanism behind this coating event is still not well understood.

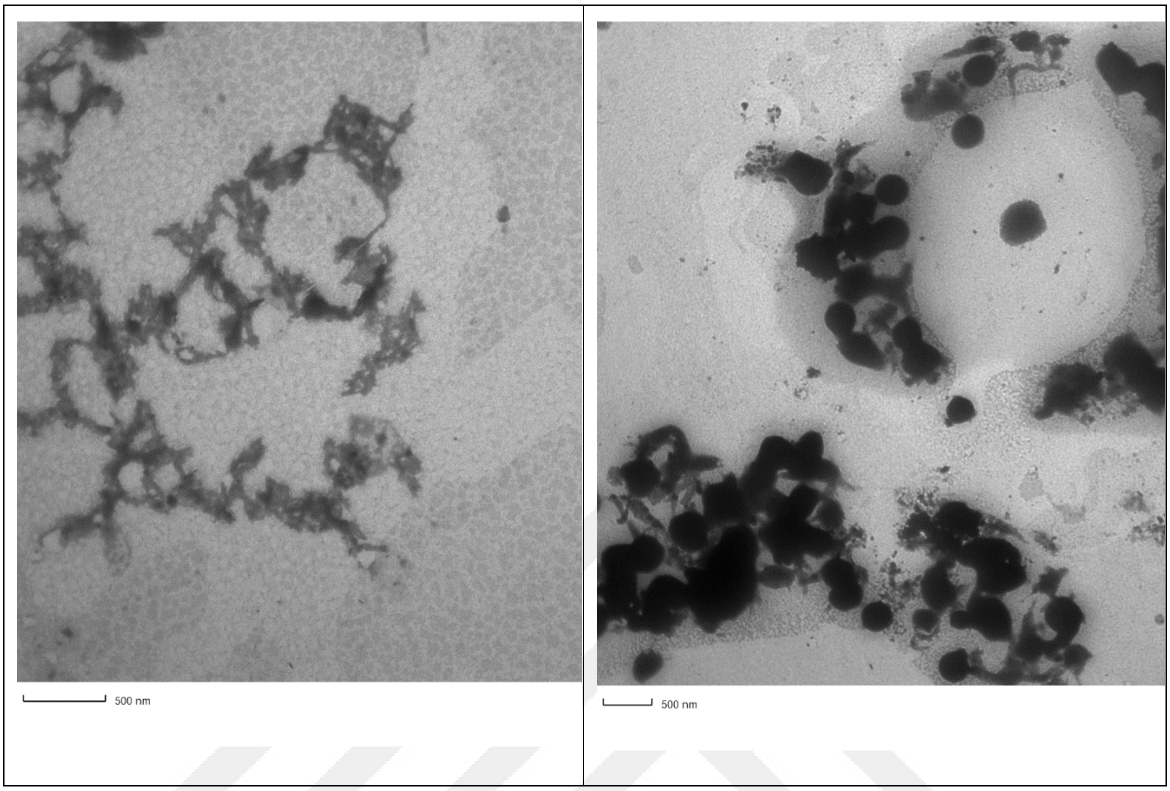

Figure 3.42 TEM micrographs of iron oxide nanoparticles coated with phosphonate-based polymer (**P2A**)

3.1.7 Thermal Analysis of Carborane and Phosphorus Based ROMP Polymers

Thermal properties of the block and random copolymers were investigated via DSC, MCC and TGA analyses. DSC was applied between 20 °C and 200 °C and it was observed that **P1**–**P6** show a broad glass transition temperature T_g, at around 119 °C, 75 °C, 60 °C, 92 °C, 65 °C and 82 °C, respectively (Figure 3.43–3.45). The Glass Transition Temperature (T_g) is one of the most important properties of any epoxy resin and is the temperature region where the polymer transitions from a hard, rigid or “glassy” state to a soft ”rubbery” state. These results show that the T_g value is directly related to the percentage of crystalline and amorphous segments in the polymer backbone. In this matter, carborane provides rigidity to the system, while phosphorus provides the mobility. Since icosahedral carboranes are thermally stable compounds, more carborane units in the structure result in higher T_g values.

TGA was performed under nitrogen as well as in air, at a heating rate of 10 °C/min between 25 °C and 600 °C (Figure 3.46–3.50). It was expected that a higher number of phosphonate units would enhance the char yield. Briefly, the results of TGA of the block copolymers can be summarized as following: under nitrogen atmosphere, char residue of **P1** (possessing the highest carborane content) is 41%; char residue of **P2** (possessing the highest phosphonate content) is 59.3%; char residue of **P3** (possessing equivalent carborane and phosphonate content) is 51.1%. The values in air are 62.4%, 48.4% and 56.8%, respectively. Moreover, char residues of the phosphoric acid- and carborane-containing block copolymers are given as follows: **P1A** is 64.20%, **P2A** is 60.60% and **P3A** is 62.75% under nitrogen, while **P1A** is 52.44%, **P2A** is 60.40% and **P3A** is 53.82% in air. Polymer **P2** (Figure 3.47), which has a higher phosphorus content, resulted in 59.3% char (Table 3.4) when compared to the other ROMP block copolymers (**P1** and **P3**). However, increasing the amount of carborane units (**P2**) in the polymer backbone resulted in increased char formation in air, due to the capture of oxygen by the boron cluster to form B_2O_3, whereas increasing the amount of phosphorus units (**P1**) in the polymer backbone resulted in increased char residue under nitrogen. Based on char residue of the molecules, the phosphoric acid- and carborane-containing polymers (**P1A**, **P2A** and **P3A**) are more heat resistant than the phosphonate ester- and carborane-containing polymers, under both conditions (nitrogen and air).

Comparing the latter values with those of the random copolymers confirmed that the ordered structures, i.e. block copolymers, generate more char residue than less ordered structures, i.e. random copolymers. For example, **P1** (block copolymer) and **P4** (random copolymer) contain the same amount of phosphonate and carborane units in their backbone. According to Table 3.4, **P1** generated higher char residue (41%) than **P4** (36.7%). This data leads us to suggest that, among the studied types of polymers, block copolymers might have superior fire-resistant properties than random copolymers.

Microscale combustion calorimetry (MCC, Fire Testing Technology, UK) is a convenient technique used in recent years for the investigation of flammability of polymers. In this study, approximately 5 mg of polymer sample was heated to 700 °C with a heating rate of 1 °C/s in a stream of nitrogen (flow = 80 cm^3/min). The volatile and anaerobic thermal degradation products in the nitrogen stream were mixed with a 20 cm^3/min stream including 20% oxygen and 80% nitrogen, prior to entering a combustion furnace at 900 °C. The MCC results are summarized in Table 3.5, which shows Heat Release Rate (HRR), Peak Heat Release Rate (PHRR) and Total Heat Release (THR)values for each polymer. The polymers **P1**, **P2**, **P3**, **P4**, **P5**, **P6**, **P1A**, **P2A** and **P3A** show HRR values of 72.8 W/g, 263.9 W/g, 223.1 W/g, 68.4 W/g, 154.8 W/g, 86.1 W/g, 41.9 W/g, 9.6 W/g and 22.8 W/g, respectively. Typically, the lower HRR values indicate higher flame retardancy properties. Random copolymers (**P4**, **P5** and **P6**) showed considerably lower HRR values than block copolymers under the same combustion conditions. Furthermore, phosphoric acid-containing polymers have lower HRR values than phosphonate ester-containing polymers.

Also, acidic polymers showed a much lower Peak Heat Release Rate (PHRR) (Figure 3.52) value than ester polymers. The same trend was observed for Total Heat Release (THR) values. These data suggest that flammability of acids is considerably lower than that of esters under the same combustion conditions.

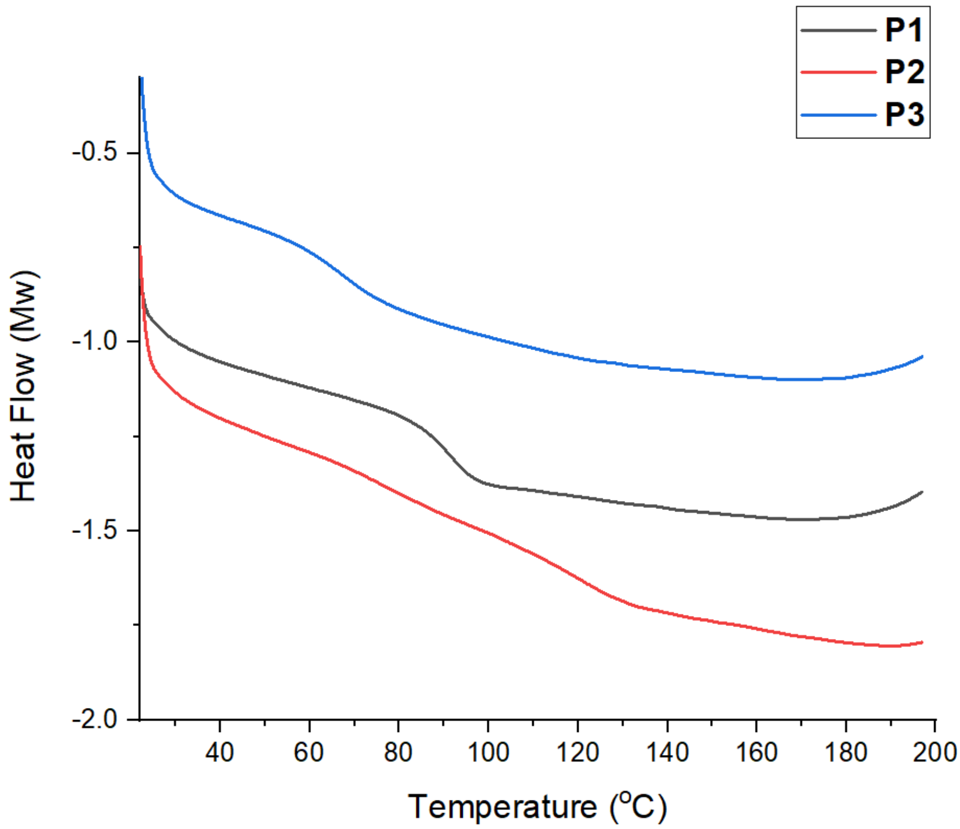

Figure 3.43 Heat flow curves of phosphonate- and carborane-containing block copolymers from DSC analysis

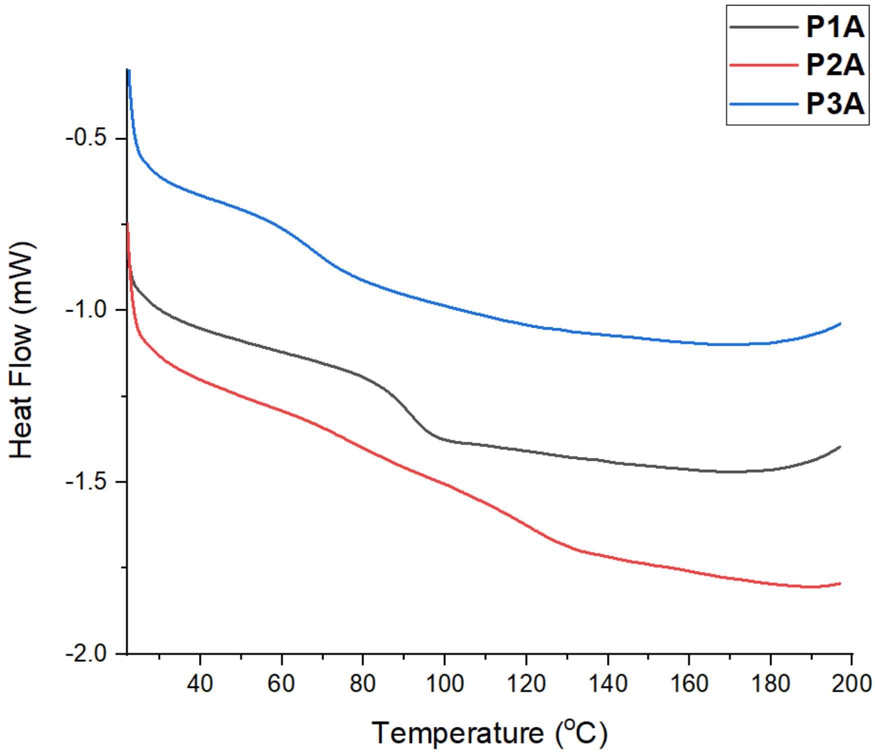

Figure 3.44 Heat flow curves of phosphoric acid- and carborane-containing block copolymers from DSC analysis

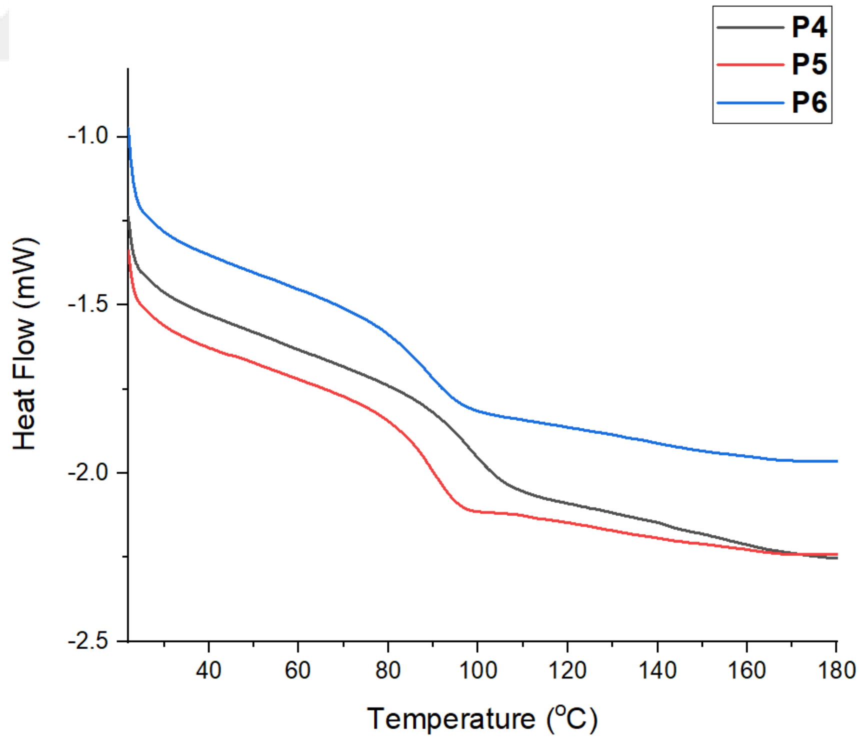

Figure 3.45 Heat flow curves of phosphonate- and carborane-containing random copolymers from DSC analysis

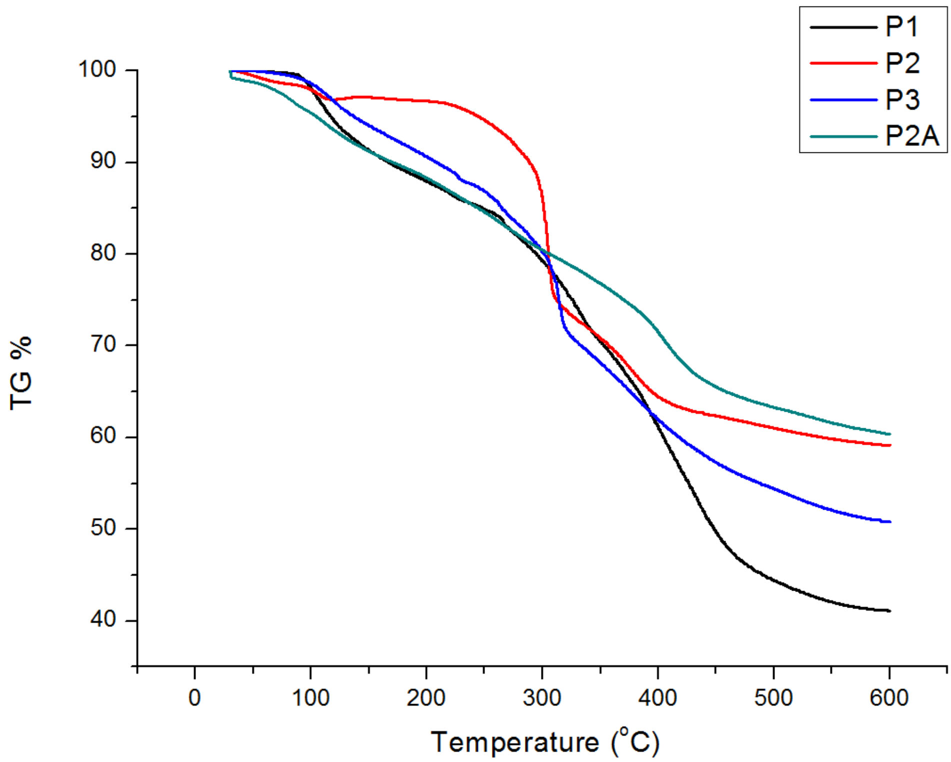

Figure 3.46 Thermogravimetric analysis of phosphonate- or phosphoric acid- and carborane-containing block copolymers under nitrogen atmosphere

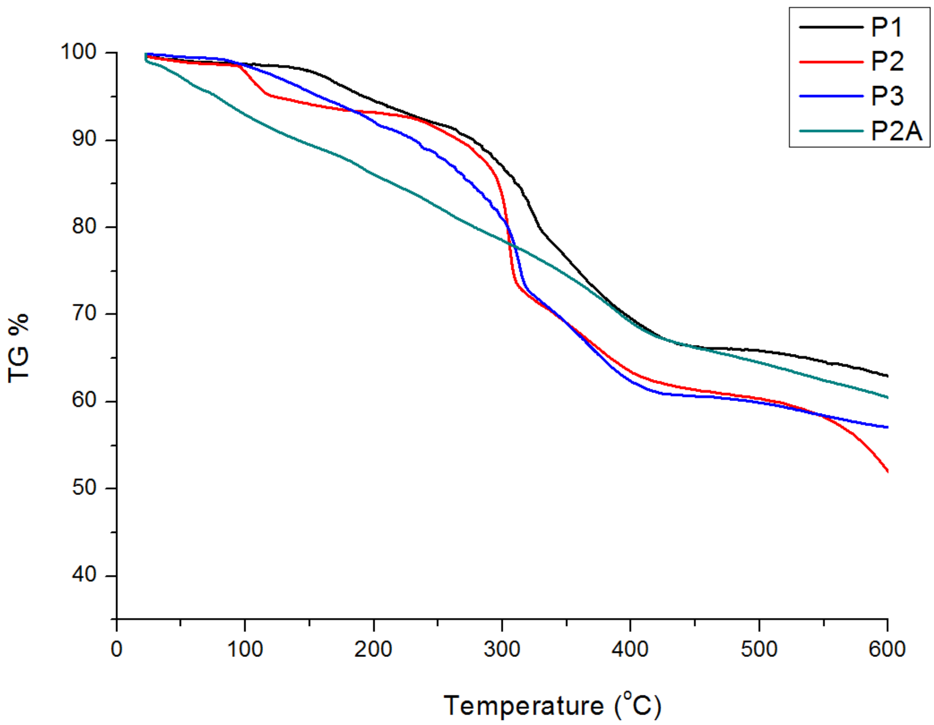

Figure 3.2 Thermogravimetric analysis of phosphonate or phosphoric acid- and carborane-bearing block copolymers in air

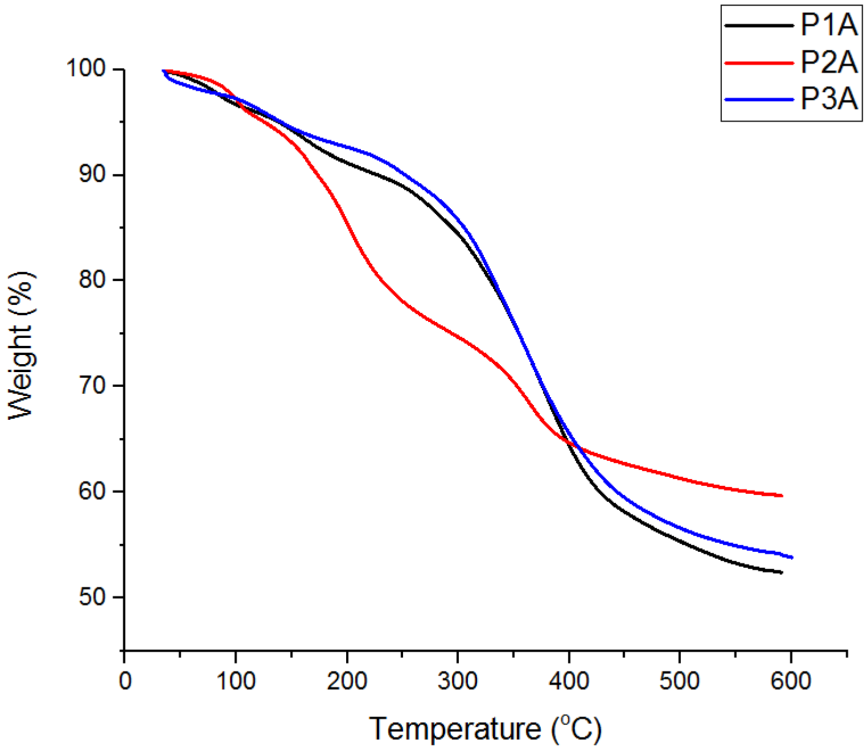

Figure 3.48 Thermogravimetric analysis of phosphoric acid- and carborane-containing block copolymers under nitrogen atmosphere

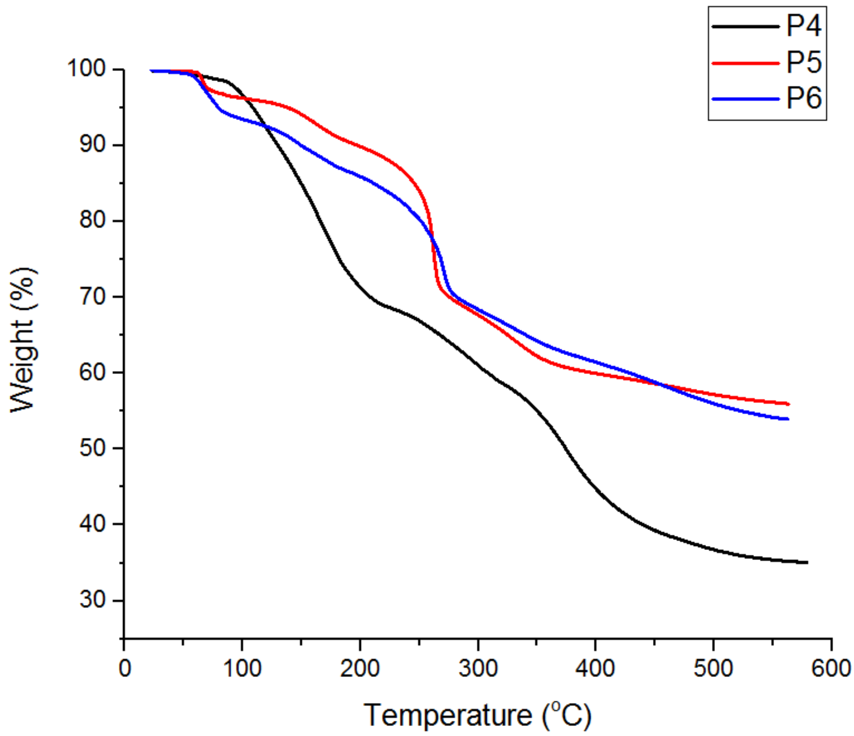

Figure 3.49 Thermogravimetric analysis of phosphonate ester- and carborane-containing random copolymers under nitrogen atmosphere

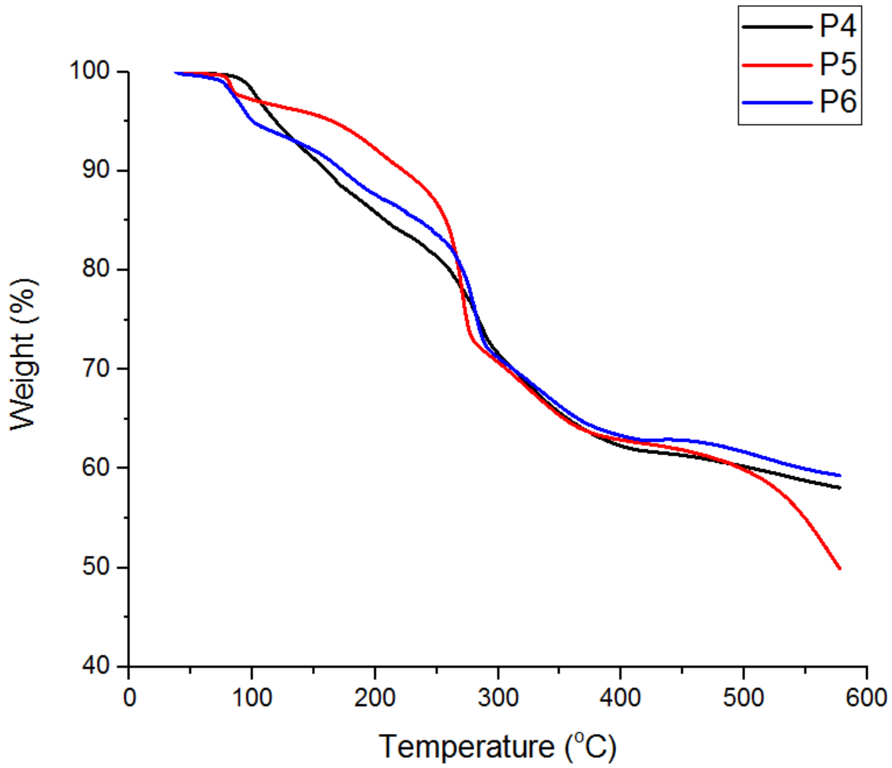

Figure 3.50 Thermogravimetric analysis of phosphonate ester- and carborane-containing random copolymers in air

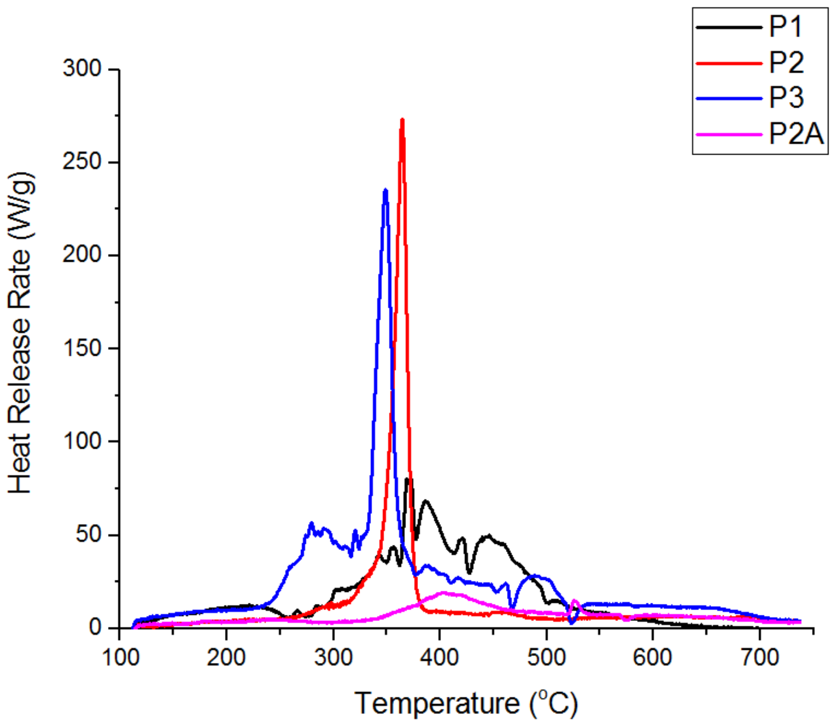

Figure 3.51 HRR curves of phosphonate- or phosphoric acid- and carborane-containing block copolymers from MCC analysis

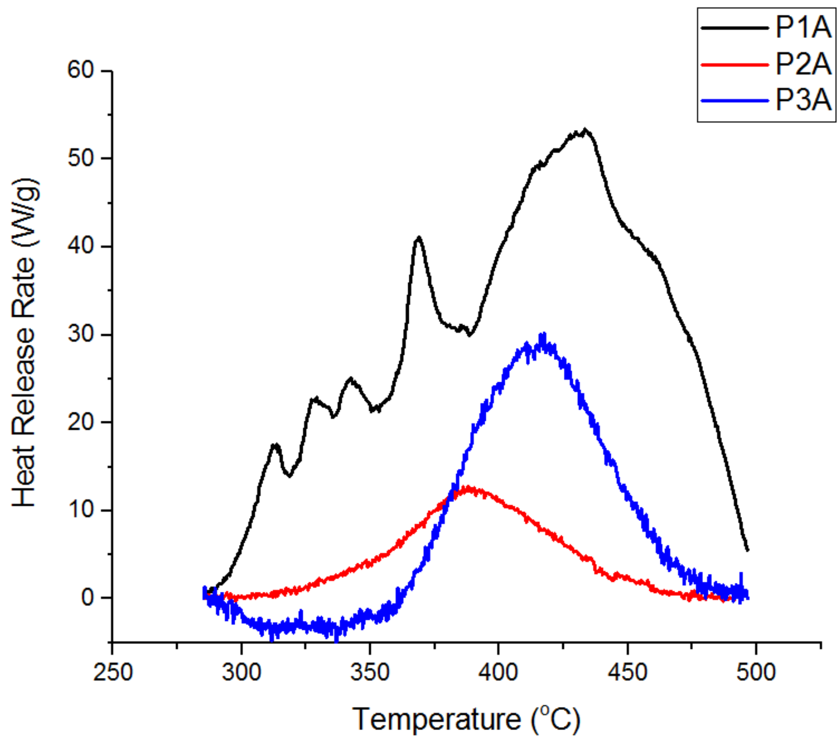

Figure 3.52 HRR curves of phosphoric acid- and carborane-containing block copolymers from MCC analysis

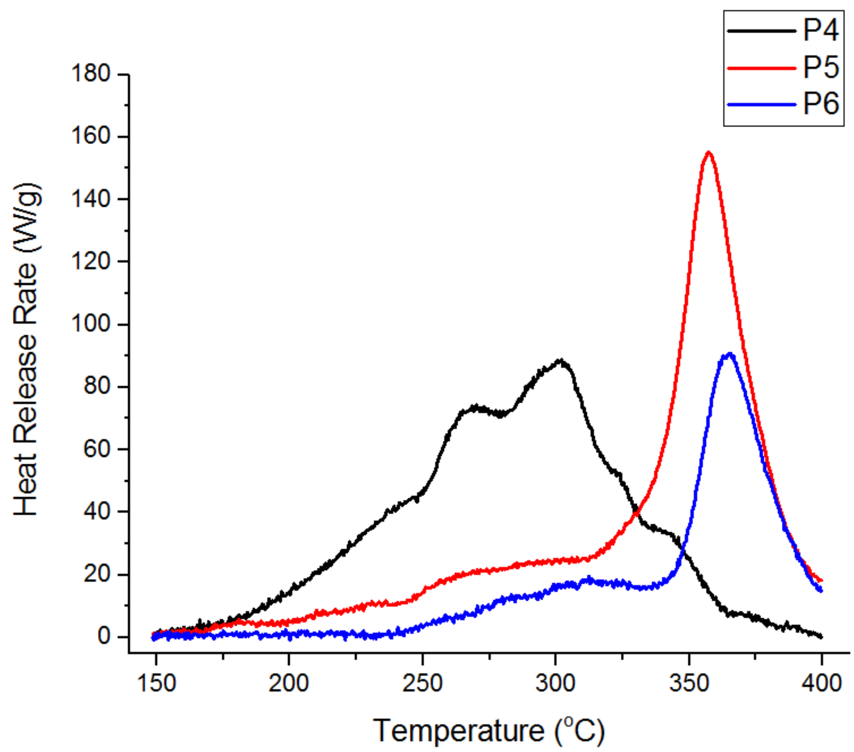

Figure 3.53 HRR curves of phosphonate- and carborane-containing random copolymers from MCC analysis

Table 3.4 Residues (%) of the compounds in this Study (N_2 and air) from TGA testing

Compound	Residue % (Under N_2)	Residue % (Under Air)	Temperature (°C)
P1	41.2	62.4	600
P2	59.3	48.4	600
P3	51.1	56.8	600
P1A	52.44	-	600
P2A	60.4	60.6	600
P3A	53.82	62.75	600
P4	36.7	58.06	600
P5	55.96	49.44	600
P6	53.94	59.24	600

Table 3.5 MCC results of the compounds in this study

Compound	HR Capacity (J/g.K)	Peak HRR (W/g)	Total HR (kJ/g)	Temperature (°C)
P1	75	72.82	6.9	368.7
P2	271	263.9	5.0	334.4
P3	226	223.1	8.8	335
P4	85	68.37	7.5	264
P5	157	154.8	8.3	358
P6	90	86.1	4.3	365.1
P1A	52	41.87	5.8	404
P2A	13	9.594	0.9	382.5
P3A	31	22.84	1.7	394.9

3.2 Mixtures with Epoxy Resin

3.2.1 Synthesis of Monomer 3

In an attempt to develop a new flame-retardant polymer, monomer **3** was synthesized following the literature procedure [133] from *o*-carborane and oxetane, after deprotonation of the $C_{cluster}$ vertices with 2.00 eq. *n*-BuLi (Scheme 3.7).

The identity of the compound was confirmed by NMR spectroscopy. In the ^{1}H NMR spectrum, three signals for the six methylene protons are found at 3.67 ppm, 2.34 ppm and 1.79 ppm, respectively. The $^{11}B\{^{1}H\}$ NMR spectrum shows two signals with a ratio 8:2.

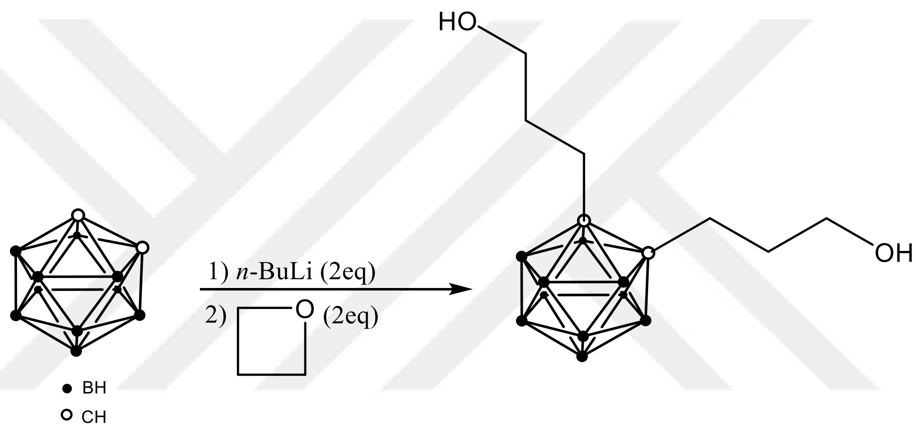

Scheme 3.7 Synthesis of monomer **3**

3.2.2 Synthesis of the Oligomer (P7)

The synthetic pathway to phospha-carborane-containing oligomer **P7** is shown in Scheme 3.8. Reaction conditions were varied, namely solvent, temperature, reaction time and relative ratio of the reagents. Optimal conditions were found to be dry toluene at room temperature for 3 h, then under reflux for 4 h. Monomer **3** was used as end-capping agent to terminate the reaction. The obtained product (**P7**) was obtained as a colorless sticky solid and was characterized by NMR spectroscopy, DSC and TGA techniques.

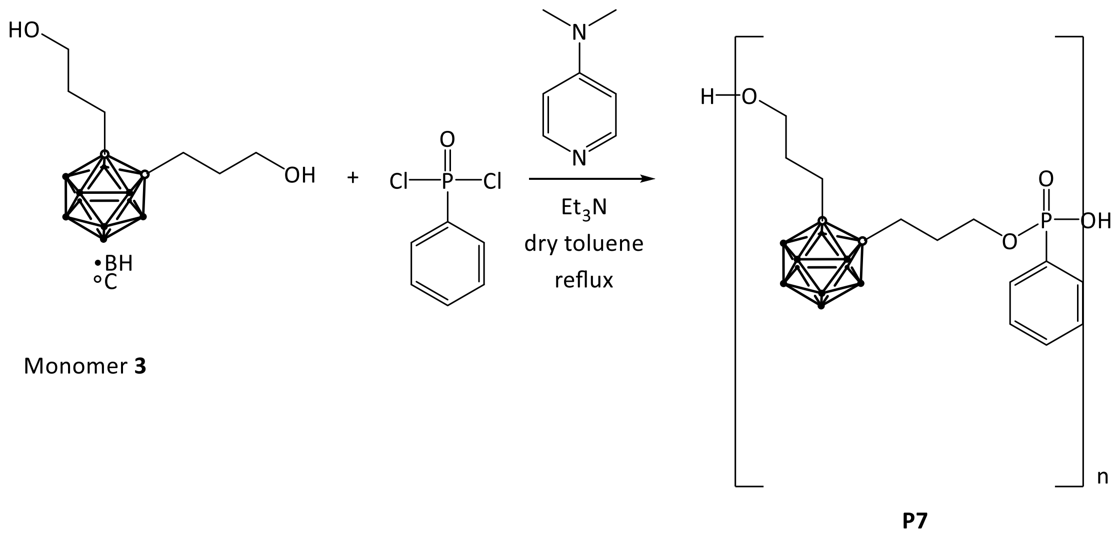

Scheme 3.8 Synthesis of phospha-carborane containing polymer via solution polymerization

The ^{1}H NMR spectrum of **P7** is shown in Figure 3.54. The signal at 9.48 ppm is attributed to the O**H** proton. The multiplet at 7.73–7.66 ppm corresponds to the *ortho* (**H**^{d}), at 7.44–7.34 ppm corresponds to *meta* (**H**^{e}) and at 7.17–7.09 ppm corresponds to *para* protons (**H**^{f}) in the phenyl ring. The multiplet at 3.49–3.37 ppm corresponds to the –CH_2O- protons (**H**^{a} and **H**^{g} in Figure 3.54). The multiplet at 2.34–2.15 ppm corresponds to the –CH_2- protons (b-h). The multiplet between 1.94 and 1.78 ppm corresponds to the –CH_2- protons **H**^{c} and **H**^{i}.

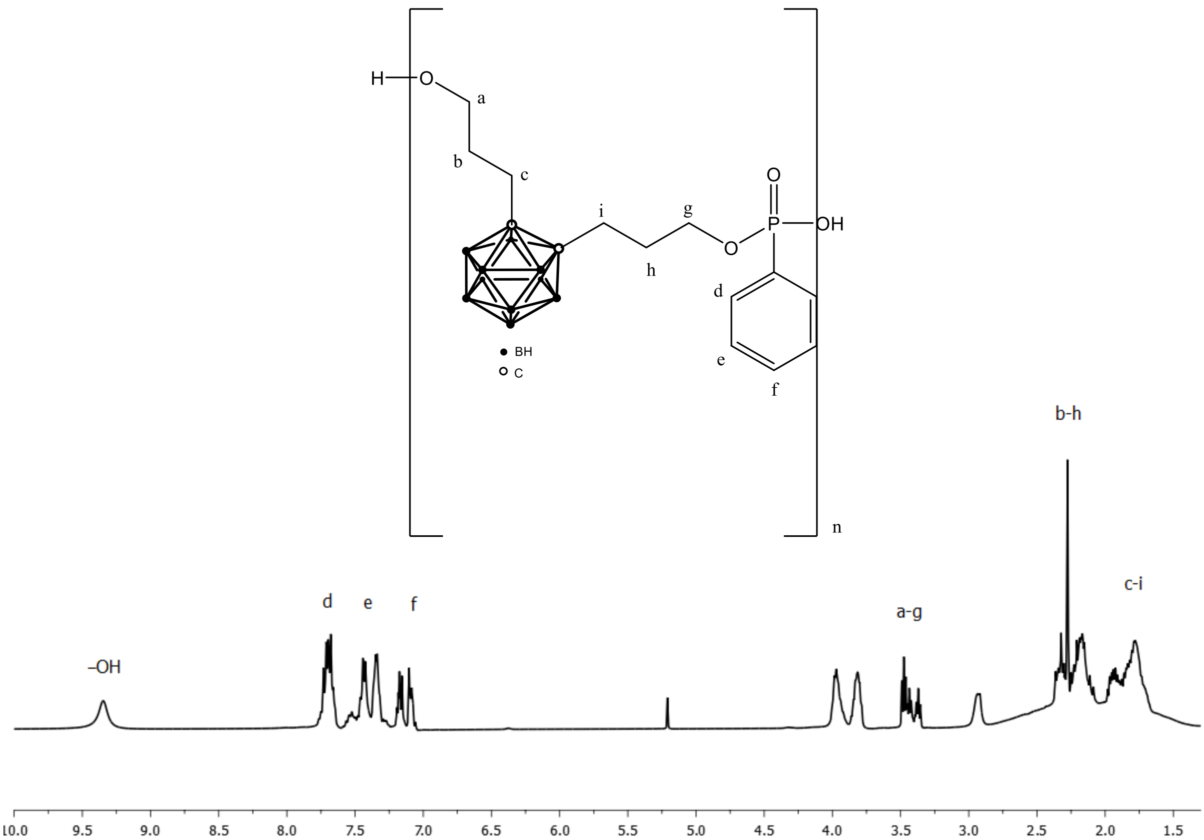

Figure 3.54 ^{1}H NMR (400.13 MHz) spectrum in $CDCl_3$of phospha-carborane-containing copolymer (**P7**)

To evaluate the flame retardant properties of oligomer **P7**, first the classic formulation with epoxy resin was used, adding different amounts of **P7** to the resin, according to the literature [134]. Four different weight % of **P7** were used for the formulation, 5% (**P7$_{5\%}$**), 7.5% (**P7$_{7.5\%}$**), 12.5% (**P7$_{12.5\%}$**) and 20% (**P7$_{20\%}$**).

Table 3.6 Formulation of **P7**-containing epoxy resin mixtures (no solvent, at 100 °C)

Formulation	P7 % in Epoxy Resin
P7$_{5\%}$	5%
P7$_{7.5\%}$	7.5%
P7$_{12.5\%}$	12.5%
P7$_{20\%}$	20%

Epoxy resins are polymer materials with a wide area of applications, either unmodified or as matrices for composite materials. In all of these applications a curing process is involved in which the monomeric or oligomeric polyfunctional epoxide is transformed into a crosslinked macromolecular structure. An understanding of these curing reactions, together with the availability of reliable methods of monitoring them, are important in order to obtain consistent products with the desired physical and mechanical properties. The technique of differential scanning calorimetry (DSC) was used to provide a convenient and useful method of monitoring the course of exothermic reaction between -OH terminal groups of **P7** and epoxy resin. Measurement conditions were the same for all experiments, namely temperature range 10–220 ^{o}C, with heat flow of 0.5 W/g per minute. DSC analysis of commercial, additive-free epoxy resin was also performed, and its response curve was used as reference. In the case of epoxy resin samples doped with **P7**, it was observed that the curve between 150 and 200 ^{o}C differed from the reference for each formulation (Figure 3.55). Here, the results confirm that the ring-opening reaction of the epoxy resin was accompanied by heat release, i.e. an exothermic process. Additionally, the integration area of the peak maxima increases upon increasing content of **P7** doping.

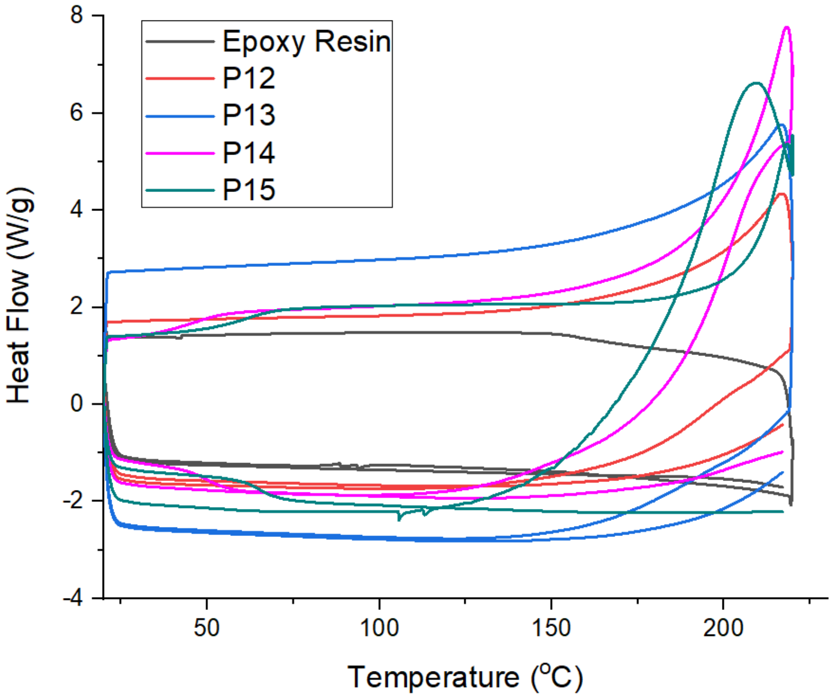

Figure 3.55 Heat flow curves of epoxy resin with different doping amounts of **P7** from DSC analysis. Non-doped epoxy resin is also shown, as reference.

TGA analysis was performed in air and under nitrogen atmosphere. The char residue (%) for monomer **3** was 34.13% under nitrogen and 58.58% in air, due to oxidation of the carborane cluster. However, oligomer **P7** surprisingly formed less char (Table 3.7) than monomer **3** in either case (under N_2 and in air), even though it contains both phosphorus and boron, which are both known for possessing flame retardant properties, independently. This could be due to unstable O=P–O bonds under the applied measurement conditions, where volatile species might be induced to escape from the polymer matrix.

Table 3.7 Residues (weight %) of monomer **3** and oligomer **P7** under N_2 atmosphere and in air at 900 °C, from TGA analysis.

Compound	**Residue % (Under N_2)**	**Residue % (Under Air)**	**Temperature (°C)**
Monomer **3**	34.13	58.58	900
P7	30.56	36.26	900

As already discussed before (section 3.1.7) the lower the heat release rate (HRR), total heat release (THR) and peak heat release rate (PHRR) values, the higher are the flame-retardant properties of the material. According to the HRR, PHRR and THR data for monomer **3**, oligomer **P7** and the respective doped epoxy resins (Table 3.8, Figures 3.58 and 3.59), the most effective flame-retardant properties are displayed by the epoxy resin sample doped with 7.5% **P7**, followed by, in decreasing order, 20% and 12.5% dopings. On the other hand, addition of 5% **P7** to the epoxy resin resulted in the highest HR capacity (203 J/g·K) and maximum PHRR (163 W/g), i.e. the lowest flame-retardant properties.

Table 3.8 Results from MCC analysis for monomer **3**, oligomer **P7** and the **P7**-doped epoxy resins

Compound	HR Capacity (J/g·K)	Peak HRR (W/g)	Total HR (kJ/g)	Temperature (ºC)
Monomer 3	151	149.8	10.2	396.9
P7	124	119.7	8.5	291.3
$P7_{5\%}$	203	163.3	16.8	451.7
$P7_{7.5\%}$	120	95.55	9.8	455.8
$P7_{12.5\%}$	115	100.8	10.2	432.2
$P7_{20\%}$	134	98.9	11.9	439.7

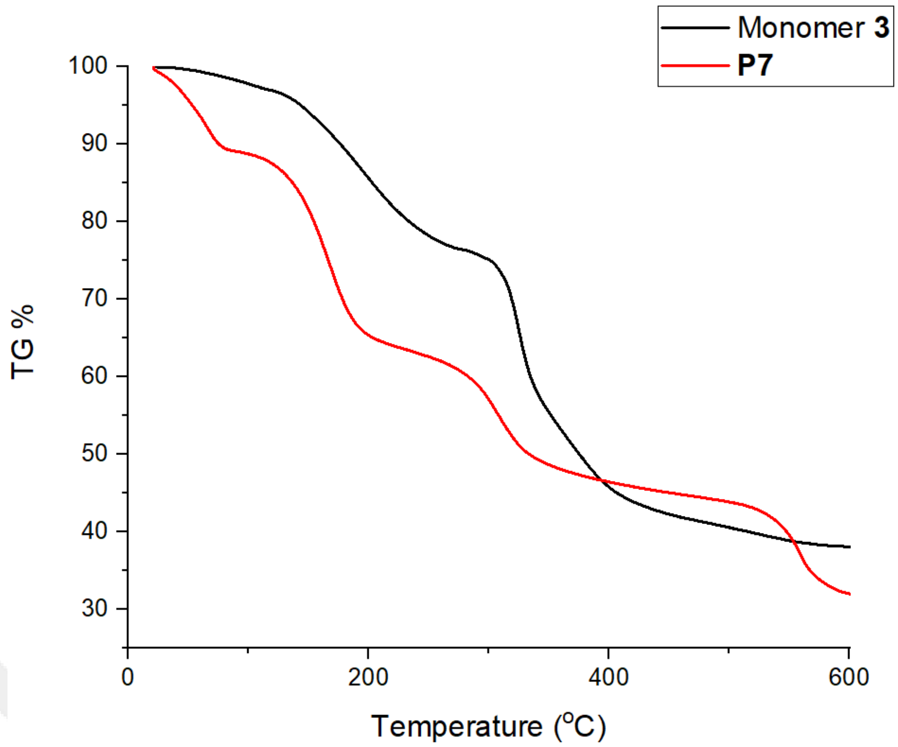

Figure 3.56 Thermogravimetric analysis of monomer **3** and oligomer **P7** under nitrogen atmosphere

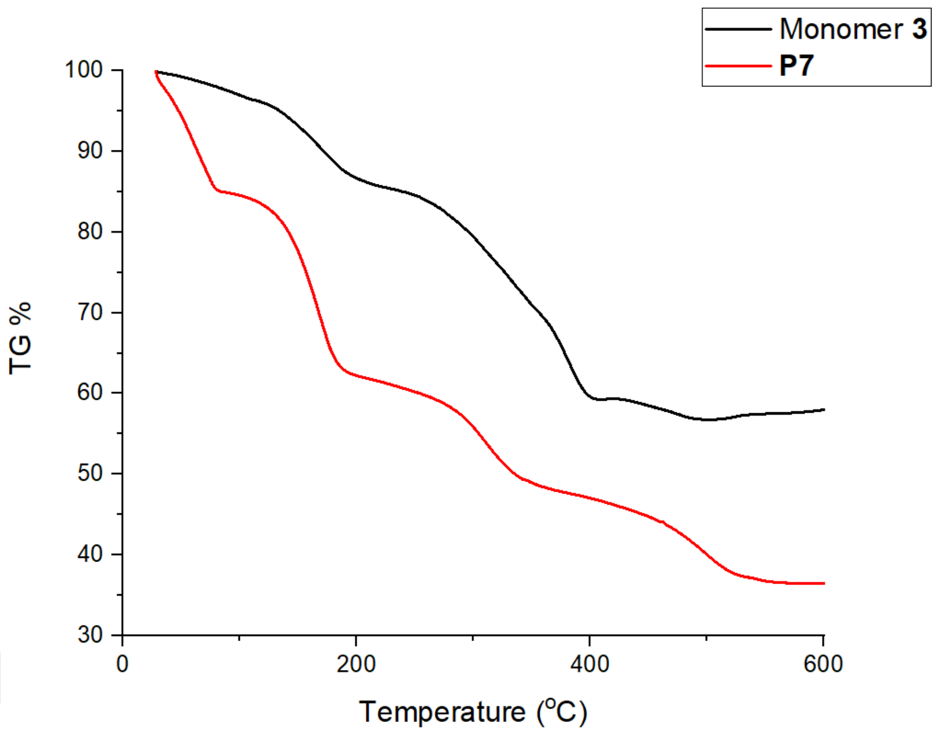

Figure 3.57 Thermogravimetric analysis of monomer **3** and oligomer **P7** in air

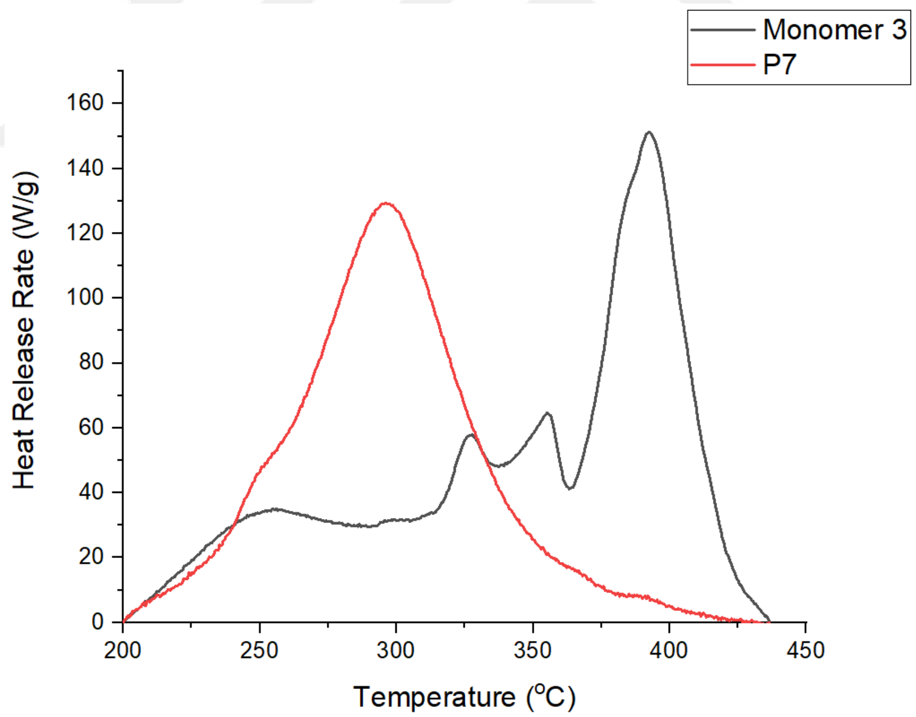

Figure 3.583 HRR curves of monomer **3** and oligomer **P7** from MCC analysis

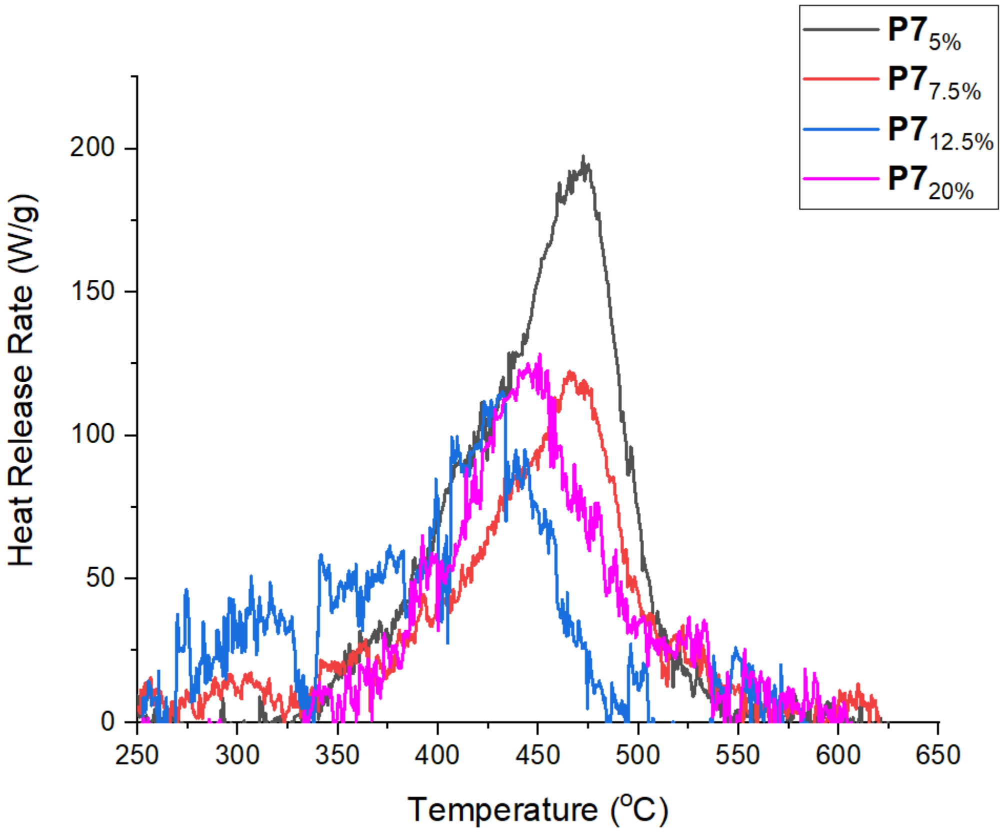

Figure 3.59 HRR curves of **P7**-doped epoxy resin from MCC analysis

3.3 Carborane-Anthracene Bearing ROMP type Polymers

3.3.1 Synthesis of Monomer 4

The synthetic pathway to monomer **4** is given in Scheme 3.9. Monomer **4** was obtained via reaction of *exo*-7-oxanorbornene-imide (**1**) and 9-(chloromethyl)anthracene in dry DMF (dimethylformamide). In the ^{1}H NMR spectrum of monomer **4** (Figure 3.60) the methylene protons (C**H**$_2$–N) appear as singlet at 5.22 ppm, and the aromatic protons are found between 7.51 and 8.50 ppm. Signals for the oxanorbornene moiety appear at 6.42 ppm (C**H**$_2$=CH$_2$), 5.59 ppm (C=C–C**H**–O) and 2.62 ppm (–CH–C**H**–(C=O)). The ^{13}C{^{1}H} NMR spectrum (Figure 3.61) shows the methylene carbon at 47 ppm. Aromatic carbons of anthracene were found in the range 126–131 ppm.

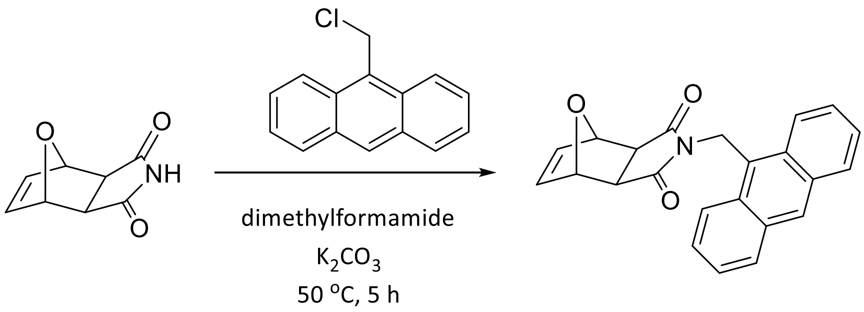

Scheme 3.9 synthesis of monomer **4**

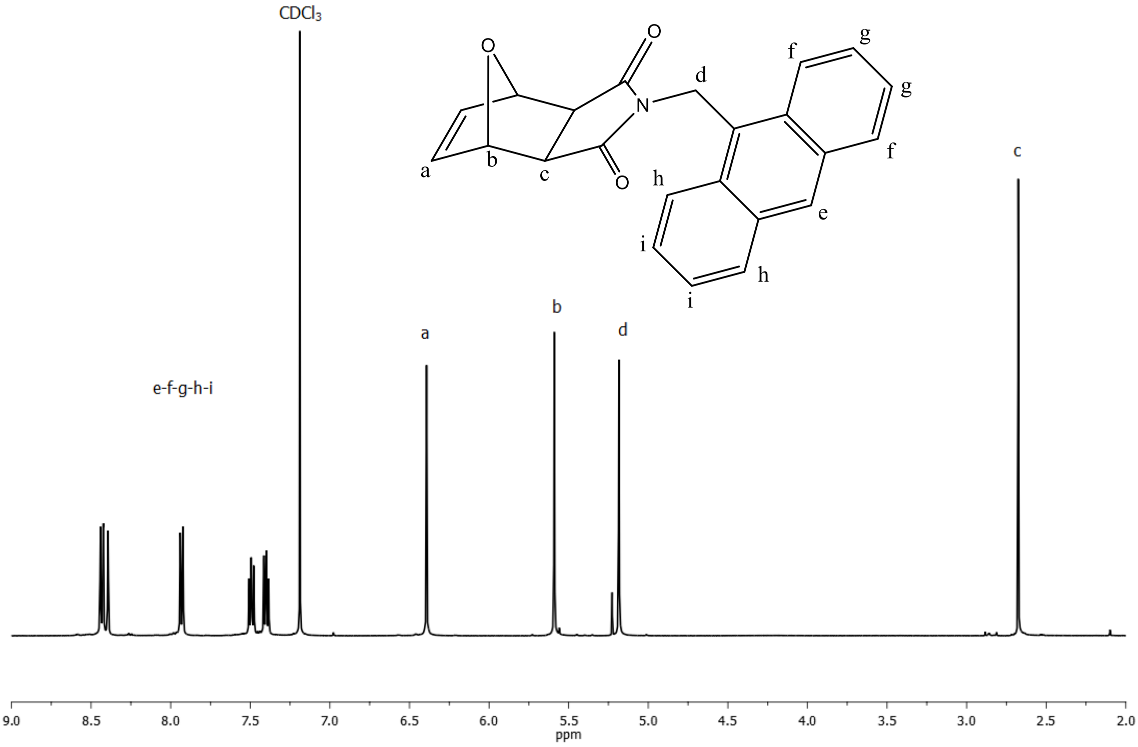

Figure 3.60 ^{1}H NMR (400.13 MHz) spectrum in $CDCl_3$of monomer **4**

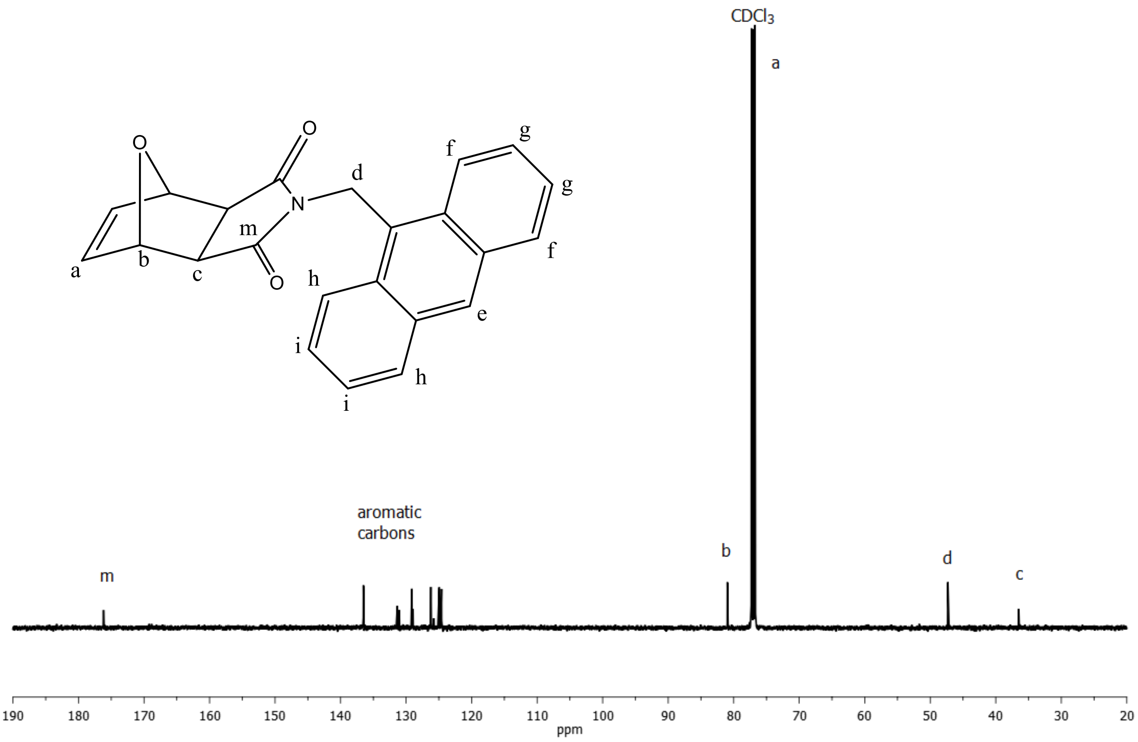

Figure 3.61 $^{13}C\{^{1}H\}$ NMR (100.16 MHz) spectrum in $CDCl_3$ of monomer **4**

3.3.2 Copolymer synthesis via ROMP

The synthetic pathway to the polymers is shown in Scheme 3.10. In order to obtain random copolymer structures, ring-opening metathesis polymerization (ROMP) was used. The designed polymers (**P8**, **P9** and **P10**) have a total weight of 80 kDa and consist of 1:7, 2:6 and 3:5 anthracene/carborane unit ratios in the polymer backbone, respectively. After drying in vacuum, the synthesized polymers were kept under nitrogen. Copolymer **P10** was stirred in *o*-xylene at reflux, in the presence of *p*-toluene sulfonyl hydrazide, yielding the hydrogenated copolymer **P11** (Scheme 3.11).

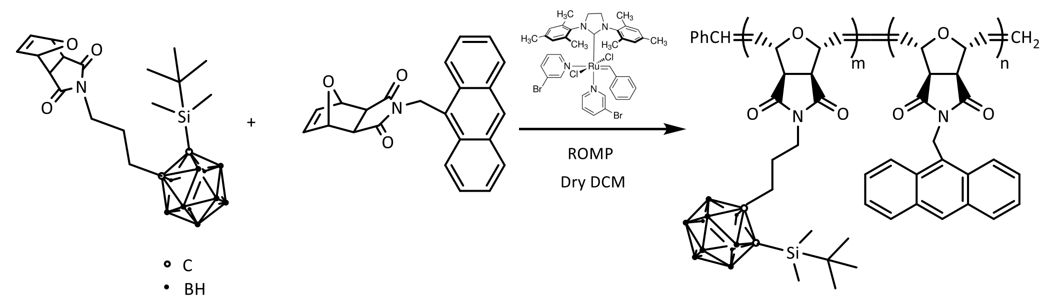

Monomer **2** Monomer **4**

P8: 70kDa-10kDa Random Copolymer
P9: 60kDa-20kDa Random Copolymer
P10: 50kDa-30kDa Random Copolymer

Scheme 3.10 Synthesis of carborane- and anthracene-containing random copolymers via ROMP pathway

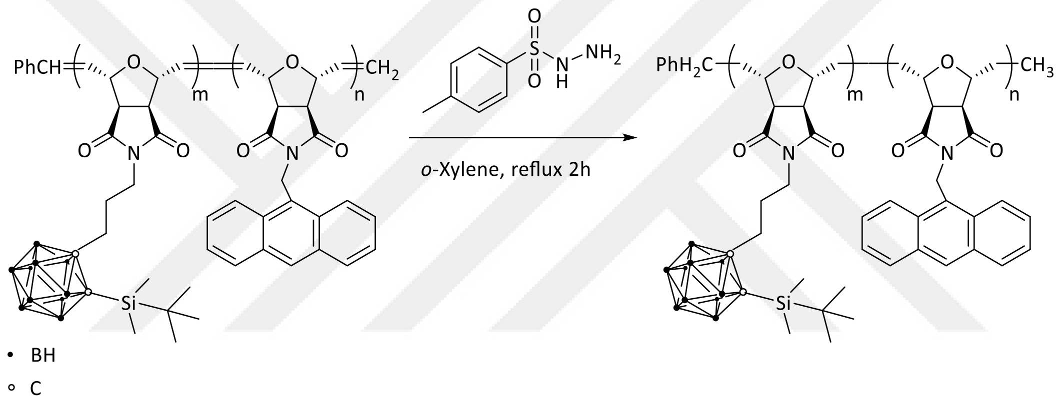

P10: 50kDa-30kDa Random Copolymer **P11:** 50kDa-30kDa Random Copolymer

Scheme 3.11 Hydrogenation of carborane- and anthracene-containing random copolymer (**P10**)

The copolymer structures were characterized by NMR spectroscopy. The relevant spectra are given in Figures 3.62–3.64. As it is expected from a polymer molecule due to its proton multiplicity, broader peaks are observed in the ^{1}H NMR spectrum. In general, the characteristic oxanorbornene peaks at 6.39, 5.59 and 2.68 ppm shift upon polymerization and become broader. The signals for the anthracene groups appear as broad, ill-resolved multiplets between 7.38 and 8.49 ppm. In the ^{1}H NMR spectrum of **P8**, the characteristic olefin protons peak at 6.50 ppm of the monomers disappeared, while the backbone double bond (*cis*/*trans*) signals appear between 5.48 and 6.00 ppm. Analogous observations can be made for the ^{1}H NMR spectra of copolymers **P9** and **P10**. The relative ratio of *cis*/*trans* isomers of the polymers was assessed via integration of the respective ^{1}H NMR signals and is reported in Table 3.9. The intensity of the signals for the *trans* isomers is, for all copolymers, lower than that of the respective *cis* protons.

Table 3.9 Characterization of the carborane-anthracene-based random copolymers.

Polymer	m[a]	n[b]	Mole Ratio Th (m/n)[c]	Mole Ratio Obs (m/n)[d]	$M_{n/random}$ Th (g/mol)[e]	$M_{n/random}$ GPC (g/mol)[f]	PDI[f]	*cis/trans* Ratio[g]	Stereo-isomer[h] %
P8	151	28	5.4	6.33	80,000	48,452	1.62	1.68	63 *cis* 37 *trans*
P9	129	56	2.3	2.75	80,000	46,090	1.29	1.23	55 *cis* 45 *trans*
P10	108	84	1.28	1.7	80,000	48,993	1.12	1.17	54 *cis* 46 *trans*

[a] Theoretical degree of polymerization (DP) of monomer **2**.

[b] Theoretical DP of monomer **4**.

[c] Theoretical ratio of monomers in the random copolymer.

[d] Calculated mole ratio by using NMR spectroscopy.

[e] Theoretical molecular weight of the polymer.

[f] M_n and polydispersity index (PDI) are determined by GPC.

[g] *cis*/*trans* ratio in the polymer backbone are calculated by using ^{1}H NMR spectroscopy.

[h] Percentage of stereoisomers in the polymer backbone are calculated by ^{1}H NMR spectroscopy.

The ratios of monomer **2** and **4** for each copolymer were calculated via quantitative ^{1}H NMR (qNMR) spectroscopy. The number of the carborane repeating units and the number of anthracene repeating units (m and n in Scheme 3.10, respectively) are analyzed by NMR spectroscopy. The ratio of the aromatic anthracene peaks to the carborane-containing unit peaks for compound **P8** is 1.90 to 0.30, resulting in the copolymer ratio of m:n = 6.33. GPC analysis was used to determine the molecular weight distribution and the polydispersity index (Đ) of the random copolymers, using THF as eluent. Đ indicates the distribution of molecular mass in a polymer which refers to ratio of weight average molecular weight (M_w) to number average molecular weight (M_n). A polydispersity index (Đ) = 1 indicates the polymer chain to be monodisperse. However, normally it is difficult to synthesize polymer chains of identical M_w or M_n. Therefore, all polymers in the literature have Đ > 1. According to GPC results in this study, narrow molecular weight distributions with a *Đ* between 1.12 and 1.62 were determined (Table 3.9).

GPC-determined M_n values are almost half of the theoretical ones for all three copolymers. For example, the theoretical molecular weight of **P8** is 80,000 g/mol, while the observed M_n is 46,090 g/mol. The explanation of this can be that GPC separates molecules in polymers by size, it only provides the molecular weight distribution of a material, not the exact molecular weight. In general M_n of the respective polymers can be also calculated by end group analysis of the purified polymers. Even though styrenic end groups coming from the carbene moiety of the catalyst are visible at ca. 7.20–7.50 ppm and can be used to calculate the degree of polymerization, it was not possible to apply this specific method in this study, because the aromatic protons of the polymer backbone overlapped with the aromatic protons of the appended anthracene group.

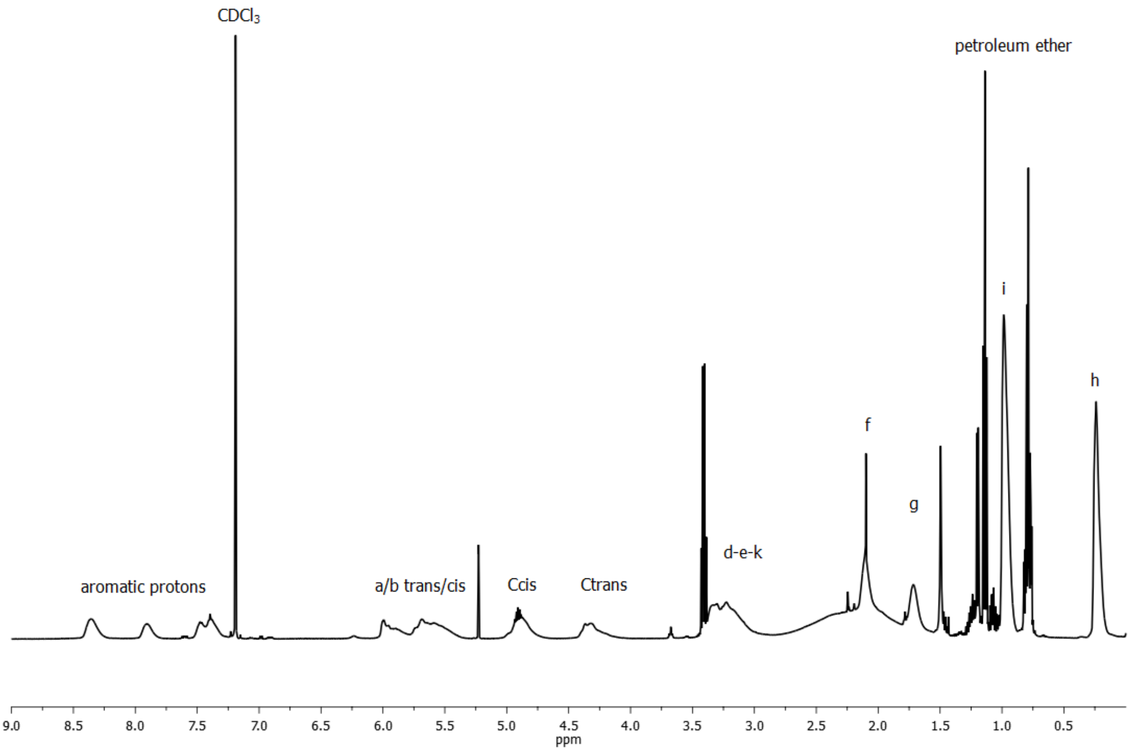

Figure 3.62 [1]H NMR (400.13 MHz) spectrum in $CDCl_3$ of carborane-anthracene-based random copolymer **P8**

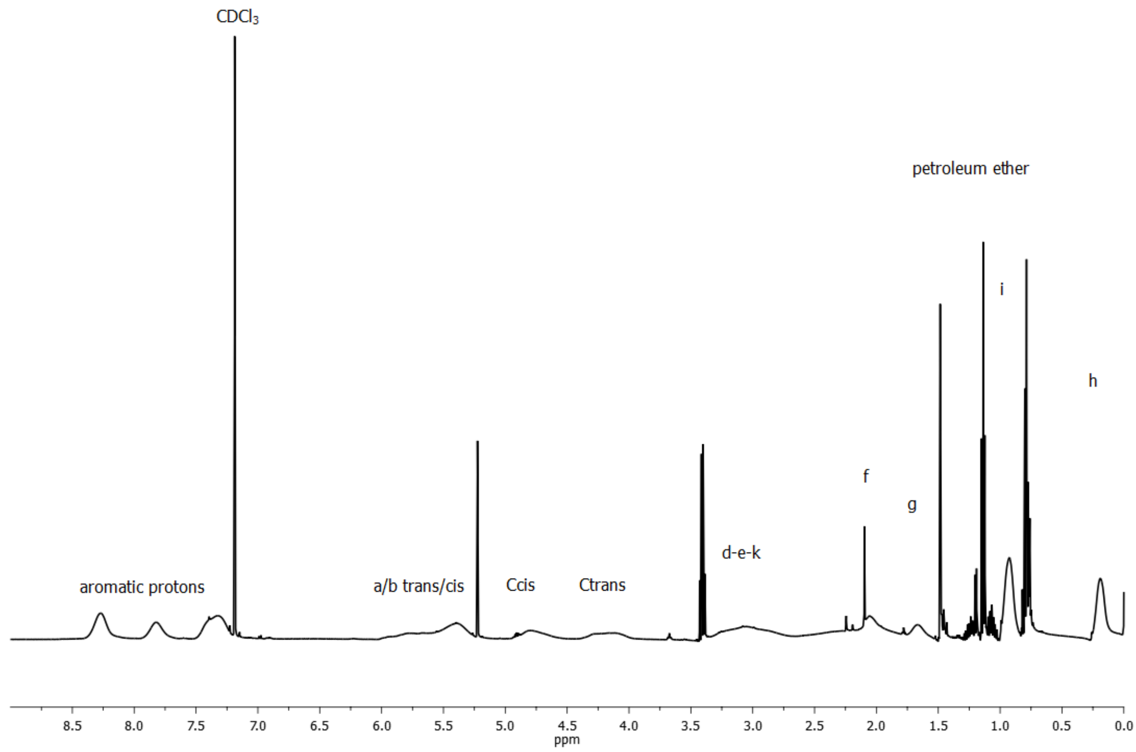

Figure 3.63 [1]H NMR (400.13 MHz) spectrum in $CDCl_3$of carborane-anthracene-based random copolymer **P9**

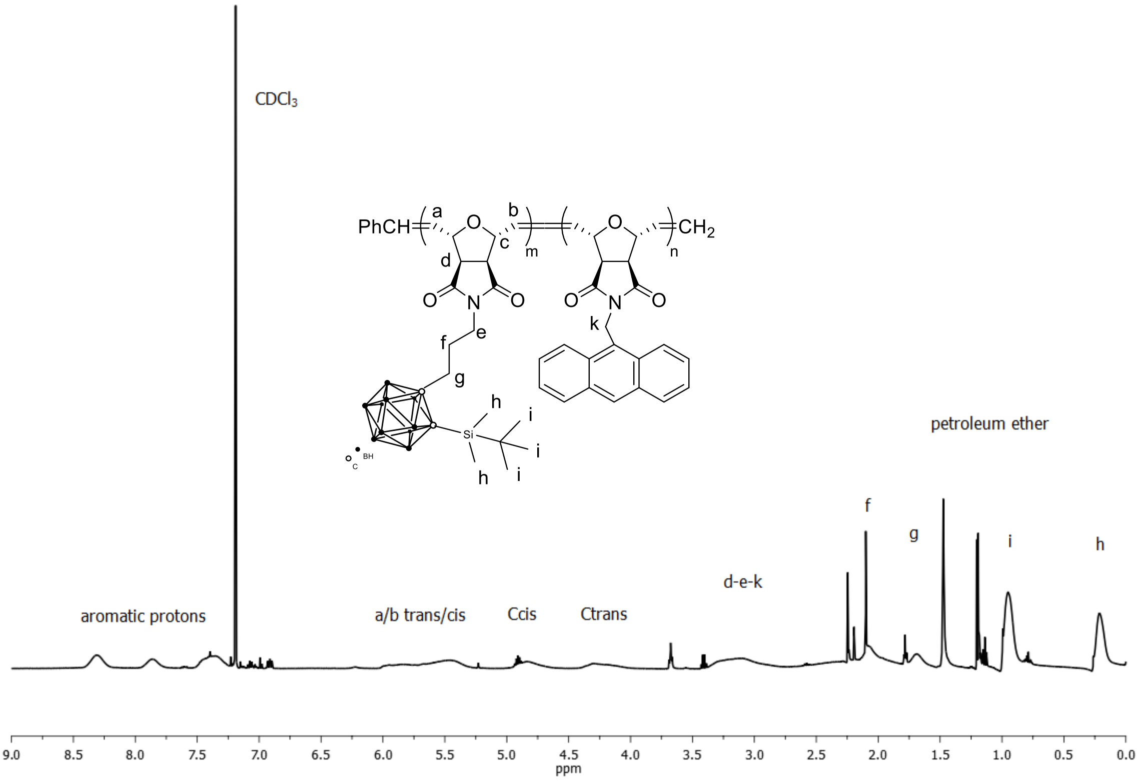

Figure 3.64 ^{1}H NMR (400.13 MHz) spectrum in $CDCl_3$ of carborane-anthracene-based random copolymer **P10**

3.3.3 Photodimerization Studies

In this work, we chose anthracene as a cross-linker for its well-known ability to undergo a photoinduced [4 π + 4 π] cycloaddition when irradiated with UV light of 350 nm, resulting in dimers that can be reversed via irradiation with wavelengths less than 300 nm or thermally at temperatures higher than 180 °C. We investigated the structure-property relationship of **P8**–**P11** of carborane-anthracene in the copolymer series derived via ROMP. Photoswitchable properties have been studied by irradiating the samples at 350 nm and 254 nm. Photodimerization studies of the polymers were performed as described in the literature [106]. Figures 3.65–3.72 show the time-dependent UV-vis spectra of **P8**–**P11**, upon irradiation at 350 or 254 nm.

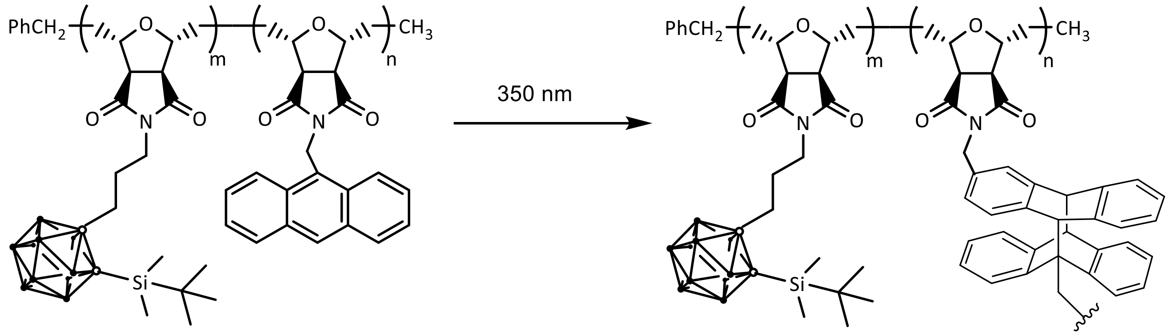

P11: 50kDa-30kDa Random Copolymer

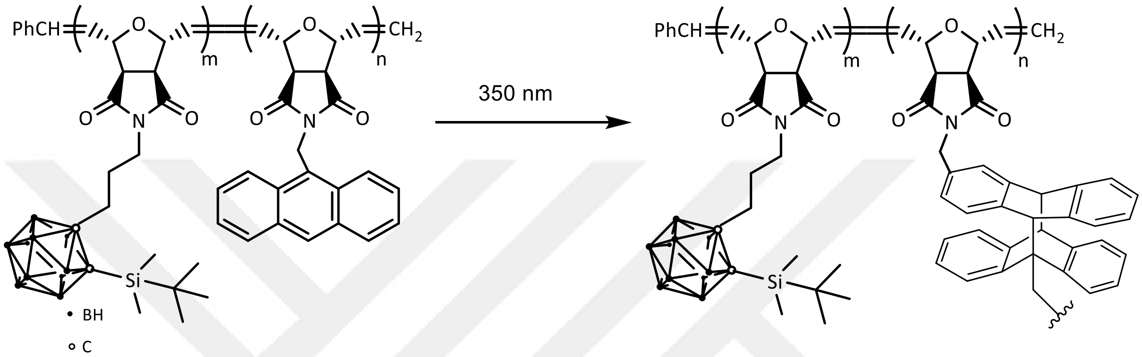

P8: 70kDa-10kDa Random Copolymer
P9: 60kDa-20kDa Random Copolymer
P10: 50kDa-30kDa Random Copolymer

Scheme 3.12 Irradiation of the polymers at 350 nm

Photodimerization is confirmed by the disappearance (Figures 3.65–3.68) of the characteristic anthracene π−π* absorption peak at ≈370 nm measured by UV–vis spectroscopy. Conversely, upon re-irradiation at 254 nm (Figures 3.69–3.72), re-appearance of the characteristic anthracene absorption peaks confirms that the dimer has been broken and the original copolymer was reformed.

Table 3.10 lists the amount of conversion (%) for each polymer, after irradiation at 350 nm, and then at 254 nm. The conversion (in %) of carborane-anthracene-based polymers is directly related to the amount of anthracene in the polymer backbone. More anthracene in the polymer backbone means more conversion after irradiating the polymers at 350 nm (photodimerization) and 254 nm (photocleavage).

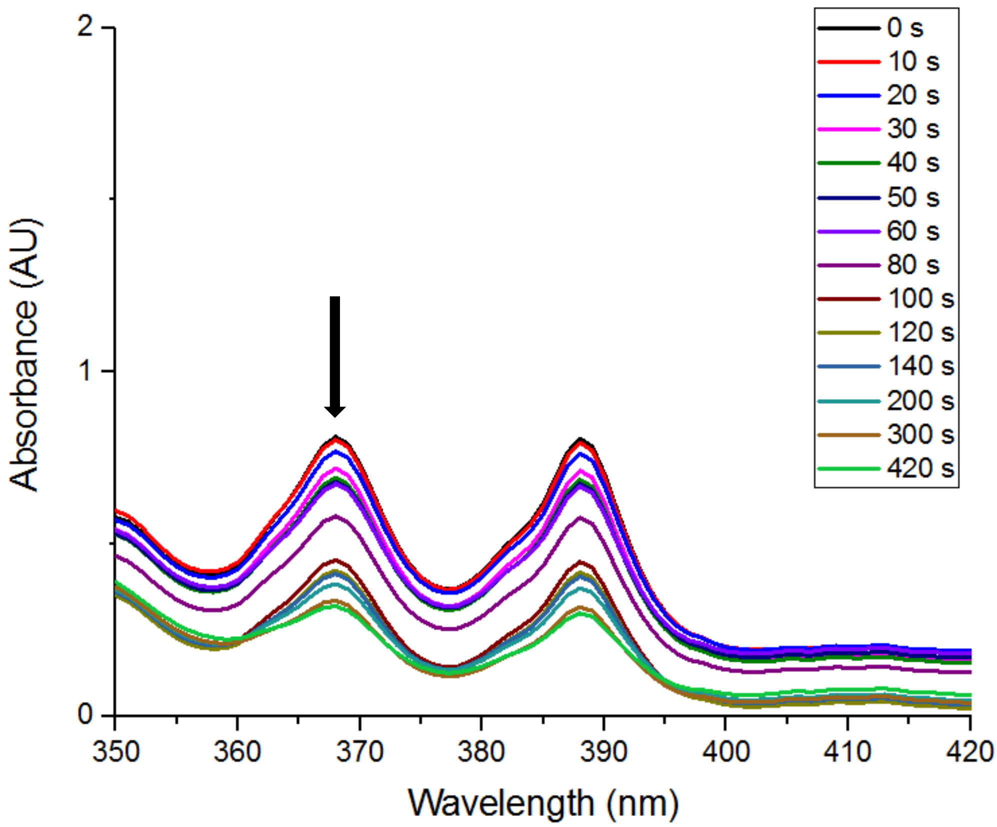

Figure 3.65 Overlay of UV–vis spectra for **P8**, confirming dimerization by monitoring the disappearance of the characteristic anthracene absorption (≈370 nm). Irradiation at 350 nm; irradiation time 420 s

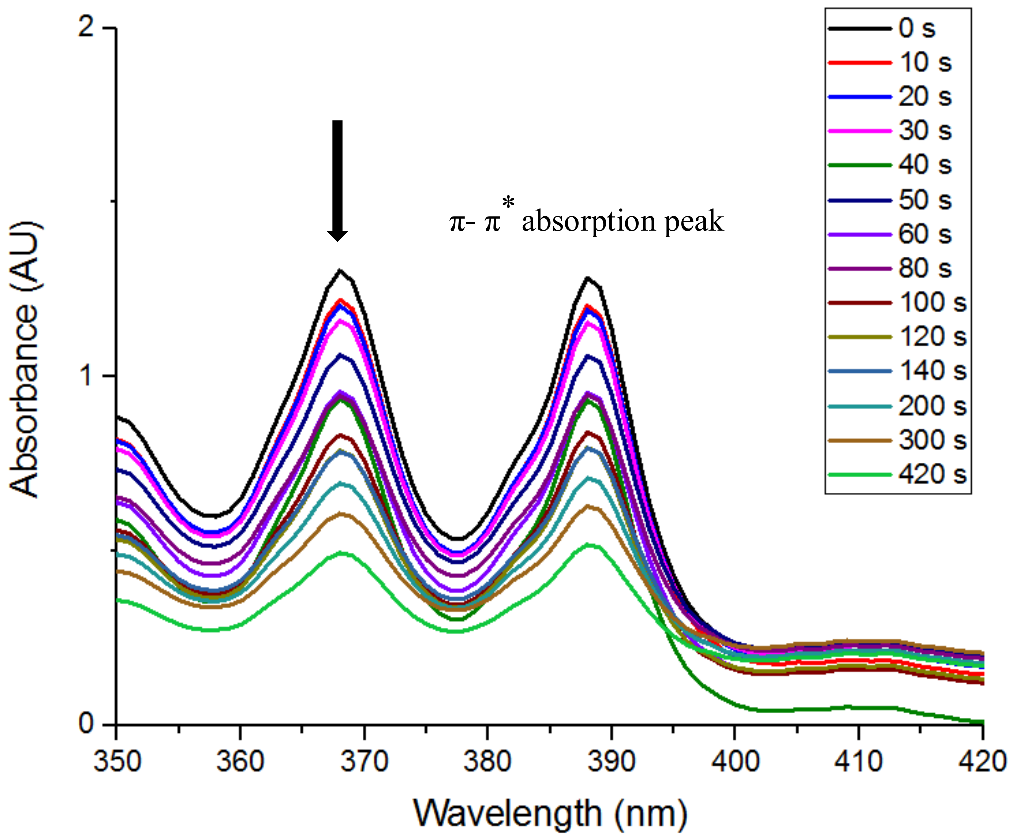

Figure 3.66 Overlay of UV–vis spectra for **P9**, confirming dimerization by monitoring the disappearance of the characteristic anthracene absorption (≈370 nm). Irradiation at 350 nm; irradiation time 420 s

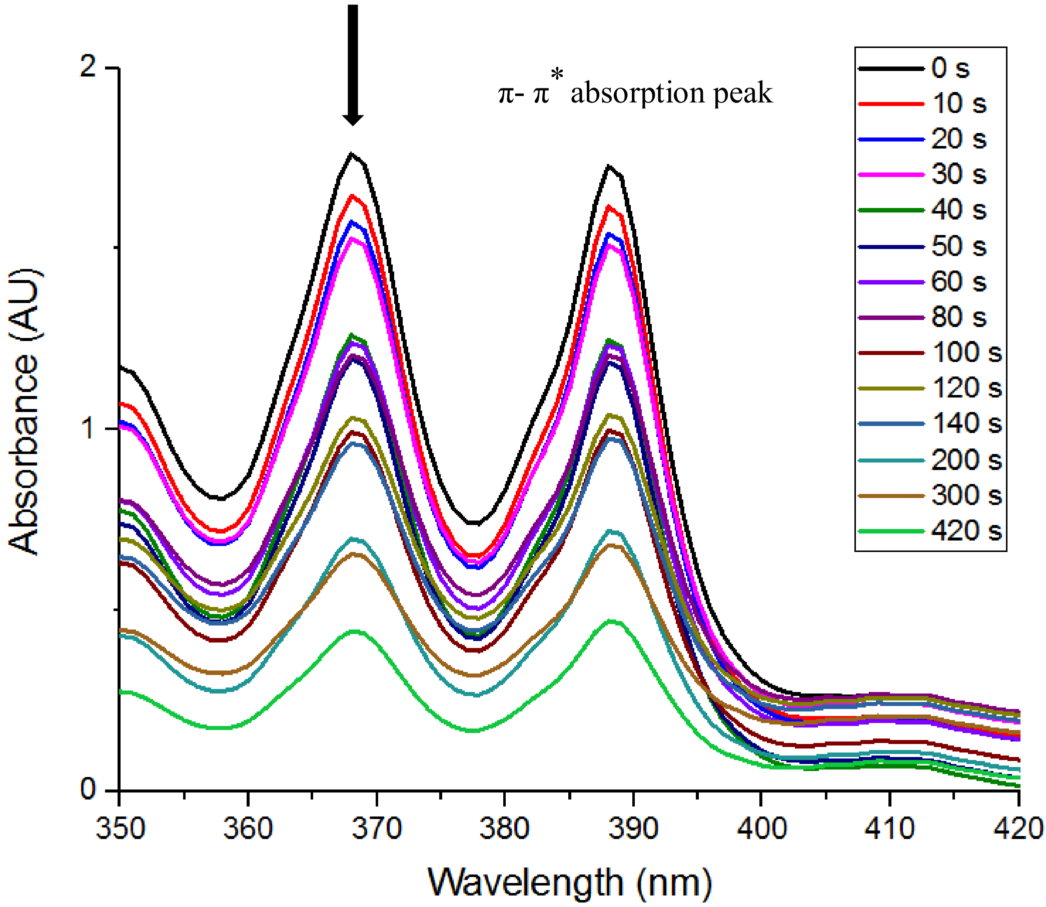

Figure 3.67 Overlay of UV–vis spectra for **P10**, confirming dimerization by monitoring the disappearance of the characteristic anthracene absorption (≈370 nm). Irradiation at 350 nm; irradiation time 420 s

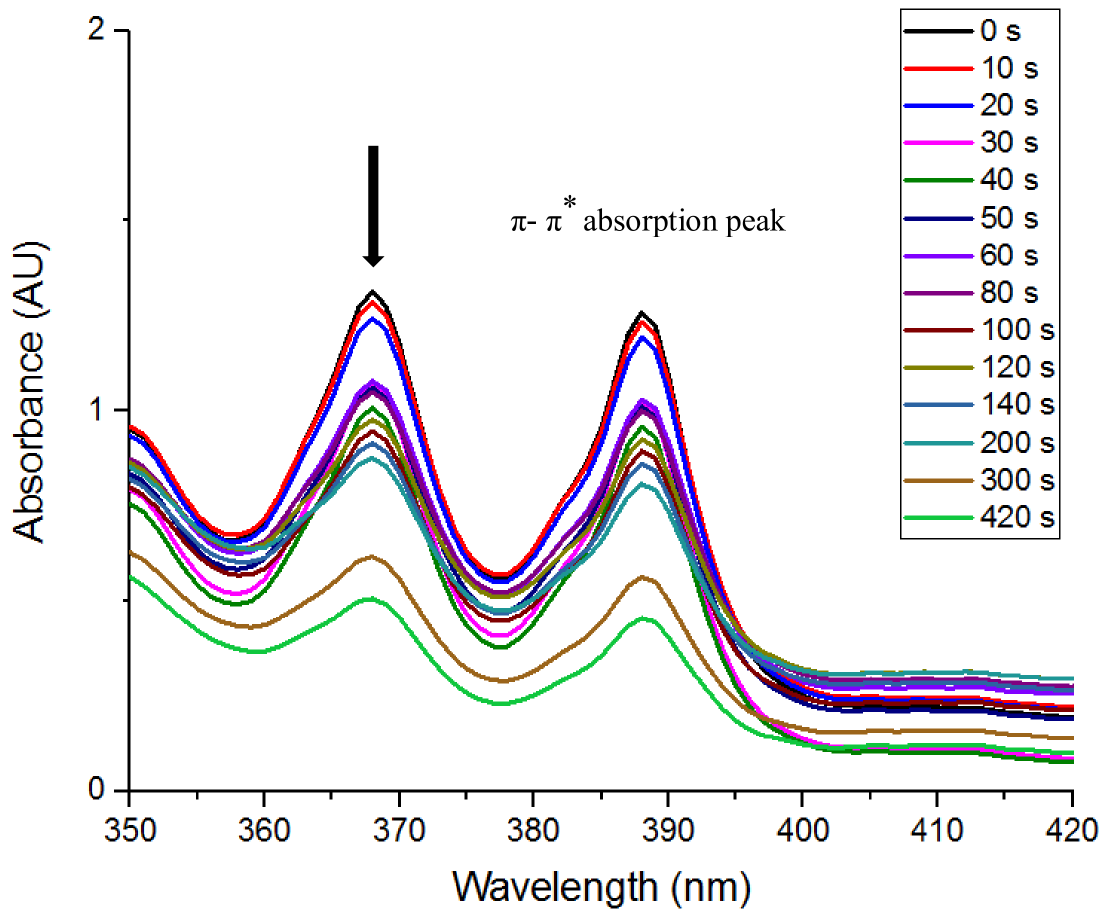

Figure 3.68 Overlay of UV–vis spectra for **P11**, confirming dimerization by monitoring the disappearance of the characteristic anthracene absorption (≈370 nm). Irradiation at 350 nm; irradiation time 420 s

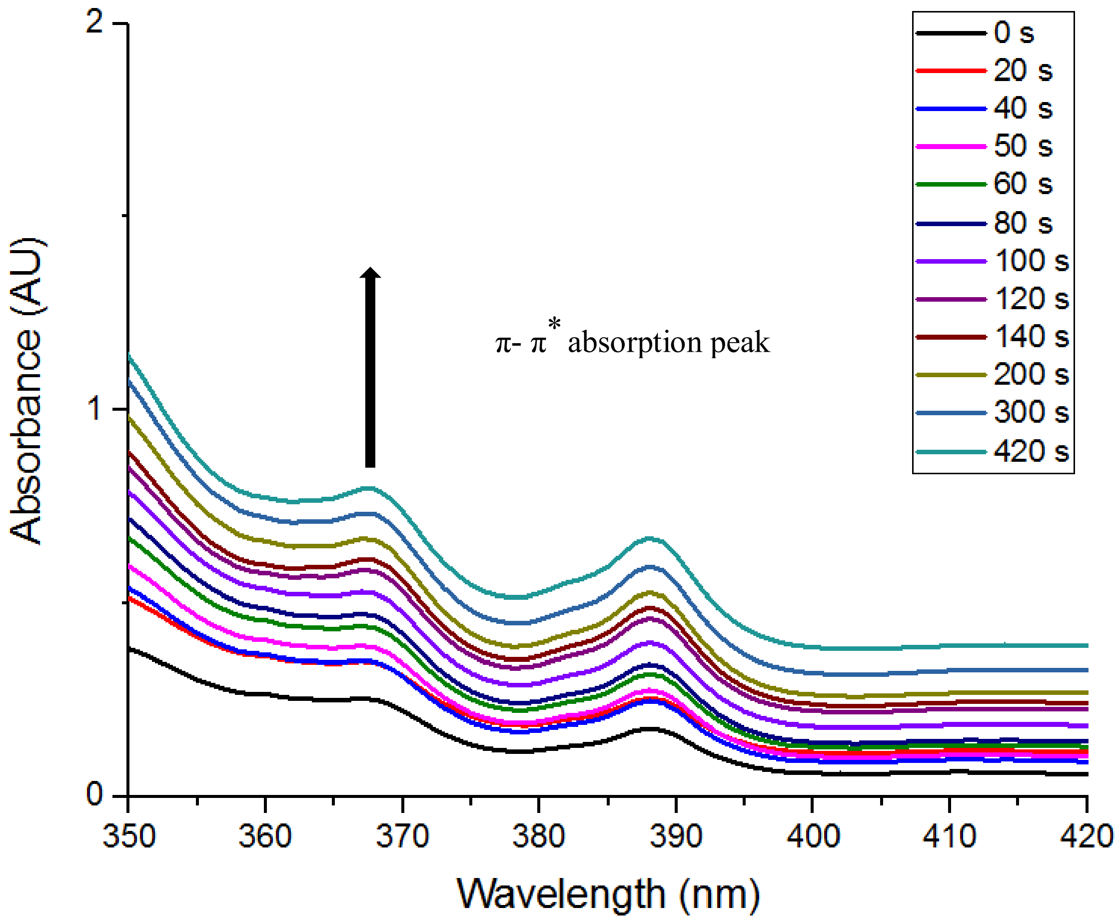

Figure 3.69 Overlay of UV–vis spectra for **P8**, confirming cleavage of the dimers by monitoring the appearance of the characteristic anthracene absorption (≈370 nm). Irradiation at 254 nm; irradiation time 420 s

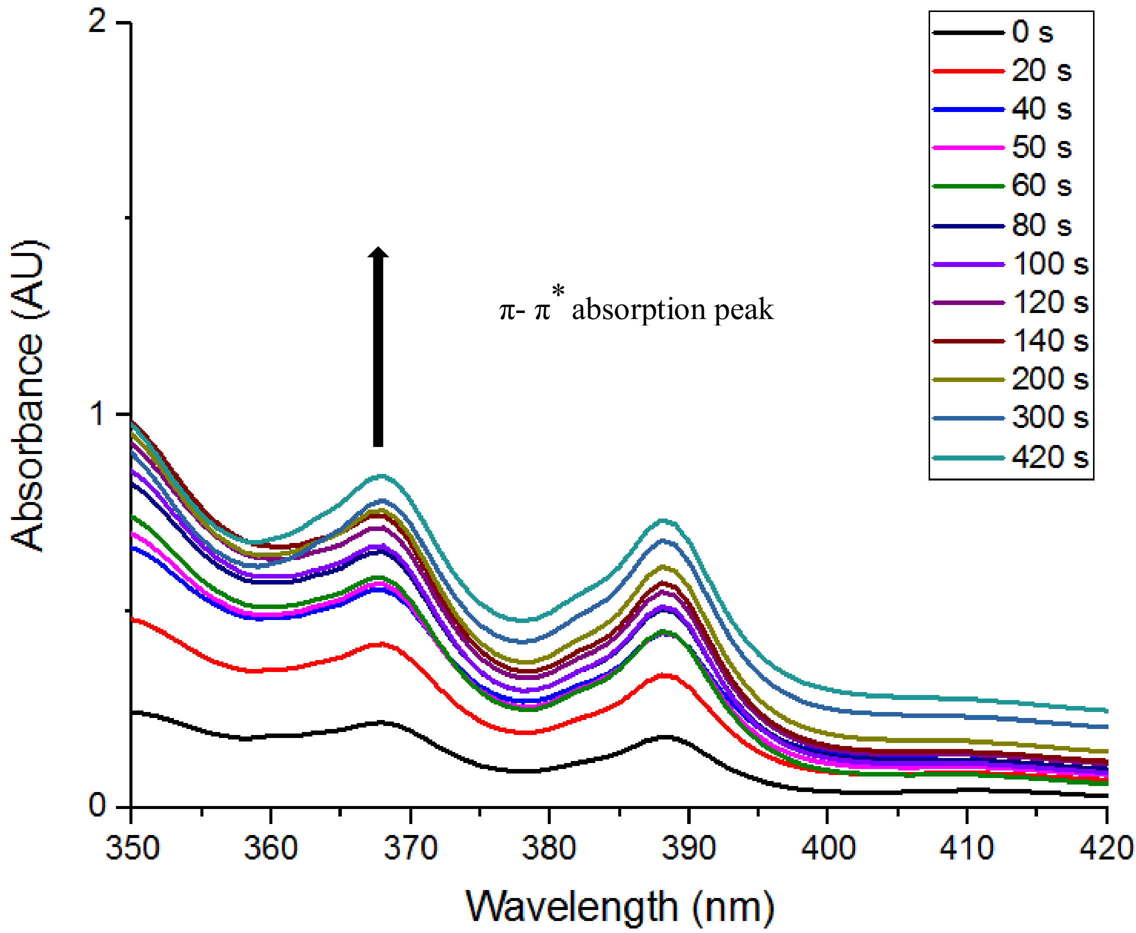

Figure 3.70 Overlay of UV–vis spectra for **P9**, confirming cleavage of the dimers by monitoring the appearance of the characteristic anthracene absorption (≈370 nm). Irradiation at 254 nm; irradiation time 420 s

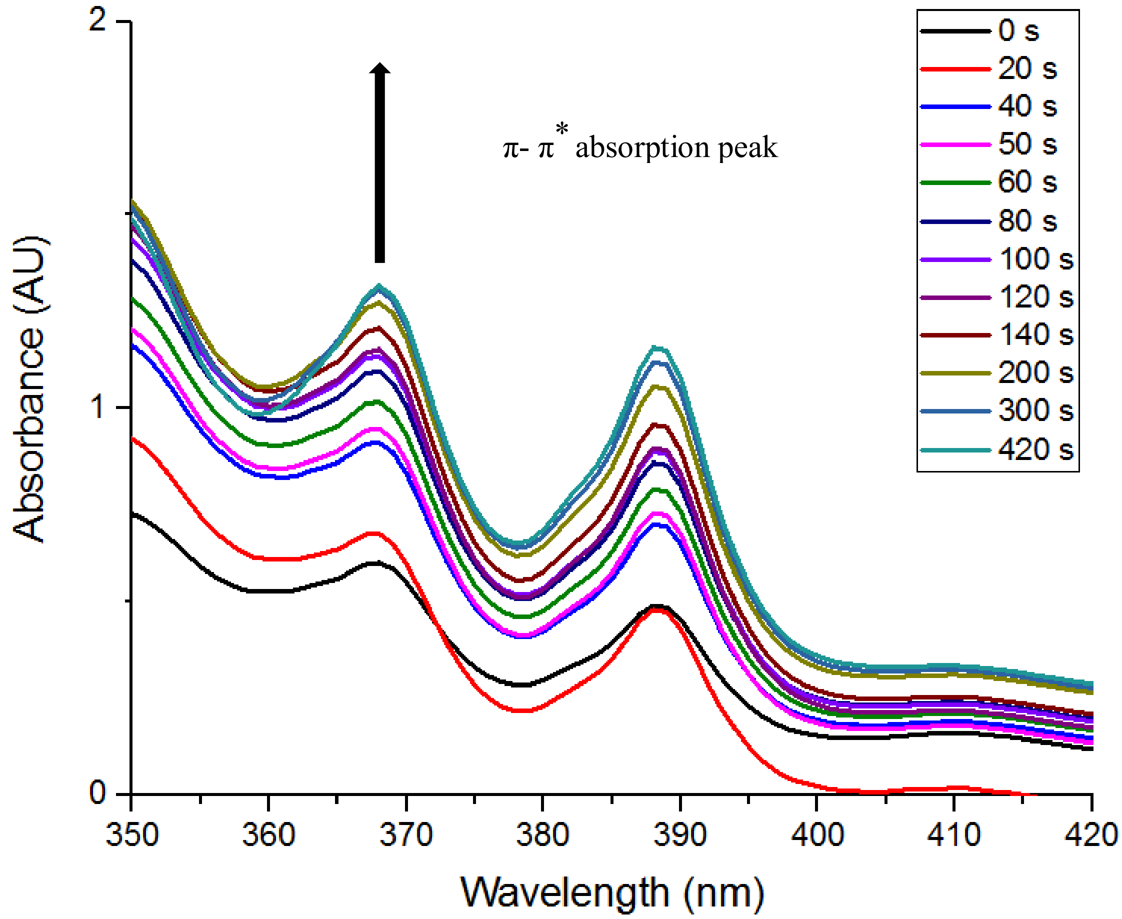

Figure 3.71 Overlay of UV–vis spectra for **P10**, confirming cleavage of the dimers by monitoring the appearance of the characteristic anthracene absorption (≈370 nm). Irradiation at 254 nm; irradiation time 420 s

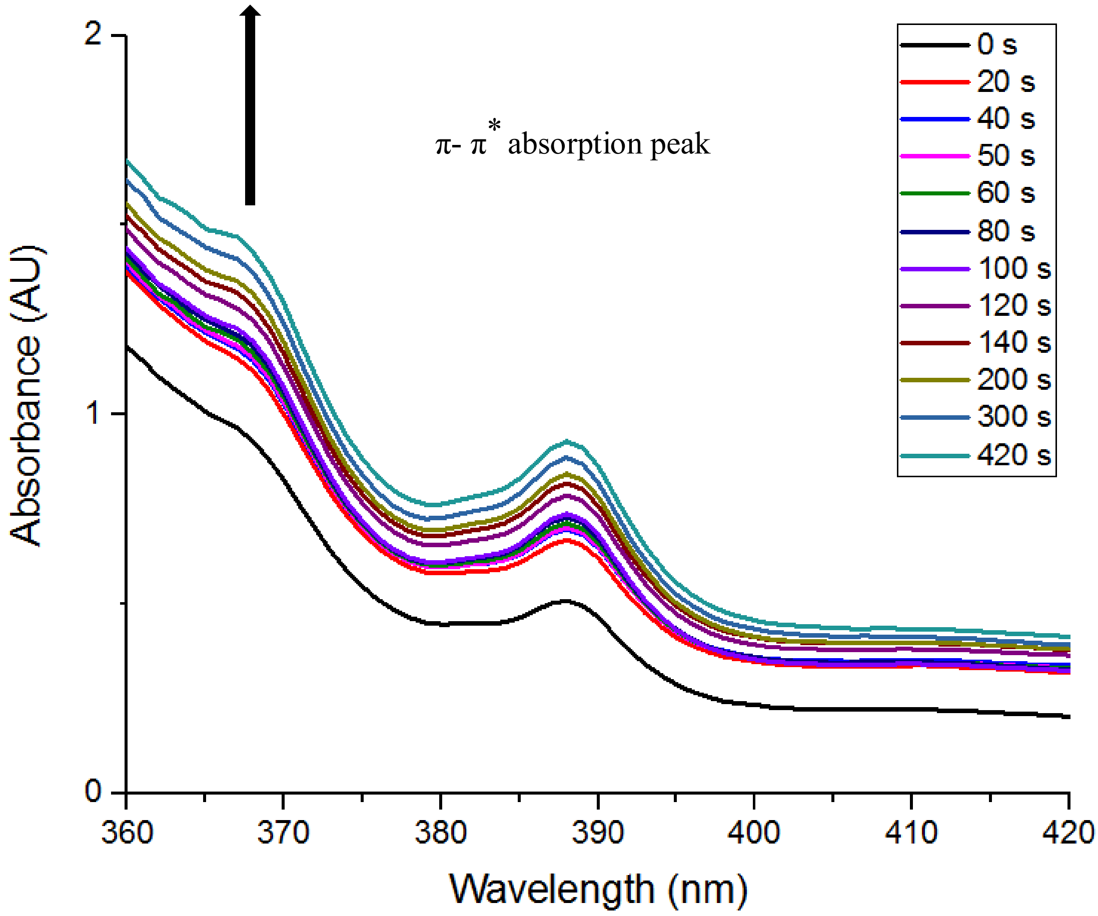

Figure 3.724 Overlay of UV–vis spectra for **P11**, confirming cleavage of the dimers by monitoring the appearance of the characteristic anthracene absorption (≈370 nm). Irradiation at 254 nm; irradiation time 420 s

Table 3.10 Conversion % of carborane-anthrecene-based random copolymers

Polymer	**Conversion % At 350 nm Photo Dimerization**	**Conversion % At 254 nm Photo Cleavage**
P7	60.6	59.9
P8	79.3	78.8
P9	75	54.6
P10	62.5	57.5

TGA was performed for copolymers **P8**, **P9** and **P10** between 25 °C and 600 °C under nitrogen. First degradation starts at 210 °C for each polymer, and char residue is 9% (**P10**), 7% (**P9**) and 5% (**P8**) by weight. While **P8** has the highest carborane content, its char residue was the lowest of the series. Therefore, it is suggested that the higher anthracene content is responsible for the higher flame resistance in these types of polymers under nitrogen.

Even though the polymers **P8**–**P10** contain thermally stable rigid groups such as carborane and anthracene, their char residues are less than 10% at 600 °C. Moreover, we observed much higher char yields for ROMP-type copolymers that contain both phosphorus and anthracene units in the backbone, in our previous work [94]. Therefore, we concluded that the flame-retardant properties of phosphorus-based blocks outstand those of icosahedral carborane clusters, for the specific case of anthracene-containing polymers, under nitrogen atmosphere.

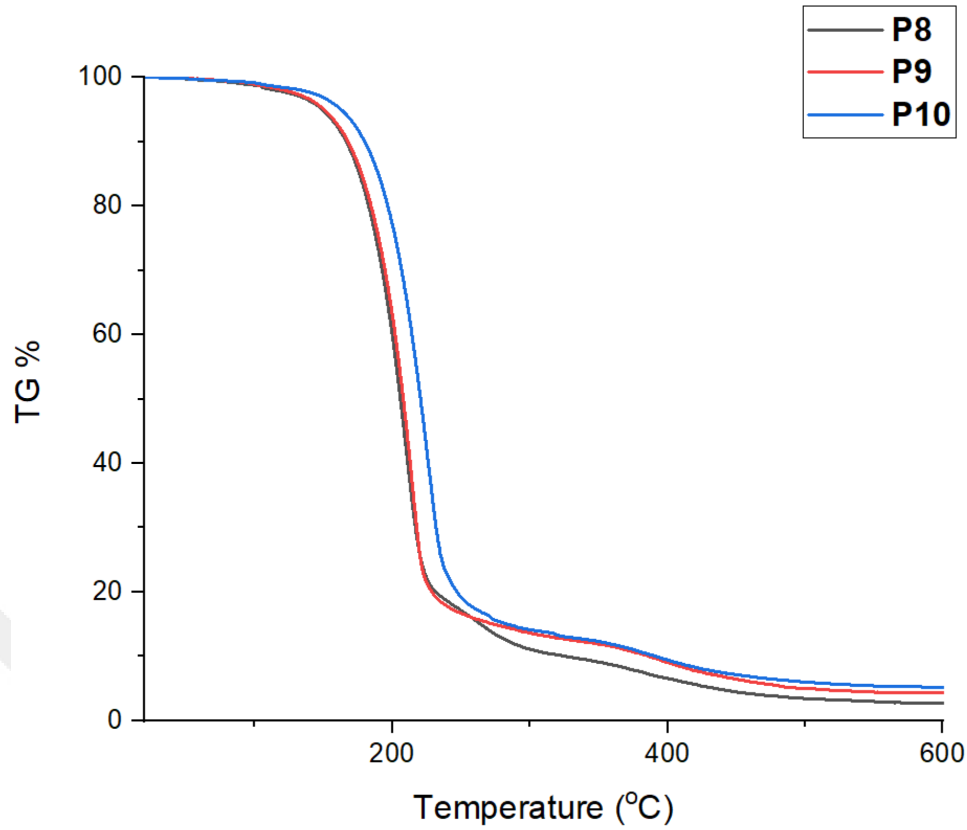

Figure 3.73 Thermogravimetric analysis of carborane- and anthracene-bearing random copolymers under nitrogen atmosphere

3.4 Conclusion

In the first part of the study (sections 3.1.3 and 3.1.4), we have successfully synthesized and characterized well-defined ROMP block copolymers, which contain carborane and phosphonate ester groups (**P1–P3**), with the calculated ratio of blocks 4:1 (**P1**), 1:4 (**P2**) and 1:1 (**P3**), and the same total molecular weight (50 kDa). Hydrolysis of the phosphonate esters yielded the corresponding phosphoric acid-containing block copolymers **P1A–P3A**. Thermogravimetric analysis (TGA) results indicated that phosphoric acid-containing polymers produce more char residue than the corresponding phosphonate ester polymers, both under nitrogen atmosphere and in air. Furthermore, polymers **P2** and **P2A**, which contain the highest amount of phosphorus, produced the highest char residue under nitrogen atmosphere (**P2** 59.3 weight%; **P2A** 60.4 weight%), while **P1**, which has a higher carborane content, gave the highest char residue in air (62.4%), due to the oxidation to B_2O_3. Micro combustion calorimetry (MCC) revealed that **P1A**, which has the higher carborane content, gave the lowest HRR (9.6 W/g). Since the lower HRR values (in MCC) and higher char residue (in TGA) indicate higher flame retardancy properties, the carborane-rich polymers can be highly effective as flame-retardants.

In section 3.1.6, the coating efficiency of **P1A**, **P2A** and **P3A** on bare iron oxide nanoparticles was investigated. ICP-MS analysis revealed that polymer **P2A**, which possesses the highest phosphoric acid content, had the highest coating efficiency of the series of tested polymers. Moreover, phosphoric acid groups showed, in general, better chelating efficiencies than phosphonate ester groups.

The carborane-phosphorus-based ROMP random copolymers (**P4**–**P6**) were also synthesized and characterized. They showed different thermal properties than block copolymers. For example, **P3** (block copolymer) and **P6** (random copolymer) both contain phosphonate ester and carborane groups in a 1:1 ratio in the polymer backbone but gave significantly different char residues in air and under nitrogen atmosphere. Based on the MCC studies, random ROMP copolymers **P5** and **P6** show less combustibility than the corresponding block copolymers **P2** and **P3** of the same composition.

In the second part of the study (section 3.2), after synthesizing carborane-diol monomer **3**, phospha-carborane-containing oligomer (**P7**) was obtained via condensation polymerization. Synthesized oligomer (**P7**) was used for doping epoxy resin with varying weight percentage from 5 %–20% (**$P7_{5\%}$– $P7_{20\%}$**). According to MCC results, the optimal amount of flame-retardant (**P7**) loading was found to be 7.5% by weight in the epoxy resin.

In the last part of the study (section 3.3.3), the photo-switchable properties of carborane- and anthracene-containing polymers (**P8–P10**) were investigated. The molecular weight of the polymers was kept constant (80 000 g/mol), with varying monomer weight ratios (1:7, 2:6, and 3:5, for **P8**, **P9** and **P10**, respectively), in order to investigate the structure-photochemical properties relationship depending on the relative carborane to anthracene content. Intramolecular photodimerization of anthracene was observed for each polymer of the series. The formation of anthracene photo dimers upon irradiation with UV light (350 nm) was followed via UV-vis spectroscopy, by observing the disappearance of the characteristic $\pi-\pi^*$ absorption peak of anthracene at $\approx$ 370 nm. To study the reversibility of the anthracene photodimerization, the photo-dimerized samples were then irradiated with UV light at 254 nm. The UV-vis spectra show the partial reappearance of the anthracene absorption peak. The conversion (monomer–dimer) of the polymers (in %) upon irradiation is directly depending on the amount of anthracene in the polymer backbone. Calculated values after photodimerization for **P10**, which has the highest content of anthracene, is 75%, whereas for **P8**, which has the lowest content of anthracene, it is 60.6%.

The polymers synthesized in this study showed very interesting properties for applications in several fields. For example, the phospha-carborane-containing ROMP-based polymers and condensation oligomer should be further investigated for application as flame retardants. Furthermore, iron oxide nanoparticles coated with carborane- and phosphoric acid-containing polymers could be possibly used for medical applications, such as magnetic resonance imaging (MRI) agents. Finally, the carborane-anthracene containing polymers have the potential of being implemented as smart materials for the development of novel shape memory polymers.

REFERENCES

[1] Sanchez, C. Lebeau, B. Chaput, F. ve Boilot, J.P., (2003). "Optical properties of functional hybrid organic–inorganic nanocomposites", Advanced Materials, 15: 1969-1994.

[2] Orilall, M.C. ve Wiesner, U., (2011). "Block copolymer based composition and morphology control in nanostructured hybrid materials for energy conversion and storage: solar cells, batteries, and fuel cells", Chemical Society Reviews, 40: 520-535.

[3] Hadjichristidis, N. Pispas, S. ve Floudas, G., (2003). Block copolymers: synthetic strategies, physical properties, and applications: John Wiley & Sons.

[4] Al-Badri, Z.M. Maddikeri, R.R. Zha, Y. Thaker, H.D. Dobriyal, P. Shunmugam, R. Russell, T.P. ve Tew, G.N., (2011). "Room temperature magnetic materials from nanostructured diblock copolymers", Nature communications, 2: 482.

[5] Belfield, K.D. ve Zhang, L., (2006). "Norbornene-functionalized diblock copolymers via ring-opening metathesis polymerization for magnetic nanoparticle stabilization", Chemistry of materials, 18: 5929-5936.

[6] Discher, D.E. ve Eisenberg, A., (2002). "Polymer vesicles", Science, 297: 967-973.

[7] Gao, Z. Varshney, S.K. Wong, S. ve Eisenberg, A., (1994). "Block copolymer" Crew-Cut" micelles in water", Macromolecules, 27: 7923-7927.

[8] Gref, R. Minamitake, Y. Peracchia, M.T. Trubetskoy, V. Torchilin, V. ve Langer, R., (1994). "Biodegradable long-circulating polymeric nanospheres", Science, 263: 1600-1603.

[9] Hayward, R.C. ve Pochan, D.J., (2010). "Tailored assemblies of block copolymers in solution: it is all about the process", Macromolecules, 43: 3577-3584.

[10] Mai, Y. ve Eisenberg, A., (2012). "Self-assembly of block copolymers", Chemical Society Reviews, 41: 5969-5985.

[11] Pu, L. Wang, J. Li, N. Chai, Q. Irache, J.M. Wang, G. Tang, J.Z. ve Gu, Z., (2016). "Synthesis of Electroneutralized Amphiphilic Copolymers with Peptide Dendrons for Intramuscular Gene Delivery", ACS applied materials & interfaces, 8: 13724-13734.

[12] Schacher, F.H. Rupar, P.A. ve Manners, I., (2012). "Functional block copolymers: nanostructured materials with emerging applications", Angewandte Chemie International Edition, 51: 7898-7921.

[13] Xu, H. Yang, P. Ma, H. Yin, W. Wu, X. Wang, H. Xu, D. ve Zhang, X., (2016). "Amphiphilic block copolymers-based mixed micelles for noninvasive drug delivery", Drug Delivery, 23: 3063-3071.

[14] Rüttiger, C. Hübner, H. Schöttner, S. Winter, T. Cherkashinin, G. Kuttich, B.r. Stühn, B. ve Gallei, M., (2018). "Metallopolymer-Based Block Copolymers for the Preparation of Porous and Redox-Responsive Materials", ACS applied materials & interfaces, 10: 4018-4030.

[15] Xiong, H. Wei, X. Zhou, D. Qi, Y. Xie, Z. Chen, X. Jing, X. ve Huang, Y., (2016). "Amphiphilic polycarbonates from carborane-installed cyclic carbonates as potential agents for boron neutron capture therapy", Bioconjugate chemistry, 27: 2214-2223.

[16] Eren, T. ve Tew, G.N., (2009). "Phosphonic acid-based amphiphilic diblock copolymers derived from ROMP", Journal of Polymer Science Part A: Polymer Chemistry, 47: 3949-3956.

[17] Queffélec, C. Petit, M. Janvier, P. Knight, D.A. ve Bujoli, B., (2012). "Surface modification using phosphonic acids and esters", Chemical Reviews, 112: 3777-3807.

[18] Boyer, C. Whittaker, M.R. Bulmus, V. Liu, J. ve Davis, T.P., (2010). "The design and utility of polymer-stabilized iron-oxide nanoparticles for nanomedicine applications", NPG Asia Materials, 2: 23.

[19] Qiu, Z. Ren, S. ve Xie, Z., (2011). "Transition metal– carboryne complexes: synthesis, bonding, and reactivity", Accounts of chemical research, 44: 299-309.

[20] Zhang, J. ve Xie, Z., (2014). "Synthesis, structure, and reactivity of 13-and 14-vertex carboranes", Accounts of chemical research, 47: 1623-1633.

[21] Schleyer, P.v.R. ve Najafian, K., (1998). "Stability and Three-Dimensional Aromaticity of closo-Monocarbaborane Anions, CB n-1Hn-, and closo-Dicarboranes, C2B n-2H n", Inorganic chemistry, 37: 3454-3470.

[22] Chattaraj, P.K., (2009). Chemical reactivity theory: a density functional view: CRC press.

[23] McArthur, S.G. Jay, R. Geng, L. Guo, J. ve Lavallo, V., (2017). "Below the 12-vertex: 10-vertex carborane anions as non-corrosive, halide free, electrolytes for rechargeable Mg batteries", Chemical Communications, 53: 4453-4456.

[24] Chan, T.L. ve Xie, Z., (2018). "Synthesis, structure and aromaticity of carborane-fused carbo-and heterocycles", Chemical science, 9: 2284-2289.

[25] Axtell, J.C. Kirlikovali, K.O. Jung, D. Dziedzic, R.M. Rheingold, A.L. ve Spokoyny, A.M., (2017). "Metal-Free Peralkylation of the closo-Hexaborate Anion", Organometallics, 36: 1204-1210.

[26] Li, J. Logan, C.F. ve Jones, M., (1991). "Simple syntheses and alkylation reactions of 3-iodo-o-carborane and 9,12-diiodo-o-carborane", Inorganic chemistry, 30: 4866-4868.

[27] Hofmann, M. Fox, M.A. Greatrex, R. Schleyer, P.v.R. ve Williams, R.E., (2001). "Empirical and ab Initio Energy/Architectural Patterns for 73 nido-6〈V〉-Carborane Isomers, from B6H9- to C4B2H6", Inorganic chemistry, 40: 1790-1801.

[28] Kiani, F.A. ve Hofmann, M., (2006). "Ortho-, Meta-, and Para-Directing Influence of Transition-Metal Fragments in 12-Vertex closo-Cyclopentadienylmetallaheteroboranes: Additive Nature of Structural Increments", Organometallics, 25: 485-490.

[29] Bregadze, V.I., (1992). "Dicarba-closo-dodecaboranes C2B10H12 and their derivatives", Chemical Reviews, 92: 209-223.

[30] Kalinin, V.N. ve Ol'shevskaya, V.A., (2008). "Some aspects of the chemical behavior of icosahedral carboranes", Russian Chemical Bulletin, 57: 815-836.

[31] Grimes, R.N., (2015). "Carboranes in the chemist's toolbox", Dalton Transactions, 44: 5939-5956.

[32] Plesek, J., (1992). "Potential applications of the boron cluster compounds", Chemical Reviews, 92: 269-278.

[33] Hatanaka, H. ve Nakagawa, Y., (1994). "Clinical results of long-surviving brain tumor patients who underwent boron neutron capture therapy", International Journal of Radiation Oncology*Biology*Physics, 28: 1061-1066.

[34] Laramore, G.E. Wootton, P. Livesey, J.C. Wilbur, D.S. Risler, R. Phillips, M. Jacky, J. Buchholz, T.A. Griffin, T.W. ve Brossard, S., (1994). "Boron neutron capture therapy: A mechanism for achieving a concomitant tumor boost in fast neutron radiotherapy", International Journal of Radiation Oncology*Biology*Physics, 28: 1135-1142.

[35] Taylor, H.J. ve Goldhaber, M., (1935). "Detection of Nuclear Disintegration in a Photographic Emulsion", Nature, 135: 341-341.

[36] Huang, X. Zhang, Q. Meng, Z. Gu, J. Jia, X. ve Xi, K., (2015). "Greatly enhanced thermo-oxidative stability of polybenzoxazine thermoset by incorporation of m-carborane", Journal of Polymer Science Part A: Polymer Chemistry, 53: 973-980.

[37] Liu, S. Zhou, Q. Peng, Z. Song, N. ve Ni, L., (2017). "Silicon alkyne hybrid polymers containing Si–H and Si–CH3: Synthesis, characterization, and thermal and oxidative properties", High Performance Polymers, 30: 259-266.

[38] Tong, D. Wang, H. Wang, L. Chen, L. ve Li, Z., (2017). "Coating of poly(carborane-carbosilane-phenylacetylene) on carbon fibers with excellent oxidation protection", Surface and Coatings Technology, 319: 335-344.

[39] Coderre, J.A. Turcotte, J.C. Riley, K.J. Binns, P.J. Harling, O.K. ve Kiger, W.S., (2003). "Boron Neutron Capture Therapy: Cellular Targeting of High Linear Energy Transfer Radiation", Technology in Cancer Research & Treatment, 2: 355-375.

[40] Sun, Y.-L. Zheng, B.-B. ve Zhang, W., (2017). "Role of crystallization water molecules on hydrogen-bonded structures and dielectric phase transitions in amino trimethylene phosphonic acid-based crystals", New Journal of Chemistry, 41: 5142-5150.

[41] Lu, S.-Y. ve Hamerton, I., (2002). "Recent developments in the chemistry of halogen-free flame retardant polymers", Progress in Polymer Science, 27: 1661-1712.

[42] Woodward, G. Harris, C. ve Manku, J., (1999). "Design of New Organophosphorus Flame Retardants", Phosphorus, Sulfur, and Silicon and the Related Elements, 144: 25-28.

[43] Weil, E.D. Levchik, S.V. Ravey, M. ve Zhu, W., (1999). "A Survey of Recent Progress in Phosphorus-Based Flame Retardants and Some Mode of Action Studies", Phosphorus, Sulfur, and Silicon and the Related Elements, 144: 17-20.

[44] Chen, L. ve Wang, Y.-Z., (2010). "Aryl polyphosphonates: useful halogen-free flame retardants for polymers", Materials, 3: 4746-4760.

[45] Lu, X. Xia, G. Lemmon, J.P. ve Yang, Z., (2010). "Advanced materials for sodium-beta alumina batteries: Status, challenges and perspectives", Journal of Power Sources, 195: 2431-2442.

[46] Shaw, S., (2010). Halogenated Flame Retardants: Do the Fire Safety Benefits Justify the Risks?, ed^eds. Reviews on Environmental Health. 261.

[47] Ranganathan, T. Zilberman, J. Farris, R.J. Coughlin, E.B. ve Emrick, T., (2006). "Synthesis and Characterization of Halogen-Free Antiflammable Polyphosphonates Containing 4,4‘-Bishydroxydeoxybenzoin", Macromolecules, 39: 5974-5975.

[48] Ranganathan, T. Ku, B.-C. Zilberman, J. Beaulieu, M. Farris, R.J. Coughlin, E.B. ve Emrick, T., (2007). "Poly(arylate-phosphonate) copolymers with deoxybenzoin in the backbone: Synthesis, characterization, and thermal properties", Journal of Polymer Science Part A: Polymer Chemistry, 45: 4573-4580.

[49] Wang, C. Huang, F. Jiang, Y. Li, J. Zhou, Y. ve Du, L., (2012). "Oxidation behavior of carbon materials derived from a carborane- and silicon-incorporated polymer", Ceramics International, 38: 3081-3088.

[50] Avci, D. ve Albayrak, A.Z., (2003). "Synthesis and copolymerization of new phosphorus-containing acrylates", Journal of Polymer Science Part A: Polymer Chemistry, 41: 2207-2217.

[51] Procházková, S. Böhmová, Z. Kubíček, V. Kotek, J. Hermann, P. ve Lukeš, I., (2014). "Phosphinate Analogues of Ida and Nta with Low Basicity of Nitrogen Atom: Acid-Base and Complexation Properties", Phosphorus, Sulfur, and Silicon and the Related Elements, 189: 933-945.

[52] Britze, A. Moosmann, K. Jähne, E. Adler, H.-J. ve Kuckling, D., (2006). "Synthesis of Block Copolymers Modified with Phosphonate Ester Groups Using Nitroxide-Mediated Radical Polymerization", Macromolecular Rapid Communications, 27: 1906-1912.

[53] David, G. Ortega, E. Chougrani, K. Manseri, A. ve Boutevin, B., (2011). "Grafting of phosphonate groups onto PVA by acetalyzation. Evaluation of the anti-corrosive properties for the acetalyzed PVA coatings", Reactive and Functional Polymers, 71: 599-606.

[54] Nowack, B., (2003). "Environmental chemistry of phosphonates", Water Research, 37: 2533-2546.

[55] Vega, C. ve Abascal, J.L.F., (2011). "Simulating water with rigid non-polarizable models: a general perspective", Physical Chemistry Chemical Physics, 13: 19663-19688.

[56] Nowack, B. ve Stone, A.T., (2000). "Degradation of Nitrilotris(methylenephosphonic Acid) and Related (Amino)Phosphonate Chelating Agents in the Presence of Manganese and Molecular Oxygen", Environmental Science & Technology, 34: 4759-4765.

[57] Alcala, M. Criado, J. Real, C. Grygar, T. Nejezchleba, M. Subrt, J. ve Petrovsky, E., (2004). "Synthesis of nanocrystalline magnetite by mechanical alloying of iron and hematite", Journal of Materials Science, 39: 2365-2370.

[58] Zhang, D. Zhang, X. Ni, X. Song, J. ve Zheng, H., (2007). "Fabrication and Characterization of Fe3O4 Octahedrons via an EDTA-Assisted Route", Crystal Growth & Design, 7: 2117-2119.

[59] Cornell, R.M. ve Schwertmann, U., (2003). The iron oxides: structure, properties, reactions, occurrences and uses: John Wiley & Sons.

[60] Schwertmann, U. ve Cornell, R.M., (2000). Iron oxides in the laboratory: Wiley Online Library.

[61] Gupta, A.K. ve Gupta, M., (2005). "Synthesis and surface engineering of iron oxide nanoparticles for biomedical applications", Biomaterials, 26: 3995-4021.

[62] Liang, J. Li, L. Luo, M. ve Wang, Y., (2011). "Fabrication of Fe3O4 octahedra by a triethanolamine-assisted hydrothermal process", Crystal Research and Technology, 46: 95-98.

[63] Wu, W. He, Q. ve Jiang, C., (2008). "Magnetic iron oxide nanoparticles: synthesis and surface functionalization strategies", Nanoscale research letters, 3: 397.

[64] Nadagouda, M.N. ve Varma, R.S., (2007). "A greener synthesis of core (Fe, Cu)-shell (Au, Pt, Pd, and Ag) nanocrystals using aqueous vitamin C", Crystal Growth and Design, 7: 2582-2587.

[65] Roy, S. ve Das, T.K., (2015). "Plant Mediated Green Synthesis of Silver Nanoparticles-A", A Review. Int. J. Plant Biol. Res, 3: 1044-1055.

[66] Saeedi, M.S. Tangestaninejad, S. Moghadam, M. Mirkhani, V. Mohammadpoor-Baltork, I. ve Khosropour, A.R., (2013). "Magnetic nanoparticles supported manganese (III) tetrapyridylporphyrin catalyst via covalent interaction: A highly efficient and reusable catalyst for the oxidation of hydrocarbons", Polyhedron, 49: 158-166.

[67] Yong, Y. Bai, Y. Li, Y. Lin, L. Cui, Y. ve Xia, C., (2008). "Preparation and application of polymer-grafted magnetic nanoparticles for lipase immobilization", Journal of Magnetism and Magnetic Materials, 320: 2350-2355.

[68] Bradford, M.M., (1976). "A rapid and sensitive method for the quantitation of microgram quantities of protein utilizing the principle of protein-dye binding", Analytical biochemistry, 72: 248-254.

[69] Price, P.M. Dittmar, J.W. Carlson, K. Lawson, B.P. Reilly, A.K. Stein, B.D. Cheng, H. Zholobko, O. Kohut, A. ve Voronov, A., (2019). "Clustering of

Iron Oxide Nanoparticles with Amphiphilic Invertible Polymer Enhances Uptake and Release of Drugs and MRI Properties", Particle & Particle Systems Characterization: 1900112.

[70] Gómez-Vallejo, V. Puigivila, M. Plaza-García, S. Szczupak, B. Piñol, R. Murillo, J.L. Sorribas, V. Lou, G. Veintemillas, S. ve Ramos-Cabrer, P., (2018). "PEG-copolymer-coated iron oxide nanoparticles that avoid the reticuloendothelial system and act as kidney MRI contrast agents", Nanoscale, 10: 14153-14164.

[71] Patten, T. Xia, J. ve Abernathy, T., (1998). "Science (Washington, DC) 272, 866 (1996);(b) TE Patten and K. Matyjaszewski", Adv. Mat, 10: 901.

[72] Hawker, C.J., (1997). "“Living” free radical polymerization: a unique technique for the preparation of controlled macromolecular architectures", Accounts of chemical research, 30: 373-382.

[73] Chiefari, J. Chong, Y. Ercole, F. Krstina, J. Jeffery, J. Le, T.P. Mayadunne, R.T. Meijs, G.F. Moad, C.L. ve Moad, G., (1998). "Living free-radical polymerization by reversible addition− fragmentation chain transfer: the RAFT process", Macromolecules, 31: 5559-5562.

[74] Rizzardo, E. Chiefari, J. Chong, B.Y. Ercole, F. Krstina, J. Jeffery, J. Le, T.P. Mayadunne, R.T. Meijs, G.F. ve Moad, C.L., (1999). "Tailored polymers by free radical processes": Wiley Online Library.

[75] Wenzel, A.G. ve Grubbs, R.H., (2006). "Ruthenium metallacycles derived from 14-electron complexes. New insights into olefin metathesis intermediates", Journal of the American Chemical Society, 128: 16048-16049.

[76] Grubbs, R.H. Wenzel, A.G. O'Leary, D.J. ve Khosravi, E., (2015). Handbook of metathesis: Wiley Online Library.

[77] Ivin, K.J. ve Mol, J.C., (1997). Olefin metathesis and metathesis polymerization: Elsevier.

[78] Odian, G., (2004). Principles of polymerization: John Wiley & Sons.

[79] Lynn, D.M. Kanaoka, S. ve Grubbs, R.H., (1996). "Living ring-opening metathesis polymerization in aqueous media catalyzed by well-defined ruthenium carbene complexes", Journal of the American Chemical Society, 118: 784-790.

[80] Choi, T.-L. ve Grubbs, R.H., (2003). "Controlled Living Ring-Opening-Metathesis Polymerization by a Fast-Initiating Ruthenium Catalyst", Angewandte Chemie International Edition, 42: 1743-1746.

[81] Maughon, B.R. ve Grubbs, R.H., (1997). "Ruthenium Alkylidene Initiated Living Ring-Opening Metathesis Polymerization (ROMP) of 3-Substituted Cyclobutenes", Macromolecules, 30: 3459-3469.

[82] Hillmyer, M.A. Laredo, W.R. ve Grubbs, R.H., (1995). "Ring-Opening Metathesis Polymerization of Functionalized Cyclooctenes by a Ruthenium-Based Metathesis Catalyst", Macromolecules, 28: 6311-6316.

[83] Patton, P.A. Lillya, C.P. ve McCarthy, T.J., (1986). "Olefin metathesis of cyclohexene", Macromolecules, 19: 1266-1268.

[84] Dounis, P. James Feast, W. ve Kenwright, A.M., (1995). "Ring-opening metathesis polymerization of monocyclic alkenes using molybdenum and tungsten alkylidene (Schrock-type) initiators and 13C nuclear magnetic resonance studies of the resulting polyalkenamers", Polymer, 36: 2787-2796.

[85] Schrock, R.R. Yap, K.B. Yang, D.C. Sitzmann, H. Sita, L.R. ve Bazan, G.C., (1989). "Evaluation of cyclopentene-based chain-transfer agents for living ring-opening metathesis polymerization", Macromolecules, 22: 3191-3200.

[86] Trzaska, S.T. Lee, L.-B.W. ve Register, R.A., (2000). "Synthesis of Narrow-Distribution "Perfect" Polyethylene and Its Block Copolymers by Polymerization of Cyclopentene", Macromolecules, 33: 9215-9221.

[87] Nuyken, O. ve Pask, S.D., (2013). "Ring-Opening Polymerization—An Introductory Review", Polymers, 5: 361-403.

[88] Lyon, C.K. Prasher, A. Hanlon, A.M. Tuten, B.T. Tooley, C.A. Frank, P.G. ve Berda, E.B., (2015). "A brief user's guide to single-chain nanoparticles", Polymer Chemistry, 6: 181-197.

[89] Grubbs, R.H., (2006). "Olefin-Metathesis Catalysts for the Preparation of Molecules and Materials (Nobel Lecture)", Angewandte Chemie International Edition, 45: 3760-3765.

[90] Schrock, R.R., (2006). "Multiple Metal–Carbon Bonds for Catalytic Metathesis Reactions (Nobel Lecture)", Angewandte Chemie International Edition, 45: 3748-3759.

[91] Chauvin, Y., (2006). "Olefin Metathesis: The Early Days (Nobel Lecture)", Angewandte Chemie International Edition, 45: 3740-3747.

[92] Jani, J.M. Leary, M. Subic, A. ve Gibson, M.A., (2014). "A review of shape memory alloy research, applications and opportunities", Materials & Design (1980-2015), 56: 1078-1113.

[93] Yang, D. Huang, W. Yu, J. Jiang, J. Zhang, L. ve Xie, M., (2010). "A novel shape memory polynorbornene functionalized with poly (ε-caprolactone) side chain and cyano group through ring-opening metathesis polymerization", Polymer, 51: 5100-5106.

[94] lşıksel, E. Kahraman, G. Ceren Süer, N. Wang, D.-Y. ve Eren, T., (2019). "Synthesis and characterization of phosphonate and aromatic-based polynorbornene polymers derived from the ring opening metathesis polymerization method and investigation of their thermal properties", Journal of Applied Polymer Science, 136: 47085.

[95] Aktas Eken, G. ve Acar, M.H., (2019). "PVDF-based shape memory polymers", European Polymer Journal, 114: 249-254.

[96] Jiang, H.Y. Kelch, S. ve Lendlein, A., (2006). "Polymers Move in Response to Light", Advanced Materials, 18: 1471-1475.

[97] Leng, J. Lu, H. Liu, Y. Huang, W.M. ve Du, S., (2011). "Shape-Memory Polymers—A Class of Novel Smart Materials", MRS Bulletin, 34: 848-855.

[98] Feng, Y. Lu, J. Behl, M. ve Lendlein, A., (2011). "Degradable Depsipeptide-Based Multiblock Copolymers with Polyester or Polyetherester Segments", The International Journal of Artificial Organs, 34: 103-109.

[99] Hu, J. Meng, H. Li, G. ve Ibekwe, S.I., (2012). "A review of stimuli-responsive polymers for smart textile applications", Smart Materials and Structures, 21: 053001.

[100] El Feninat, F. Laroche, G. Fiset, M. ve Mantovani, D., (2002). "Shape Memory Materials for Biomedical Applications", Advanced Engineering Materials, 4: 91-104.

[101] Lendlein, A. ve Kelch, S., (2002). "Shape-Memory Polymers", Angewandte Chemie International Edition, 41: 2034-2057.

[102] Ahn, S.-k. Kasi, R.M. Kim, S.-C. Sharma, N. ve Zhou, Y., (2008). "Stimuli-responsive polymer gels", Soft Matter, 4: 1151-1157.

[103] Zhou, Y. Xu, M. Yi, T. Xiao, S. Zhou, Z. Li, F. ve Huang, C., (2007). "Morphology-Tunable and Photoresponsive Properties in a Self-Assembled Two-Component Gel System", Langmuir, 23: 202-208.

[104] Thomsen, D.L. Keller, P. Naciri, J. Pink, R. Jeon, H. Shenoy, D. ve Ratna, B.R., (2001). "Liquid Crystal Elastomers with Mechanical Properties of a Muscle", Macromolecules, 34: 5868-5875.

[105] Andreopoulos, F.M. Deible, C.R. Stauffer, M.T. Weber, S.G. Wagner, W.R. Beckman, E.J. ve Russell, A.J., (1996). "Photoscissable Hydrogel Synthesis via Rapid Photopolymerization of Novel PEG-Based Polymers in the Absence of Photoinitiators", Journal of the American Chemical Society, 118: 6235-6240.

[106] Frank, P.G. Tuten, B.T. Prasher, A. Chao, D. ve Berda, E.B., (2014). "Intra-Chain Photodimerization of Pendant Anthracene Units as an Efficient Route to Single-Chain Nanoparticle Fabrication", Macromolecular Rapid Communications, 35: 249-253.

[107] Han, D. Lu, H. Li, W. Li, Y. ve Feng, S., (2017). "Light- and heat-triggered reversible luminescent materials based on polysiloxanes with anthracene groups", RSC Advances, 7: 56489-56495.

[108] Becker, H.D., (1993). "Unimolecular photochemistry of anthracenes", Chemical Reviews, 93: 145-172.

[109] Chen, W. Wang, J.-Y. Zhao, W. Li, L. Wei, X. Balazs, A.C. Matyjaszewski, K. ve Russell, T.P., (2011). "Photocontrol over the Disorder-to-Order Transition in Thin Films of Polystyrene-block-poly(methyl methacrylate) Block Copolymers Containing Photodimerizable Anthracene Functionality", Journal of the American Chemical Society, 133: 17217-17224.

[110] Wang, C.-H. Hsieh, C.-Y. ve Hwang, J.-C., (2011). "Flexible Organic Thin-Film Transistors with Silk Fibroin as the Gate Dielectric", Advanced Materials, 23: 1630-1634.

[111] Frath, D. Massue, J. Ulrich, G. ve Ziessel, R., (2014). "Luminescent Materials: Locking π-Conjugated and Heterocyclic Ligands with Boron(III)", Angewandte Chemie International Edition, 53: 2290-2310.

[112] Naito, H. Nishino, K. Morisaki, Y. Tanaka, K. ve Chujo, Y., (2017). "Highly-efficient solid-state emissions of anthracene–o-carborane dyads with various substituents and their thermochromic luminescence properties", Journal of Materials Chemistry C, 5: 10047-10054.

[113] Chen, Y. Abdellatif, M.M. ve Nomura, K., (2018). "Olefin metathesis polymerization: Some recent developments in the precise polymerizations for synthesis of advanced materials (by ROMP, ADMET)", Tetrahedron, 74: 619-643.

[114] Leitgeb, A. Wappel, J. ve Slugovc, C., (2010). "The ROMP toolbox upgraded", Polymer, 51: 2927-2946.

[115] Kolonko, E.M. Pontrello, J.K. Mangold, S.L. ve Kiessling, L.L., (2009). "General synthetic route to cell-permeable block copolymers via ROMP", Journal of the American Chemical Society, 131: 7327-7333.

[116] Simon, Y.C. ve Coughlin, E.B., (2010). "Ring-opening metathesis copolymerization of cyclooctene and a carborane-containing oxanorbornene", Journal of Polymer Science Part A: Polymer Chemistry, 48: 2557-2563.

[117] Smith, D. Pentzer, E.B. ve Nguyen, S.T., (2007). "Bioactive and therapeutic ROMP polymers", Journal of Macromolecular Science, Part C: Polymer Reviews, 47: 419-459.

[118] Pawar, G.M. Lalancette, R.A. Bonder, E.M. Sheridan, J.B. ve Jäkle, F., (2015). "ROMP-Derived Pyridylborate Block Copolymers: Self-Assembly, pH-Responsive Properties, and Metal-Containing Nanostructures", Macromolecules, 48: 6508-6515.

[119] Love, J.A. Morgan, J.P. Trnka, T.M. ve Grubbs, R.H., (2002). "A Practical and Highly Active Ruthenium-Based Catalyst that Effects the Cross Metathesis of Acrylonitrile", Angewandte Chemie International Edition, 41: 4035-4037.

[120] Som, A. Reuter, A. ve Tew, G.N., (2012). "Protein Transduction Domain Mimics: The Role of Aromatic Functionality", Angewandte Chemie International Edition, 51: 980-983.

[121] Simon, Y.C. Ohm, C. Zimny, M.J. ve Coughlin, E.B., (2007). "Amphiphilic Carborane-Containing Diblock Copolymers", Macromolecules, 40: 5628-5630.

[122] Mitsunobu, O., (1980). THE USE OF DIETHYL AZODICARBOXYLATE-TRIPHENYLPHOSPHINE SYSTEM IN THE SYNTHESIS AND TRANSFORMATION OF NATURAL PRODUCTS, W.J. Stec, ed. Phosphorus Chemistry Directed Towards Biology. Pergamon, 213-218.

[123] Elson, K.E. Jenkins, I.D. ve Loughlin, W.A., (2003). "The Hendrickson reagent and the Mitsunobu reaction: a mechanistic study", Organic & Biomolecular Chemistry, 1: 2958-2965.

[124] Hughes, D.L., (1996). "PROGRESS IN THE MITSUNOBU REACTION. A REVIEW", Organic Preparations and Procedures International, 28: 127-164.

[125] Mitsunobu, O. ve Yamada, M., (1967). "Preparation of Esters of Carboxylic and Phosphoric Acid via Quaternary Phosphonium Salts", Bulletin of the Chemical Society of Japan, 40: 2380-2382.

[126] Fletcher, S., (2015). "The Mitsunobu reaction in the 21st century", Organic Chemistry Frontiers, 2: 739-752.

[127] Baraldi, P.G. Guarneri, M. Moroder, F. Pollini, G.P. ve Simoni, D., (1982). "Synthesis of 1-Phthalimidoalkanephosphonates", Synthesis, 1982: 653-655.

[128] Schmider, M. Müh, E. Klee, J.E. ve Mülhaupt, R., (2005). "A Versatile Synthetic Route to Phosphonate-Functional Monomers, Oligomers, Silanes, and Hybrid Nanoparticles", Macromolecules, 38: 9548-9555.

[129] Kahraman, G. Wang, D.-Y. von Irmer, J. Gallei, M. Hey-Hawkins, E. ve Eren, T., (2019). "Synthesis and Characterization of Phosphorus- and Carborane-Containing Polyoxanorbornene Block Copolymers", Polymers, 11: 613.

[130] N'Guyen, T.T.T. Duong, H.T.T. Basuki, J. Montembault, V. Pascual, S. Guibert, C. Fresnais, J. Boyer, C. Whittaker, M.R. Davis, T.P. ve Fontaine, L., (2013). "Functional Iron Oxide Magnetic Nanoparticles with Hyperthermia-Induced Drug Release Ability by Using a Combination of Orthogonal Click Reactions", Angewandte Chemie International Edition, 52: 14152-14156.

[131] Sahoo, Y. Pizem, H. Fried, T. Golodnitsky, D. Burstein, L. Sukenik, C.N. ve Markovich, G., (2001). "Alkyl Phosphonate/Phosphate Coating on Magnetite Nanoparticles: A Comparison with Fatty Acids", Langmuir, 17: 7907-7911.

[132] Krekić, K. Klintuch, D. ve Pietschnig, R., (2017). "Facile access to efficiently luminescent Ln3+ phosphonic ester coordination polymers (Ln = Eu, Tb, Dy)", Chemical Communications, 53: 11076-11079.

[133] Valliant, J.F. Guenther, K.J. King, A.S. Morel, P. Schaffer, P. Sogbein, O.O. ve Stephenson, K.A., (2002). "The medicinal chemistry of carboranes", Coordination Chemistry Reviews, 232: 173-230.

[134] Zhao, X. Babu, H.V. Llorca, J. ve Wang, D.-Y., (2016). "Impact of halogen-free flame retardant with varied phosphorus chemical surrounding on the properties of diglycidyl ether of bisphenol-A type epoxy resin: synthesis, fire behaviour, flame-retardant mechanism and mechanical properties", RSC Advances, 6: 59226-59236.

CURRICULUM VITAE

PERSONAL INFORMATION

Name Surname	: GİZEM KAHRAMAN
Date of birth and place	: 02.01.1990 İSTANBUL
Foreign Languages	: English and German
E-mail	: gizemkahramann@gmail.com

EDUCATION

Degree	**Department**	**University**	**Date of Graduation**
Master	Chemistry	Yıldız Technical University	22.08.2014
Undergraduate	Chemistry	Yıldız Technical University	27.08.2012
High School	Pertevniyal Anatolian Highschool		13.06.2008

PUBLISHMENTS

Papers

1. Kahraman G., Wang D., Irmer J., Gallei M., Hey-Hawkins E., Eren T., *Polymers*, **2019**, 11, 613, DOI:10.3390/polym11040613.
2. Coburger P., Kahraman G., Straube A., Hey-Hawkins E., *Dalton Transactions*, **2019**, DOI: 10.1039/c9dt00628a.
3. Isiksel E., Kahraman G., Suer N. C., Wang D., Eren T., *J. App. Poly. Sci.*, **2018**, DOI: 10.1002/app.47085.
4. Turgut G. Isiksel E., Kahraman G., Eren T., Ozkoc G., *J. App. Poly. Sci.*, **2017**, DOI: 10.1002/app.45998.

Projects

1. TUBITAK 114Z666

AWARDS

1. TUBITAK 2214-A International Research Fellowship Programme
2. DAAD Short Term Research Grant
3. COST Action CM1302 Short Term Scientific Mission (STSM)